OPTOGENETIC TOOL TO CONTROL SINGLE MOLECULES AND ITS APPLICATION IN THE STUDY OF UNCONVENTIONAL FGF2 SECRETION

INAUGURAL DISSERTATION
to obtain the academic degree of
Doctor rerum naturalium (Dr. rer. nat)

Submitted to the

Department of Biology, Chemistry, Pharmacy
Freie Universität Berlin

by
Purba Kashyap

Berlin, April, 2023

This doctorate study was conducted from October 2017 to December 2022 under the supervision of Prof. Dr. Helge Ewers in the Department of Biology, Chemistry and Pharmacy of the Freie Universität Berlin.

1st reviewer: Prof. Dr. Helge Ewers

2nd reviewer: Dr. Francesca Bottanelli

Date of defence: 20.06.2023

Declaration of independent work

This is to confirm that this thesis was independently composed and authored by myself, using solely the referred sources and support. This thesis has not been submitted to any other doctoral procedure.

ACKNOWLEDGEMENTS

My doctorate experience has been enriching, humbling, and transformative. It is an endeavour that a single person cannot accomplish but is instead a result of contributions from many individuals. I am fortunate to have had the support of many individuals, without whom this thesis would have been impossible.

First and foremost, I would like to express my gratitude to my PI, Prof. Helge Ewers, for selecting me to join his lab and allowing me to work on interesting projects. It has been an exciting journey to explore and execute his clever and elegant ideas. I could not have asked for a more supportive mentor. His guidance has helped me become the independent scientist I aspired to be.

I thank Dr. Francesca Bottanelli for agreeing to be my second reviewer.

I also thank my co-PI, Prof. Walter Nickel, for his support and for allowing me to work on the fascinating topic of FGF2's secretion. Investigating FGF2's unconventional secretion from a single-molecule perspective was truly enjoyable. The Nickel lab has been very kind to me, and I would like to thank Eleni Dimou and Roberto Saleppico from the lab for their support, discussions and valuable contributions. Eleni taught me crucial experiments, and Roberto made the stable cell lines vital for this work.

I thank Jia Hui Li, who has been like a third mentor to me. We decided to meet every Monday to discuss our progress and future experiments, and it turned out to be one of the best decisions. Her insights have been invaluable to my progress.

I am grateful to all the present and former members of the Ewers group for their support, friendship, and scientific discussions. Special thanks to Claire Schlack, who taught me everything I know about cloning, Mengfei Gao, who showed me experiments initially, and Amin Zehtabian for his advice and help with coding. I would

also like to thank Andrea Senge and Carolin Knappe for their technical help, Markus and Jakob for scientific discussions and Ando, Raluca and Suse for their friendship.

I have been fortunate to receive help from many talented bachelor's and master's students, including Fenja Blank, whose contributions were enormous and resurrected the PhoCl project, Adolf Bierhuizen, who established the beginning slower phase of the PhoCl project with great care, and Daria Shyshko, who provided crucial help during the last pressing months of my doctorate.

Throughout my doctorate study, I have had opportunities to collaborate with many labs. I am grateful to Prof. Tobias Stauber for his consistent optimistic outlook, and I would like to thank Yulia Kolobkova for a great collaboration in the PhoCl-based VRAC reconstitution project. I would also like to thank Prof. Andrew Plested for another great collaboration. I want to thank Sara Bertellli from the Plested lab for her consistent effort, which resulted in detecting functional ion channels with PhoCl uncaging. Both the Stauber lab and Plested lab members were very warm and welcoming. I want to thank Prof. Robert Campbell and Xiaocen Lu from Campbell lab, whose crucial inputs were instrumental in the success of the PhoCl project, and Prof. Robin Hiesenger and Egemen Agi for their time and help with the two-photon experiments.

I am grateful to Annalena, Jakob, Jia, Markus, Raluca and Roberto for generously giving their time and providing invaluable feedback on my thesis, helping me improve it.

Finally, I would like to thank my friends, Lena, Laura, Sneha, Ayusman, Arunav and Abhyuday, for being there.

Most importantly, I would like to express my deep appreciation to my parents for their unwavering support and hard work, which have been a constant source of inspiration. I am also grateful to my sister for her constant encouragement and JJ for believing in me.

ABSTRACT

Single-molecule microscopy is a powerful tool for investigating functional events at the plasma membrane. With the state-of-the-art microscopy method, changes in protein mobility can be correlated to cellular events or structures. Such experiments offer quantitative data that is impossible to yield from ensemble methods as they render the individual functional event in a protein's life tractable to investigation and analysis. We can visualize changes in molecular behaviour with respect to triggered or observed cellular events and thus understand the role of the observed molecule in these processes. However, setting up the conditions required for investigating stoichiometry is challenging. Single-molecule tracking requires a sparse population of the protein of interest for single-molecule visualization. This requirement is met by partially labelling the protein of interest, which occludes information like the stoichiometry of the protein and how oligomeric protein influence function. We propose control of the number of proteins at the plasma membrane by controlling its transport to achieve a low population of fully labelled proteins of interest at the site of its action. We developed an optogenetic tool for the light-controlled delivery of functional soluble and transmembrane proteins to the plasma membrane. We show that small amounts of proteins can be released optogenetically and efficiently transported to the plasma membrane using an optically cleavable fluorescent protein. Our method allows for the controlled delivery of proteins, including functional ion channels, to the plasma membrane in amounts compatible with single-molecule imaging.

Single-molecule microscopy and the developed optogenetic tool were applied to study the unconventional secretion of Fibroblast Growth Factor (FGF2). FGF2 is an essential growth factor involved in cell growth, differentiation, and development. FGF2 skips the conventional ER-Golgi route for secretion and instead adopts an unconventional secretion pathway. Through biochemical reconstitution experiments, it is known to directly interact with the plasma membrane, where it undergoes

phosphorylation and oligomerization. It is hypothesized that FGF2 oligomers form a pore in the plasma membrane where FGF2's interaction with the extracellular heparan sulphate proteoglycans facilitates its extraction from the plasma membrane. To elucidate steps in FGF2 secretion in the context of live cells and to test the current model, I aimed to visualize the FGF2 secretion using live cell single-molecule microscopy. I employed the developed optogenetic tool to synchronize FGF2 release in the cytosol to study the initial phase of FGF2 secretion. Furthermore, by observing the mobility and intensity of FGF2 molecules via single molecule tracking, I dissected the sequence of events in the FGF2 secretion process.

ZUSAMMENFASSUNG

Die Einzelmolekülmikroskopie ist ein leistungsfähiges Instrument zur Untersuchung funktioneller Ereignisse an der Plasmamembran. Mit der hochmodernen Mikroskopiemethode können Änderungen der Proteinmobilität mit zellulären Ereignissen oder Strukturen korreliert werden. Solche Experimente liefern quantitative Daten, die mit Ensemble-Methoden nicht gewonnen werden können, da sie das einzelne funktionelle Ereignis im Leben eines Proteins für die Untersuchung und Analyse zugänglich machen. Wir können Veränderungen im molekularen Verhalten im Zusammenhang mit ausgelösten oder beobachteten zellulären Ereignissen sichtbar machen und so die Rolle des beobachteten Moleküls in diesen Prozessen verstehen. Es ist jedoch eine Herausforderung, die für die Untersuchung der Stöchiometrie erforderlichen Bedingungen zu schaffen. Die Einzelmolekülverfolgung erfordert eine spärliche Population des Proteins, das für die Einzelmolekülvisualisierung von Interesse ist. Diese Anforderung wird durch die teilweise Markierung des interessierenden Proteins erfüllt, wodurch Informationen wie die Stöchiometrie des Proteins und der Einfluss oligomerer Proteine auf die Funktion verdeckt werden. Wir schlagen vor, die Anzahl der Proteine an der Plasmamembran zu kontrollieren, indem wir ihren Transport steuern, um eine geringe Population vollständig markierter Proteine am Ort ihrer Wirkung zu erreichen. Wir haben ein optogenetisches Werkzeug für die lichtgesteuerte Zuführung von funktionellen löslichen und Transmembranproteinen zur Plasmamembran entwickelt. Wir zeigen, dass kleine Mengen von Proteinen mit Hilfe eines optisch spaltbaren fluoreszierenden Proteins optogenetisch freigesetzt und effizient zur Plasmamembran transportiert werden können. Unsere Methode ermöglicht die kontrollierte Abgabe von Proteinen, einschließlich funktioneller Ionenkanäle, an die Plasmamembran in Mengen, die mit der Einzelmolekül-Bildgebung kompatibel sind.

Die Einzelmolekülmikroskopie und das entwickelte optogenetische Werkzeug wurden eingesetzt, um die unkonventionelle Sekretion des Fibroblasten-Wachstumsfaktors (FGF2) zu untersuchen. FGF2 ist ein wichtiger Wachstumsfaktor, der an Zellwachstum, Differenzierung und Entwicklung beteiligt ist. FGF2 überspringt den

konventionellen ER-Golgi-Weg für die Sekretion und nimmt stattdessen einen unkonventionellen Sekretionsweg ein. Aus biochemischen Rekonstitutionsexperimenten ist bekannt, dass es direkt mit der Plasmamembran interagiert, wo es eine Phosphorylierung und Oligomerisierung erfährt. Es wird angenommen, dass FGF2-Oligomere eine Pore in der Plasmamembran bilden, durch die FGF2 durch Interaktion mit den extrazellulären Heparansulfat-Proteoglykanen aus der Plasmamembran extrahiert werden kann. Um die einzelnen Schritte der FGF2-Sekretion in lebenden Zellen aufzuklären und das derzeitige Modell zu testen, wollte ich die FGF2-Sekretion mit Hilfe der Einzelmolekülmikroskopie in lebenden Zellen sichtbar machen. Ich setzte das entwickelte optogenetische Werkzeug zur Synchronisierung der FGF2-Freisetzung im Zytosol ein, um die Anfangsphase der FGF2-Sekretion zu untersuchen. Durch die Beobachtung der Mobilität und Intensität der FGF2-Moleküle mittels Einzelmolekül-Tracking konnte ich die Abfolge der Ereignisse im FGF2-Sekretionsprozess aufschlüsseln.

CONTENTS

FIGURES AND TABLES

ABBREVIATIONS

AcbA	acyl-coenzyme A-binding protein
AF	Alexa Fluor
ATP	Adenosine triphosphate
BK	Big Potassium
BSA	Bovine serum albumin
CCD	Charged Coupled Device
CD4	Cluster of Diferentiation-4
CHO	Chinese Hamster Ovarian
CMV	Cytomegalovirus
D	Diffusion Coefficient
DAG	Diacylglycerol
DMEM	Dulbecco's Modified Eagle Medium
DNA	Deoxyribonucleic acid
ECM	Extracellular Matrix
EGF	Epidermal Growth Factor
e.g.	Exemplum gratia
EM-CCD	Electron Multiplying Charged Coupled Device
ER	Endoplasmic reticulum
FBS	Fetal Bovine Serum
FCS	Fluorescence Correlation Spectroscopy
FGF	Fibroblast Growth Factor
GFP	Green Fluorescent Protein
GPC1	Glypican1
GPI	Glycosylphosphatidylinositol
GUV	Giant Unilamellar Vesicle
HMGB-1	High mobility group box-1
HSPG	Heparan Sulfate Proteoglycan
i.e	id est
Kb	Boltzmann Constant
LPS	Lipopolysaccharide
MAP	Microtubule Associated Protein
MSD	Mean Squared Displacement
η	viscosity
NA	Numerical Aperture
NiNTA	Nickel Nitrilotriacetic acid
nb	Nanobody
n.s	Not significant
PALM	Photoactivated localization microscopy
PI3K	Phosphoinositide 3 Kinase
$PI_{(4,5)}P_2$	Phosphatidylinositol 4,5 bisphosphate

PLCγ	Phospholipase C gamma
PM	Plasma membrane
POI	Protein of interest
PSF	Point Source Function
QD	Quantum Dot
RER	Retention in Endoplasmic Reticulum Retrieval sorting receptor1
RNA	Ribonucleic acid
ROI	Region of Interest
ROXS	Reducing-plus-Oxidizing System
RUSH	Retention Using Selective Hook
SBP	Streptavidin Binding Protein
sd	Standard Deviation
smFRET	Single Molecule Fluorescence Resonance Energy Transfer
SNR	Signal-to-Noise Ratio
SP	Signal Peptide
SPT	Single Particle Tracking
SRP	Signal Recognition Particle
ST	Sialyl transferase
STAT	Signal transducer and activator of transcription
T	Temperature
TIRF	Total Internal Reflection Fluorescence
TMD	Transmembrane Domain
TMEM/TMEM115	Transmembrane protein 115
Tyr	Tyrosine
UV	Ultraviolet
UVR8	UV-B resistance-8

1 General Introduction

'It is very easy to answer many of these fundamental biological questions; you just look at the thing! ..... Unfortunately, the present microscope sees at a scale which is just a bit too crude.'

Feynman, 1959

1.1 The skeleton of a biological process

A cell is a busy place where countless biological processes run simultaneously. A biological process is a series of chemical reactions that occurs in cells that translates into a function important for the cell's sustenance. Signal transduction is an example of such a biological process. A signal from outside is conveyed to the cell through a series of steps, mostly involving protein interactions and modifications. It begins with a growth factor (signal) that interacts with its receptor on the cell membrane. This interaction causes receptor modifications, such as dimerization or phosphorylation. The modified receptor is recognized by other proteins, passing the information to even more proteins. Thus, information from the cell's exterior is conveyed to the cell through a series of protein interactions. The cell responds to this new information by changing the cell state by initiating other biological processes, either through the gene expression of another protein or by starting another reaction cascade. In molecular

biology, biochemistry, and cell biology, biologists aim to study fundamental biological processes and their mechanisms.

1.2 THE BIOCHEMICAL APPROACH

In past decades, bulk biochemical experiments have been the most common approach for studying biological processes. Such experiments detect the presence, increase, or decrease of the protein of interest (POI) or protein interaction after an event. These experiments also involve purification of the proteins and measurement of their properties. In the example of signal transduction, key proteins, their sequence of interaction, and modifications post-interaction have been identified through this approach.

Thus, a biochemical approach is a significant and highly relevant method for understanding biological processes. However, this approach does not allow one to grasp the entire picture of a biological process in a physiological or true sense. In our example of the signal transduction process, the spatial information of the process, the dynamics of each step of the process, and the transient intermediates are missing. These details are crucial for understanding the mechanisms underlying biological processes. The biochemical approach is an indirect method used to predict a model of biological function that needs to be tested in the physiological context, that is, in live cells. The approach identifies the 'whats' or the key participating molecules but misses the 'hows' or the dynamics of a process. *In vitro* approaches miss out on the spatial information of the biological process and are limited to detecting large changes in cells. Finally, the measurements made with biochemical experiments are ensemble averages, disregarding heterogeneity and complexity of biological processes.

1.3 THE SINGLE-MOLECULE APPROACH

The models of biological processes found in textbooks inform about the participants and the sequence of events in the process. Such models give the misleading idea that these biological processes are smooth unidirectional processes, like assembly lines in factories. However, most of these biological processes are not straightforward. The molecules move in random motion owing to the thermal energy and interact stochastically with one another. This generates heterogeneity in the state of the molecule (confirmation, oligomeric state, or chemical modification) at any given time. Furthermore, stochastic interaction translates into a function through many unknown transient steps and fine details. The single-molecule approach can capture the dynamics and complexity of a biological process.

The underlying mechanism can be understood if one can see biomolecules in action during a biological process. Single-molecule methods provide the opportunity to do so. In single-molecule techniques, one follows a single molecule in its trajectory, revealing all stages that the molecules undergo. Following many such single molecules reveal the heterogeneity in the molecule's state in the system. Performing single-molecule microscopy techniques in live cells provides spatial information, heterogeneity, and dynamics of the POI in the context of cells.

The following example illustrates the strength of the single-molecule method. Biochemical experiments have shown that signal transduction results from ligand-receptor interactions and effector proteins' subsequent recruitment and modification. A single-molecule study of the process illuminates the additional conditions required for and the mechanism underlying successful signal transduction. A single-molecule study showed that T-cell receptors respond to specific ligands because the interaction is longer. The long interaction facilitates more receptor-ligand interactions in the vicinity. Aggregation of activated receptors leads to the formation of a stable substrate

for the recruitment of effector proteins and, ultimately, successful signal transduction [1].

Within a short time, single-molecule microscopy has already revealed much about the nanoscale organization and molecular dynamics of proteins[2]. The single-molecule approach has been revolutionary in understanding the functioning of molecular machines. Imaging of single motor proteins like kinesin and myosin showed that they walk in a 'hand over hand' manner with ~8 nm stepsize[3]. In live cells, it was found that a single cargo can be simultaneously attached to multiple motor proteins of all kinds (myosin, dynein, and kinesin), increasing speed and helping manoeuvre roadblocks[4–6]. Imaging single ATP synthetase complexes led to a mechanistic understanding of the molecular machine[7,8]. A single-molecule study showed that gene expression is a stochastic process that leads to burst expression of proteins[9–12]. By looking at single transcription factors, researchers found that Deoxyribonucleic acid (DNA) binding proteins combine 1D and 3D diffusion, i.e., they diffuse on the DNA (1D) as well as frequently unbind and bind other regions of the DNA (3D) to find their target sequence[13,14].

At the plasma membrane (PM), an enormous amount of single-molecule research has been done on the transmembrane receptors for growth factors and immune signalling[1,15–17]. Single-molecule studies of receptors for cell signalling highlight the heterogeneity in receptor states and modes of activation of cell signalling events. For example, it was shown that vascular endothelial growth factor receptor-2 (VEGFR) is present in multiple assembly and mobility states even before VEGF (the ligand) addition. On stimulation with VEGF, the mode of activation varies based on the receptor state prior to the stimulation[15]. Single-molecule studies have also been crucial to understanding the sequence of events that lead to successful signal transduction. Sako et al. gave the first evidence of EGFR dimerization on EGF binding in live cells. They also showed that most EGFRs are present as dimers, ligand binding to one EGFR in the dimer increases the probability of the ligand binding to the other receptor[18]. In another paper, it was shown that activation of immune receptors is based on macromolecular assemblies of receptor and effector proteins[17]. On stimulation,

interleukin-1 receptor (IL1R) forms a cluster followed by binding and oligomerization of downstream effector protein, MyD88. The success of signal transduction depends on the duration of receptor binding, translated to the size and stability of the receptor and the MyD88 cluster. This unprecedented quality and quantity of information have been possible through single-molecule microscopy.

1.4 ELEMENTS FOR SINGLE MOLECULE MICROSCOPY

1.4.1 Fluorescence

Fluorescence is a process in which a molecule emits photons in the visible range after absorbing photons and becoming excited. A simplified Jablonski diagram illustrates the process (Figure 1). An electron of an atom absorbs energy and jumps to the higher energy state, S1. The excited electron loses some energy and comes to the lowest vibrational level of the excited state. The excited electron then returns to the ground state and, in the process, emits a photon in the visible range. This radiative pathway of relaxation is called fluorescence. A fluorescent molecule undergoes absorption and emission cycles, each taking ns to μs. The excited electron may also relax via non-

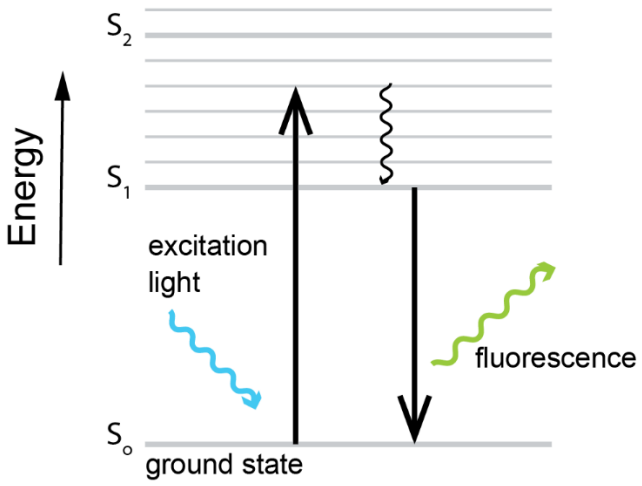

fluorescent, non-radiative pathways. The brightness of a fluorophore is defined by its quantum yield and extinction coefficient. The quantum yield is the ratio of the number of photons emitted compared to the number of photons absorbed. This value depends on the propensity of the excited electron to relax via the fluorescent pathway compared to non-radiative pathways. The extinction coefficient is the measure of the ease of absorbance of light.

1.4.2 Fluorescent probes

Many aquatic organisms like corals, frogs, jellyfish, and fish display fluorescence. Green Fluorescent Protein (GFP), purified initially from jellyfish Aequorea victoria, is the most popular fluorescent protein in bioimaging. GFP showcases green fluorescence when exposed to blue light. The Discovery of GFP has been such a breakthrough for biology research that in 2008, Roger Y. Tsien, Osamu Shimomura, and Martin Chalfie were awarded the Nobel prize for its discovery and development. By now, there are hundreds of fluorescent proteins with the colour palette of the entire visible spectrum. These were initially extracted from fluorescent organisms and later engineered for brighter, more stable, or of different colour variants. Tagging a POI with a fluorescent protein like GFP makes the protein 'visible'. Fluorescent proteins can be genetically fused to the POI to express them as fusion proteins. Genetic fusion leads to a covalent link between the fluorescent tag and the POI. It also ensures 1:1 labelling, a characteristic important for quantitative imaging studies.

Chemically synthesized, organic fluorophores are another alternative to fluorescent proteins as reporters. They are brighter, more stable and provide a wider spectral range than fluorescent proteins. Proteins are labelled at their surface cysteines and amines with fluorophores in vitro. Antibodies labelled with organic fluorophores are then used to tag the POI in the permeabilised cell indirectly.

Quantum dots are another option for tagging POI. Quantum dots are bright nanometre-sized semiconductor particles that are even brighter and more photostable

than organic fluorophores. They can be functionalised with streptavidin and targeted to the POI via biotinylated antibodies.

1.4.3 Resolution

The discovery of GFP[19] helped tag POI inside a cell and investigate the distribution of the protein using fluorescence microscopy. However, when cells express GFP-tagged recombinant protein, usually, one does not see single GFP molecules in the cell but rather a green cloud occupying an area inside the cell. This problem arises because when the cell is crowded with many GFP molecules, spatial resolution limitations of the imaging system inhibit the visualization of single molecules.

According to Abbe's diffraction limit, particles within a certain distance cannot be resolved when observed through a microscope[20]. The limit arises from the wave nature of light. When light waves from a point source pass a lens aperture, they diffract and interfere, forming a large and patterned image of the object[21](Figure 2a). The diffraction pattern of a point source is called the Point Source Function (PSF), and it is defined by the imaging system. This 2D image of the PSF with a bright central spot and alternating dark and bright rings is called an Airy disk (Figure 2a). The size of the airy disk depends on the wavelength (λ) of the exciting light and the objective lens's numerical aperture (NA), a measure of the objective lens's ability to collect and focus light. In the example of a GFP-tagged protein in a cell, each GFP molecule is a point source and will give rise to a PSF. When there is a dense population of the fluorescently tagged protein, closely located point sources cannot be resolved because their PSFs would overlap. Abbe's limit is formulated as λ/2NA. Most NA can vary between 1 to 1.35. Therefore, when using visible light for imaging, molecules located closer than half of the wavelength (~300 nm) are indistinguishable. Therefore, one must dilute the point sources to resolve them as single molecules.

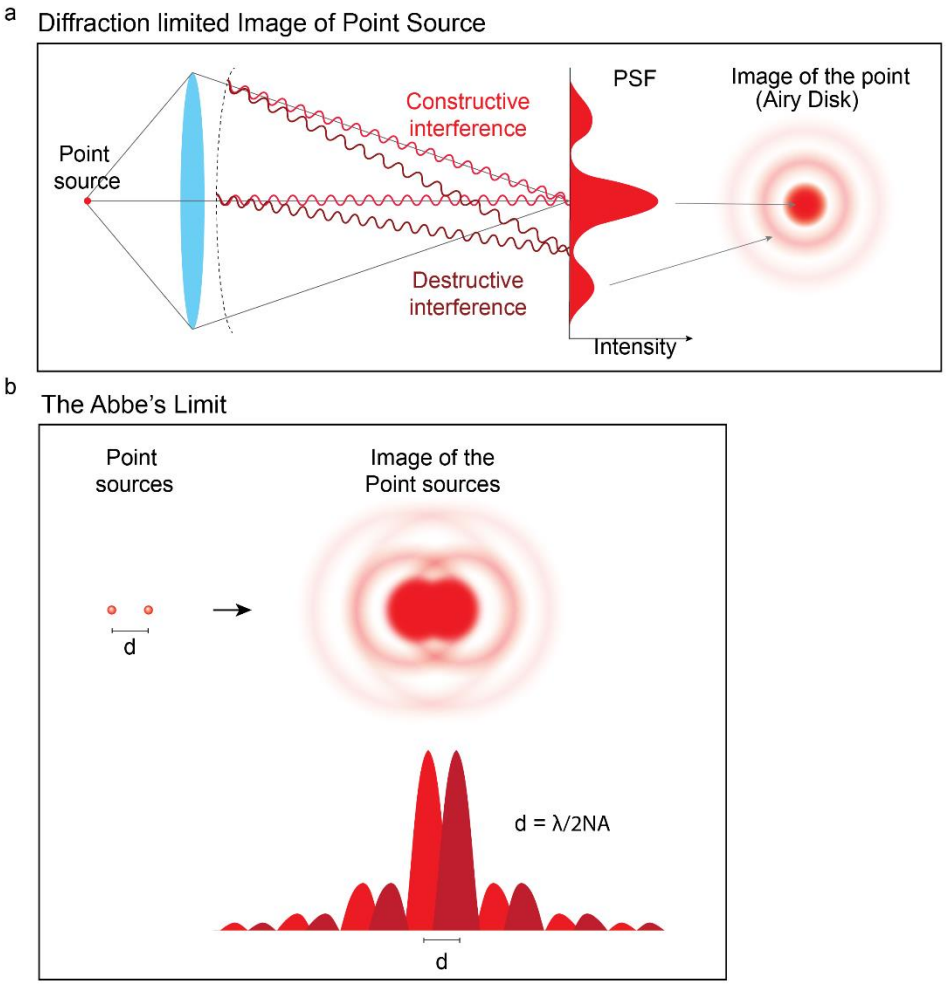

Figure 2: Diffraction limited resolution. (a) Light waves diffract and interfere to form an airy pattern. (b) According to the Rayleigh criterion, two emitters can be resolved if the maxima of one's PSF fall on the minima of the second particle's PSF.

1.4.4 How to see single molecules in live cells

As mentioned earlier, when imaging fluorescently tagged proteins with visible wavelength, each fluorescent probe will result in a larger image. Therefore, to resolve single molecules, the point sources need to be more than ~300 nm distance apart, ideally much more. Different approaches can be used to visualise single molecules.

One approach is to express the fluorescently tagged proteins at very low levels. In conventional fluorescence microscopy, when we express GFP-tagged recombinant proteins, we usually express them at high levels under strong promoters. The GFP-tagged recombinant proteins at such dense concentrations cannot be resolved. If we instead lower the concentration of the tagged protein and, thus, increase the separation between the molecules, we can see single GFP molecules. Microscopists use multiple strategies to achieve single-molecule visualisation of the recombinant protein. Weak expression of the protein can be mediated through a weak promoter or via gene editing and expression at endogenous levels. Researchers also microinject low levels of protein or mRNA into individual cells to achieve a low level of expression.

Another approach is to control the concentration of fluorescent tags instead of regulating the expression of the POI. Photobleaching the majority of the GFP-tagged protein can ensure a low number of 'visible' and hence, resolvable proteins. Researchers also use photoswitchable or photoconvertible proteins to achieve a low number of 'visible' proteins. Photoswitchable proteins are modified fluorescent proteins that are non-fluorescent in the beginning. Illumination with Ultraviolet (UV) light changes the conformation of the protein and makes it fluorescent. Under low amounts of UV light, very few tagged proteins would be stochastically 'switched on' and become fluorescent. Photoconvertible proteins are based on a similar concept, except instead of switching on from dark, they change their emission wavelength on UV illumination. Imaging a green-to-red photoconvertible protein in the red channel would show no fluorescent proteins before photoconversion. Illuminating the sample with controlled levels of UV would 'switch on' a few tagged proteins in the red channel.

Fluorescent protein-tagged proteins are fusion proteins, i.e., these proteins are expressed as fluorescently tagged versions. Proteins can also be tagged with a fluorophore after their expression. For single molecule microscopy of membrane proteins, the extracellular sites of the proteins can be tagged from outside with organic fluorophores via antibody or with quantum dots. The number of tagged proteins is limited by using very low concentrations (pM to nM) of antibodies or quantum dots. Organic fluorophores and quantum dots are superior alternatives to fluorescent

proteins because they are brighter and more photostable. However, intracellular targets in live cells are inaccessible by fluorophore-tagged antibodies or quantum dots due to their large sizes and the selective permeability of the PM. Self-labelling tags like the SNAP-tag or the Halo-tag come to the rescue for this problem. SNAP-tag and Halo-tag are enzymes that can be expressed as a fusion protein. The Halo-tag is a haloalkane dehalogenase enzyme that reacts with chloroalkane, while SNAP-tag is O^6-alkylguanine-DNA-alkyltransferase (AGT) which reacts with O^6benzylguanine (BG). The enzymes react and bind covalently with their substrates which are labelled with organic fluorophores. SNAP/Halo-tag, therefore, gives the best of both worlds, intracellular and quantitative tagging advantages of fluorescent proteins as well as advantages of brighter organic fluorophores. Like in the case of antibodies and quantum dots, sparse labelling is achieved by limiting the concentration of the fluorescent substrate.

1.4.5 Signal to Noise ratio

Visualisation of single molecules is contingent on the signal-to-noise ratio (SNR) of the imaging setup. A bright fluorophore choice ensures a high signal. For intracellular targets, organic fluorophores are applied via SNAP/Halo tags and for extracellular targets, quantum dots are obvious choices for high SNR. High NA objective gathers more photons from the source and hence, is another important factor in increasing the SNR. The collected photons are directed to Electron Multiplied charged coupled devices (EM-CCD cameras) for further improvement of SNR. CCD cameras are very sensitive and can collect up to ~92% of incoming photons. The EM-CCD amplifies the signal after the photons reach the camera chip.

Conventional fluorescence microscopy is performed with an epifluorescence mode where the light passes through the entire sample. Single-molecule imaging is difficult using this mode because the fluorescence background from all the planes of the sample reduces the SNR. Instead, one can illuminate only a thin section of the cell to reduce the background and improve the SNR. Total internal reflection fluorescence

microscopy (TIRF) is a mode of microscopy which uses this idea[22,23]. In a TIRF microscope, light is sent at a critical angle to the coverslip to undergo total internal reflection. Evanescent waves generated at the coverslip-liquid interface enter the sample illuminating the volume closest to the coverslip (Figure 3). In TIRF microscopy, observation of fluorophores is limited to ~100 nm from the coverslip. The technique is useful for imaging membrane proteins at the single molecule level as it dramatically reduces the fluorescent/ auto-fluorescent background from the rest of the cell.

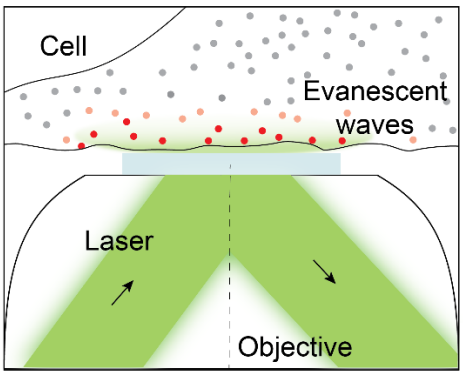

Figure 3: Schematic of TIRF microscopy. The laser hits the interface at a critical angle beyond which it undergoes total internal reflection. The evanescent waves illuminate a thin volume above the coverslip exciting only the fluorescent molecules closest to the plasma membrane.

1.5 SINGLE PARTICLE TRACKING

Once the stage is set to visualise single molecules, we can track the POI over time. The technique is called Single Particle Tracking (SPT) (Figure 4). In SPT, a movie of the proteins is acquired. For the tracking, the positions of proteins are first estimated, then the positions are linked between subsequent frames. Resolvable proteins appear as diffraction-limited spots. The position of the protein can be extracted by fitting the diffraction-limited spots with a gaussian function and obtaining the centre of the fit.

The protein positions are linked between subsequent frames in the movie according to user-defined parameters of the expected distance travelled by the molecule.

SPT can yield the following observations: the diffusion and the stoichiometry of the POI. Tracking POI in equilibrium or after an event in real-time informs of the protein's mobility and oligomer state changes. Mobility changes may represent interaction with other proteins or self-aggregation. The technique has illustrated the functioning of molecular machines like ATPsynthetase[24] and myosin motors[3], aggregation of receptors on signalling in T cells[25], dimerization of epidermal growth factor (EGF) receptors for a successful activation[18], stoichiometry of ion channels[26–28], organisation of membrane and actin-cytoskeleton cortex[29] among many other biological processes.

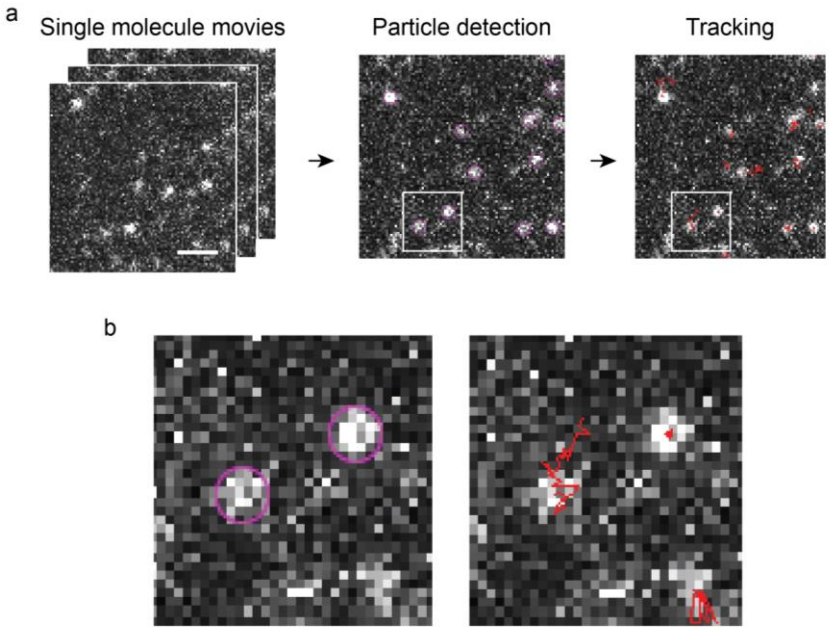

Figure 4: Pipeline of SPT. (a) Example images of sparsely labelled proteins. The analysis includes particle detection of single molecules and tracking of these molecules. Scale bar is 2 μm. (b) Magnified images to show the particles and tracks.

1.5.1 Diffusion of single molecules

Protein motion is the primary observable in an SPT experiment. The molecule's motion informs of the protein's environment and interactions. A protein's motion can be characterised by its diffusion coefficient and the type of motion. The diffusion coefficient measures how fast a molecule diffuses in a substrate. The type of motion might range between free diffusion, active motion, and confined diffusion.

Molecules under no force undergo free diffusion or the Brownian motion [30]. Brownian motion is the random motion of molecules because of collision with molecules in the solution. The motion of molecules is fuelled by the thermal energy of the surrounding media [31]. The Diffusion law can estimate the Diffusion coefficient of the POI under Brownian motion. The diffusion law, first proposed by Albert Einstein in 1905 [32], states that the area explored by the molecule, or its Mean squared Displacement (MSD), is proportional to the Diffusion Coefficient (D) and the time elapsed(t). For motion in one dimension, the relationship can be expressed as,

$$\langle (x_n)^2 \rangle = 2Dt \qquad \text{(Equation 1)}$$

where, $\langle (x_n)^2 \rangle$ is the mean squared displacement of the molecule (MSD) in $n * \Delta t$. The lag time or Δt is the smallest observable time difference. In a movie of diffusing particles, the Δt is the exposure set for the image acquisition. Each spatial dimension contributes with 2Dt to the overall MSD. Therefore, the MSD of particles diffusing in two dimensions is 4Dt. Examples include transmembrane proteins moving on the PM. MSD of particle diffusing in three dimensions is 6Dt. Examples include proteins diffusing in the cytosol.

The diffusion coefficient, D, depends on the temperature, viscosity of the substrate and radius of the molecule. It is formulated by $D = kBT/ (6\pi\eta a)$, where kB is the Boltzmann constant, T is the temperature, η is the viscosity of the media, and a is the radius of the molecule[33]. The diffusion coefficient of a protein indicates the protein size and its environment.

Other motion types, like active motion facilitated by the expenditure of ATP or confined motion due to a restrictive environment, can also be modelled by the diffusion law. Equation 1 is a specialised case of

$$\langle (r_N)^2 \rangle = 2nDt^{\alpha} \qquad \text{(Equation 2)}$$

where n is the dimension and α describes the motion of the particle. α = 1 describes Brownian motion, α >1 describes superdiffusion such as those exhibited by actively transported molecules, and α <1 describes subdiffusion. Subdiffusion is the restricted movement of the molecules due to crowding, interaction with other molecules or spatial heterogeneity. In SPT, movies of sparsely labelled proteins in cells are recorded. These movies are later analysed, where each molecule is detected and tracked. The diffusion coefficient and α are calculated for each tracked molecule and the population distribution generated.

1.5.2 Oligomerisation

Protein oligomers are ubiquitous in biological processes[34]. They are common in signalling pathways. Receptor oligomerization on ligand binding activates the receptors[35]. Receptors may further cluster to form a stable, longer-lived substrate for binding downstream signalling molecules ensuring conversion of ligand binding into successful signalling event [1]. Structural proteins like f-actin, tubulin and septins oligomerize to form the cytoskeletal organization of cells. Many proteins, like enzymes and ion channels oligomerize to form a functional unit. The composition of hetero-oligomers confers them different properties or functions. The composition of subunits in an ion channel defines its properties, such as gating and conductance [36]. Oligomeric composition of transcription factors regulates its DNA binding specificity and affinity[37,38]. Different oligomer states may also provide different functions to a protein. For example, p53, a transcription factor with multifaceted roles forms various oligomeric forms. The tetrameric p53 are the principal transcription factors, 12-16mers p53 participate in DNA looping and the dimeric p53 functions outside the nucleus [39].

Oligomers are fundamental to biological processes and diseases. It is, therefore, crucial to study how oligomers form and how proteins gain modularity in their functions through oligomeric forms. Single-molecule microscopy can elucidate the oligomeric state of proteins and their correlative function in live cells.

SPT can be used to quantify the stoichiometry of a molecular complex. The main requirements for stoichiometry determination through SPT are 1) all proteins should be fluorescently tagged, and 2) proteins must be tagged at a 1:1 ratio. The oligomer state of a complex can be determined through two methods (Figure 5a). Since each protein is labelled with a fluorescent protein, the brightness of the molecule would represent the complex's oligomer state. The brightness of monomer fluorescent protein is quantified and then used to estimate a complex's oligomer state based on its intensity[40]. Another, more rigorous method to determine stoichiometry is the Stepwise Photobleaching method[26]. On exposure to light, all fluorescent probe loses their ability to fluoresce after some time. This phenomenon is called Photobleaching, which occurs due to light-induced structural changes in the fluorophore, like breakage of bond or reaction of the fluorophore with other molecules. Each fluorescent protein in the complex would photobleach independently. The number of photobleaching steps determines the number of fluorescent proteins in the complex and hence, the number of subunits in the complex.

Stoichiometry quantification is challenging due to the method's prerequisites. As described earlier, fluorophores need to be diluted to be resolvable. For SPT, the amount of QD or Halo/SNAP conjugates is controlled to achieve a single-molecule resolution, which means not all the POI is fluorescently tagged (Figure 5b). Stoichiometry measurement demands complete, full labelling of the POI (Figure 5c). Achieving complete labelling but a sparse labelled protein population for single molecule resolution is not trivial. Protein fusion with fluorescent protein ensures 1:1 labelling of all expressed proteins of interest, and the fusion proteins must be expressed in small quantities for single-molecule resolution. The only available methods that fulfil conditions for full SPT are gene-editing cell lines with the fluorescently tagged POI for endogenous expression[41] and microinjection of a low amount of mRNA or protein

into cells[26]. Generation of gene-edited cell lines is a multi-step and time taking process, while microinjection is skill intensive and low-throughput process. Therefore, it is useful to find an easier alternative to set up the conditions required for full SPT.

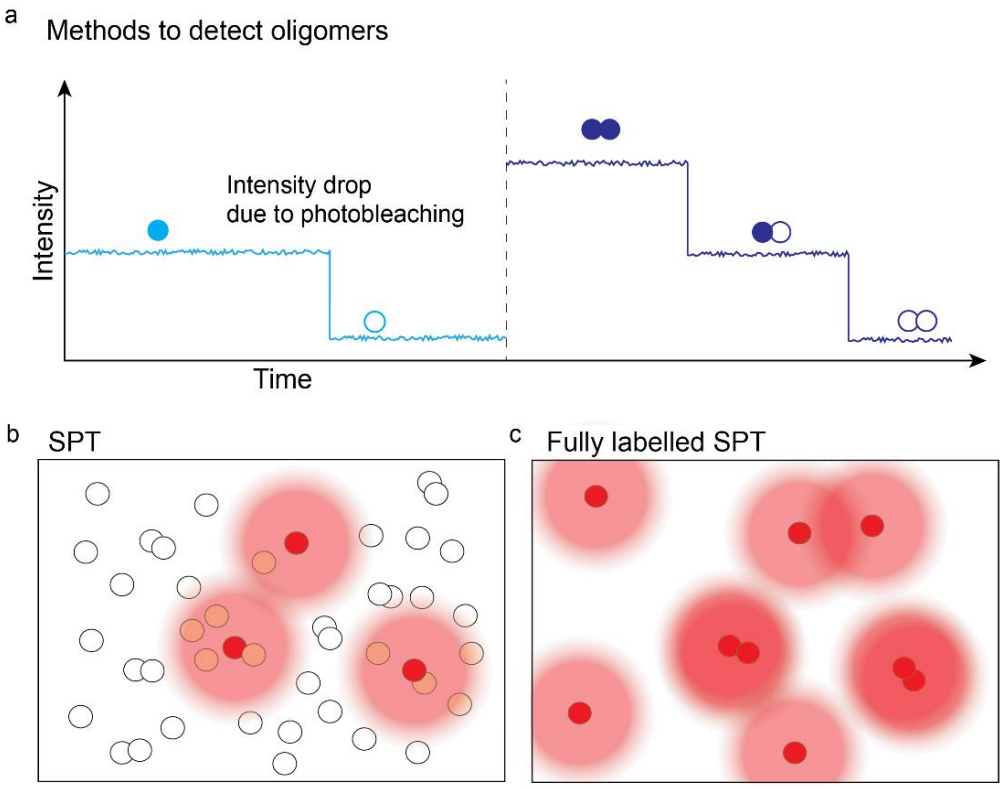

Figure 5: Detecting oligomers. (a) Intensity traces of the single molecules can reveal the oligomer state of the protein through its intensity levels and the number of photobleaching steps it showcases. (b) Partial labelling used in SPT to visualise single molecules hides dimer information in the sample. (c) Low protein levels allow fully labelled SPT that reveals the oligomer states of the protein.

2 OBJECTIVES

As the **first objective** of the thesis, I developed an optogenetic tool to control the number of proteins of interest. It is a more accessible tool to help achieve full labelling of POI with concentrations required for single-molecule microscopy. I used a photocleavable protein to cage molecules of interest away from their site of action. Induction with UV cleaves the photocleavable protein linker and releases the POI in quantities applicable for SPT. Expressing fluorescently tagged POI ensures 1:1 stoichiometry and complete labelling. Caging and releasing a quantified amount of the fusion protein controls the concentration of the proteins at its site of action.

Caging and releasing proteins at a single molecule level also gives the advantages of synchronisation. As the **second objective**, I use this tool to synchronise my POI, Fibroblast Growth Factor (FGF2) and study its unconventional secretion mechanism using SPT methods. FGF2 is a crucial developmental protein. It also plays a role in tumour survival and metastasis. FGF2 undergo an unconventional secretion pathway where the cytosolic FGF2 interacts with the PM components, undergoes modifications and oligomerisation, and gets secreted through the membrane. The model of its secretion is hypothesised based on biochemical experiments. I aim to use single-molecule microscopy to study the mechanism underlying FGF2 secretion and test the current model in live cells.

3 CHAPTER 1: DEVELOPMENT OF A TOOL FOR QUANTITATIVE SPT

3.1 INTRODUCTION

Easy control of protein number is a desirable step which will enable the study of protein oligomers and extend the potential of single-molecule microscopy assays. We propose to control protein transport to control protein number in the target compartment. We take inspiration from caging systems developed to cage POI and control their transport. In these caging systems, membrane proteins destined for the PM are sequestered midway in the Endoplasmic Reticulum (ER) or Golgi apparatus through their interaction with ER/Golgi proteins. The Retention Using Selective Hook (RUSH) system is the most notable caging system, which is based on the biotin-streptavidin affinity[42] (Figure 6a). Streptavidin linked to the Golgi/ER protein binds to the streptavidin binding protein (SBP) linked to the POI, caging the POI. The addition of biotin displaces the streptavidin-SBP bond and releases the POI. Light-based caging systems have also been developed for better spatial control [43,44] (Figure 6b). In this system, the hook and the POI are linked by adding a light-sensitive molecule. Uncaging is mediated by light illumination and subsequent breakage of the

linker. Another light-based caging tool depends on ER retention via aggregation. The POI is fused to UV-B resistance 8 (UVR8), which aggregates and, thus, traps the POI in the ER. Light-based caging systems provide better spatial control of release, but their caging is still affinity-based.

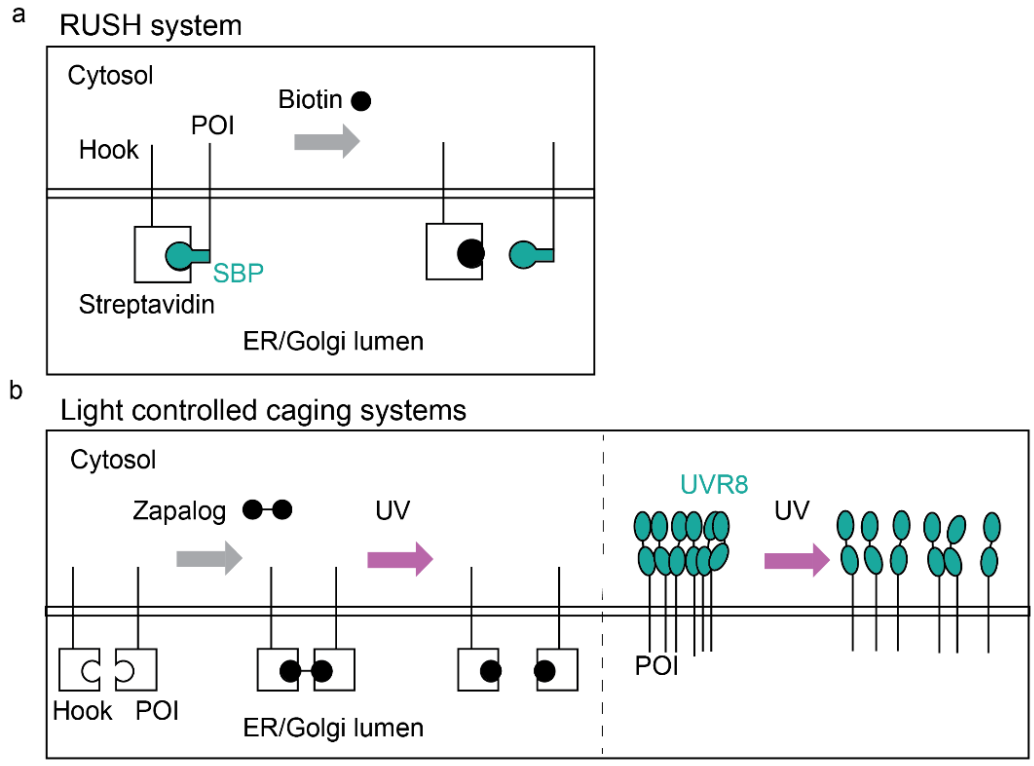

Figure 6: Caging tools. (a) RUSH system. The POI is caged using streptavidin, SBP, and a hook, that is, a Golgi or ER-resident protein. The addition of biotin releases the POI from the hook. (b, left) Light-controlled caging tools. The POI is anchored to a hook, as in the RUSH system, but via a light-sensitive molecule called Zapalog. UV light breaks zapalog and releases the POI. (b, right) POI is caged using UVR8, a homodimer. Due to the size of the oligomerized construct, the POI is caged in the ER. On UV illumination, the oligomer dissociates, and the POI is released.

These caging systems were developed to study protein trafficking and control protein availability in large-scale average-based studies, but they are unsuitable for single-molecule microscopy assays. Caging systems are leaky because they rely on affinity-based systems like streptavidin and biotin interaction in the case of the RUSH system and the zapalog, hook, and POI interaction in the case of the zapalog based caging system. In these caging systems, POI and anchor proteins (ER/Golgi protein) are synthesized separately. The caging of the POI depends on the interaction between the POI and anchor protein. POI that missed to interact with an anchor protein would be transported, rendering the caged state leaky. Leakage and lack of control in lower quantities do not allow for single-molecule microscopy.

We developed a caging tool based on a covalent linker to control the delivery of cytosolic and transmembrane POI in amounts compatible with single-molecule experiments. We used a photocleavable protein to link the anchor protein and POI and constructed a fusion protein of the three constituents. Expressing the anchor, linker, and POI as a single fusion protein ensures no leakage in the caged state. Uncaging is controlled by light, where the amount of light controls the amount of uncaging, and the illumination location within the cell provides spatial control of the release.

For the photocleavable linker in our caging system, we took advantage of a photoconvertible protein, PhoCl[45]. Photoconvertible proteins are fluorescent proteins that change their emission wavelength upon UV illumination. The UV light breaks a peptide bond in the fluorescent protein, which changes the chromophore's structure and shifts the fluorescent protein's emission wavelength (Figure 7a). The chromophore is a chemical group in the fluorescent protein responsible for fluorescence. Usually, the breakage of the peptide bond does not disintegrate the photoconvertible protein because the breakpoint is in the middle of the protein polypeptide chain, and the two halves remain stably folded. PhoCl was developed so that the protein can disintegrate on UV illumination. PhoCl is a circularly permutated version of the photoconvertible protein mMaple that disintegrates upon UV illumination. PhoCl was engineered to have its C-terminus close to the UV-mediated breakpoint (Figure 7b). Upon the

photoconversion of PhoCl, a short peptide is produced that can easily leave the β-barrel structure of the fluorescent protein disintegrating the protein (Figure 7a). The disintegration of PhoCl upon UV illumination makes it an excellent tool for caging proteins[45].

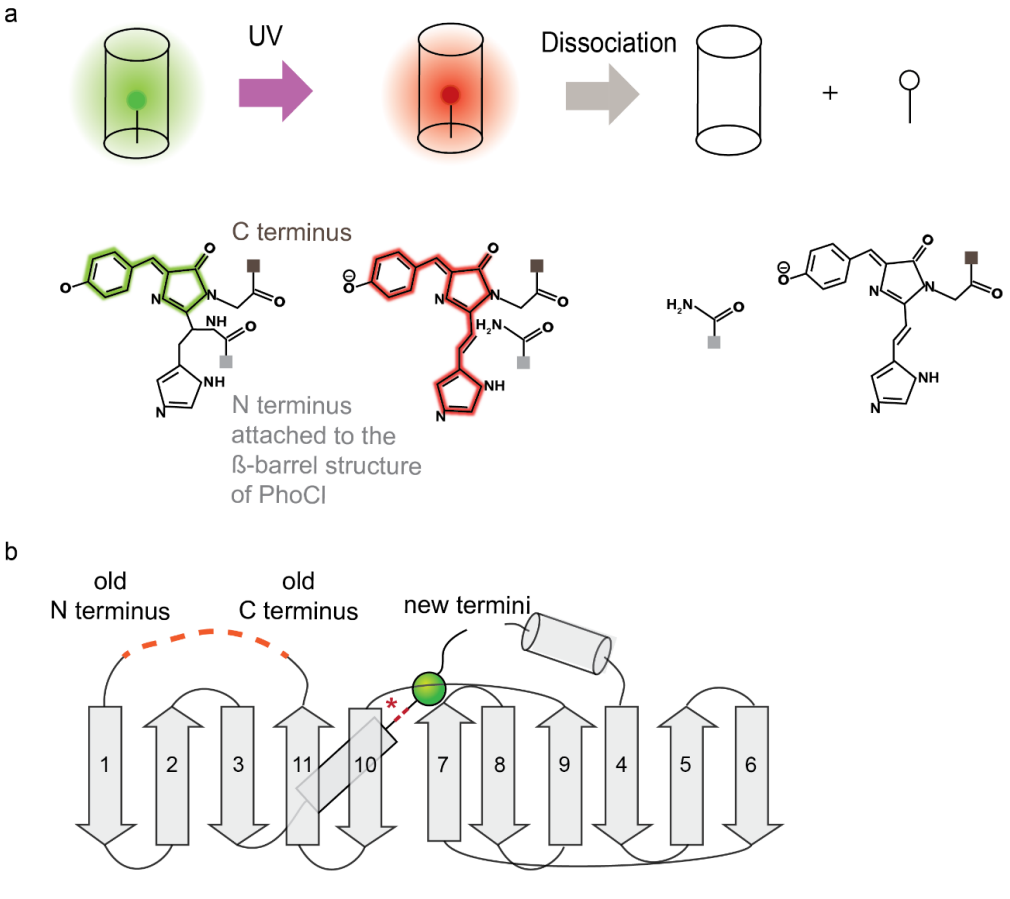

Figure 7: Structure of PhoCl. (a) Photoconversion and dissociation of PhoCl under UV light. UV light-mediated breakage of the peptide bond and the corresponding change in the structure of the chromophore. (b) Structural changes made on mMaple to generate PhoCl. The old N and C termini are joined (dashed line) and new N and C termini is created near the chromophore (green sphere). UV Illumination cleaves peptide bond near the chromophore (red star) and generates a small peptide.

The aim of chapter 1 is the establishment of a PhoCl-based caging tool to control the delivery of cytosolic and transmembrane proteins (schematically represented in Figure 8). The second aim of this chapter is to test PhoCl-based caging of large and multimeric transmembrane proteins like ion channels.

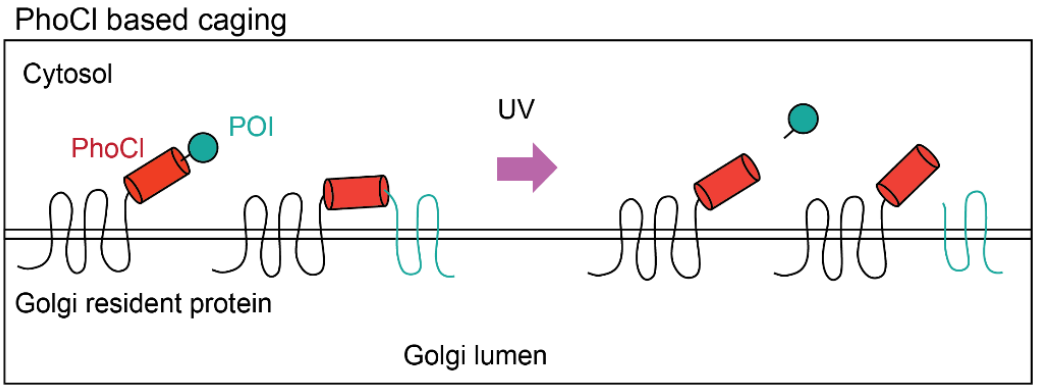

Figure 8: Schematic of PhoCl based caging tool. The POI is caged to a Golgi resident protein via PhoCl. The UV light breaks PhoCl, and the POI is released.

3.2 RESULTS

A PhoCl-based caging tool that sequesters the POI at the Golgi was designed. Sequestration at the ER or Golgi is attractive because membrane proteins can be caged mid-trafficking on their way to their destination membrane. Sequestration at the Golgi is particularly attractive because Golgi is a smaller organelle than the ER network, and hence, caged proteins can be concentrated and efficiently uncaged with UV light pulses.

First, I caged the cytosolic protein, Fibroblast Growth Factor 2 (FGF2-GFP), using PhoCl at the Golgi. FGF2 is a cytosolic protein that binds to the PM. I constructed a fusion protein composed of FGF2-GFP, PhoCl, and a Golgi-resident protein, Transmembrane protein 115 (TMEM115) (Figure 9a). Since FGF2 is a cytosolic protein, the caging construct should be designed to release the FGF2-GFP molecules in the cytosol. TMEM115, a Golgi resident protein with a C-terminus in the cytosol, was hence chosen as the Golgi hook.

Under UV illumination, PhoCl breaks, and FGF2-GFP is released into the cytosol and binds to the PM. I could show that caged FGF2-GFP was visible in the Golgi apparatus (Figure 9b). Under UV illumination, PhoCl undergoes photoconversion before disintegration. Photoconverted PhoCl was shortly visible in the 561 nm/red channel after UV illumination (Figure 9b bottom). After UV illumination-induced PhoCl cleavage, FGF2-GFP could be detected in the cytosol (Figures 9b and d). TIRF microscopy revealed the presence of PM-bound FGF2-GFP after release (Figure 9c,e).

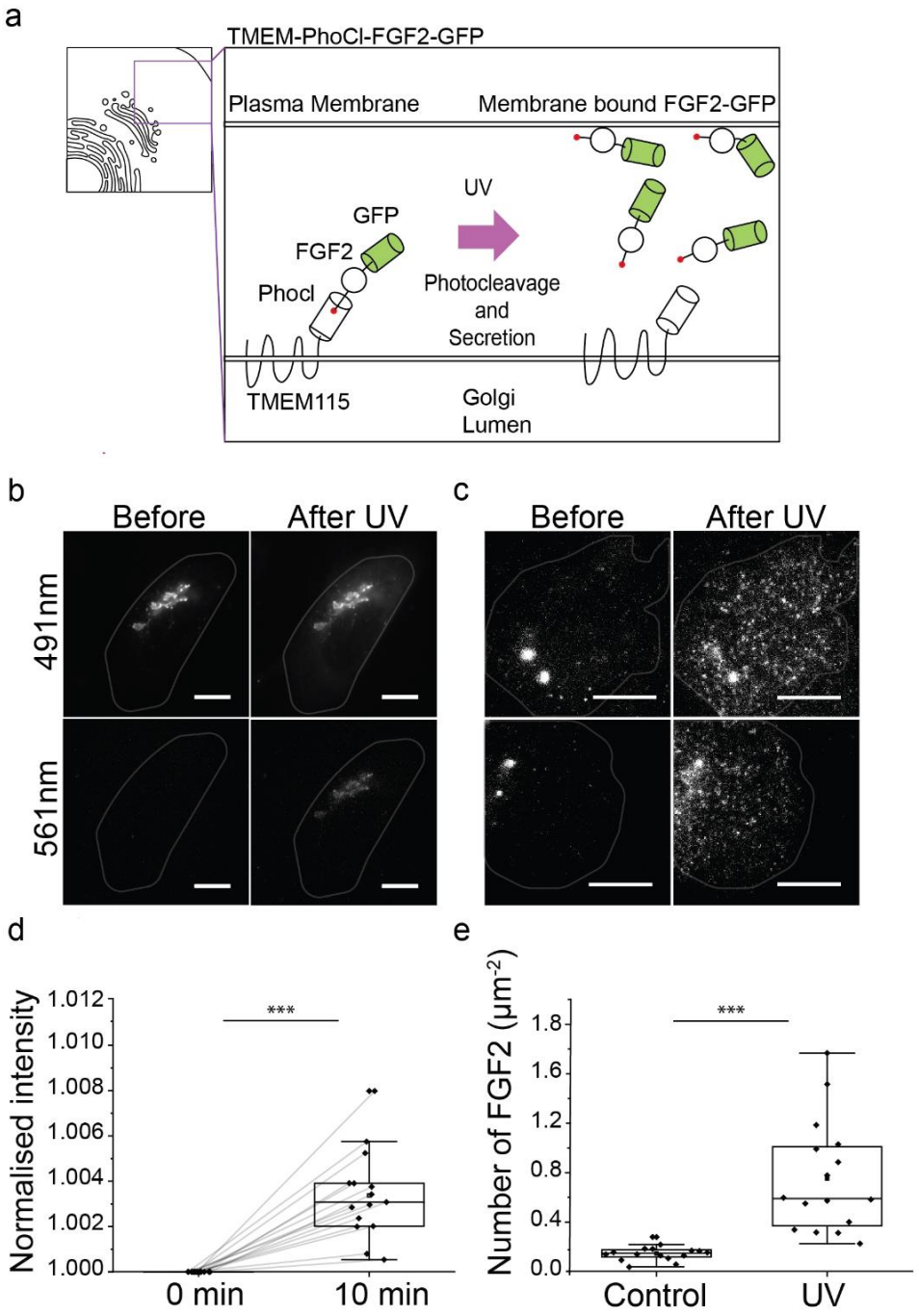

Figure 9: Caging of the cytosolic protein, FGF2. (a) Schematic representation of the fusion protein TMEM115-PhoCl-FGF2-GFP and its uncaging with UV light. (b) CHO-K1 cells expressing TMEM115-PhoCl-FGF2-GFP were observed in 491 nm and 561 nm channels using the confocal microscope. Golgi localisation of TMEM115-PhoCl-FGF2-GFP is observed in 491 nm/green channel

(top panel). Photoconverted PhoCl was visible after illumination with UV light in the 561 nm/red channel (bottom panel). (c) TIRF microscopy of the CHO-K1 cells expressing TMEM115-PhoCl-FGF2-GFP. (d) Quantification of the FGF2-GFP in the cytosol 0 min and 10 mins after activation in the same cell. Significance was tested using the paired Wilcoxon rank-sum test ($p < 0.001$) ($N_{replicate}= 1$, $N_{cells}= 15$ cells); (e) Quantification of the number of FGF2-GFP molecules observed at the PM using TIRF microscopy before (mean, sd = 0.14 ± 0.05) and after UV illumination (mean, sd = 0.75 ± 0.4) ($N_{replicate}= 2$, $N_{cells}= 16$ cells). Statistical significance was tested using the paired Wilcoxon rank-sum test ($p < 0.001$). All scale bars are 10 μm. Data for plot (e) was acquired by master student Adolf Bierhuizen as part of an internship.

Caging of cytosolic protein via PhoCl into the Golgi apparatus was accomplished relatively easily. Next, I aimed to control membrane protein delivery by Phocl. Caging membrane proteins with a Golgi resident protein is not straightforward because the membrane POI and Golgi resident anchor proteins have different cues that regulate their respective localization. Therefore, it is essential to test whether Golgi-resident proteins can retain the PM proteins. I caged the single-pass transmembrane protein, Cluster of Differentiation-4 (CD4), using PhoCl. I constructed a fusion protein consisting of mScarlet, CD4, PhoCl, and Sialyl transferase (ST), Golgi-resident proteins (Figure 10a). Under UV illumination, PhoCl should break and mScarlet- CD4 should be trafficked to the PM (Figure 10a right). Unfortunately, I detect mScarlet CD4 already on the PM before UV illumination (Figure 10b). It seems that ST is not a good Golgi anchor for the purpose, and the full fusion protein, mScarlet-CD4-PhoCl-ST, gets trafficked to the PM.

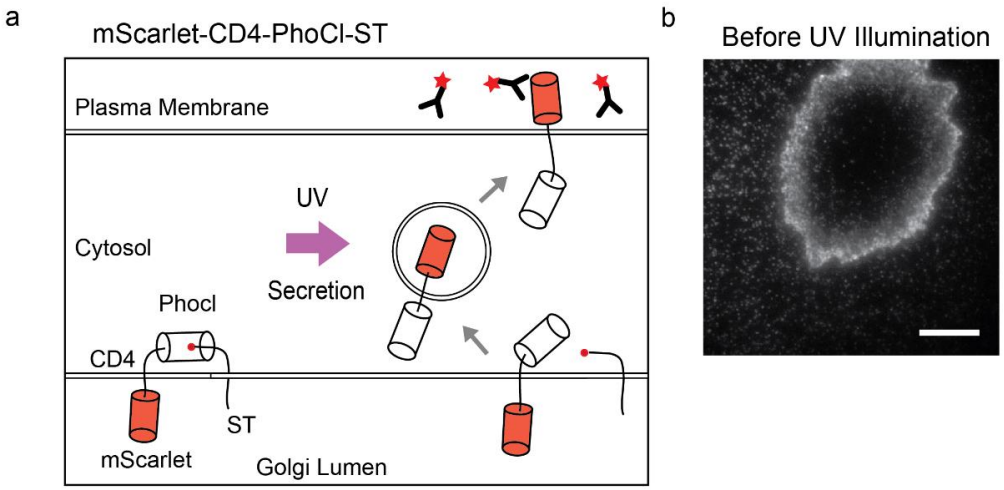

Figure 10: Caging of the transmembrane protein CD4 mScarlet using ST. (a) Schematic representation of the fusion protein mScarlet-CD4-PhoCl-ST and its uncaging with UV light. Antibodies against mScarlet is used in the extracellular media to detect the PM localised CD4. (b) TIRF microscopy of CV1 cells expressing mScarlet-CD4-PhoCl-ST shows PM localised CD4 before UV illumination. The Scale bars is 10 μm.

Next, I used a different Golgi resident protein as an anchor, Retention in Endoplasmic Reticulum Retrieval sorting receptor-1 (RER). I constructed a fusion protein consisting of Scarlet, CD4, PhoCl, and RER, Golgi-resident proteins (Figure 11a). Under UV illumination, PhoCl breaks and mScarlet-CD4 can be trafficked to the PM (Figure 11a,c). I detected Golgi localisation of the caged mScarlet-CD4 (Figure 7b). Like before, I planned to use an antibody against mScarlet in the media to detect; specifically, the PM inserted mScarlet-CD4 (Figure 11c). I detect negligible amounts of PM localised mScarlet-CD4 before UV illumination but a high number three hours after UV illumination, indicating successful caging and uncaging of the transmembrane protein (Figure 11d,e,f). I expected surface delivery of mScarlet-CD4 to take longer than that for FGF2-GFP as mScarlet-CD4 is delivered to the PM via the vesicular trafficking, and hence, the relatively late 3 hrs timepoint after uncaging was chosen to ensure a significant number of molecules has arrived at the PM.

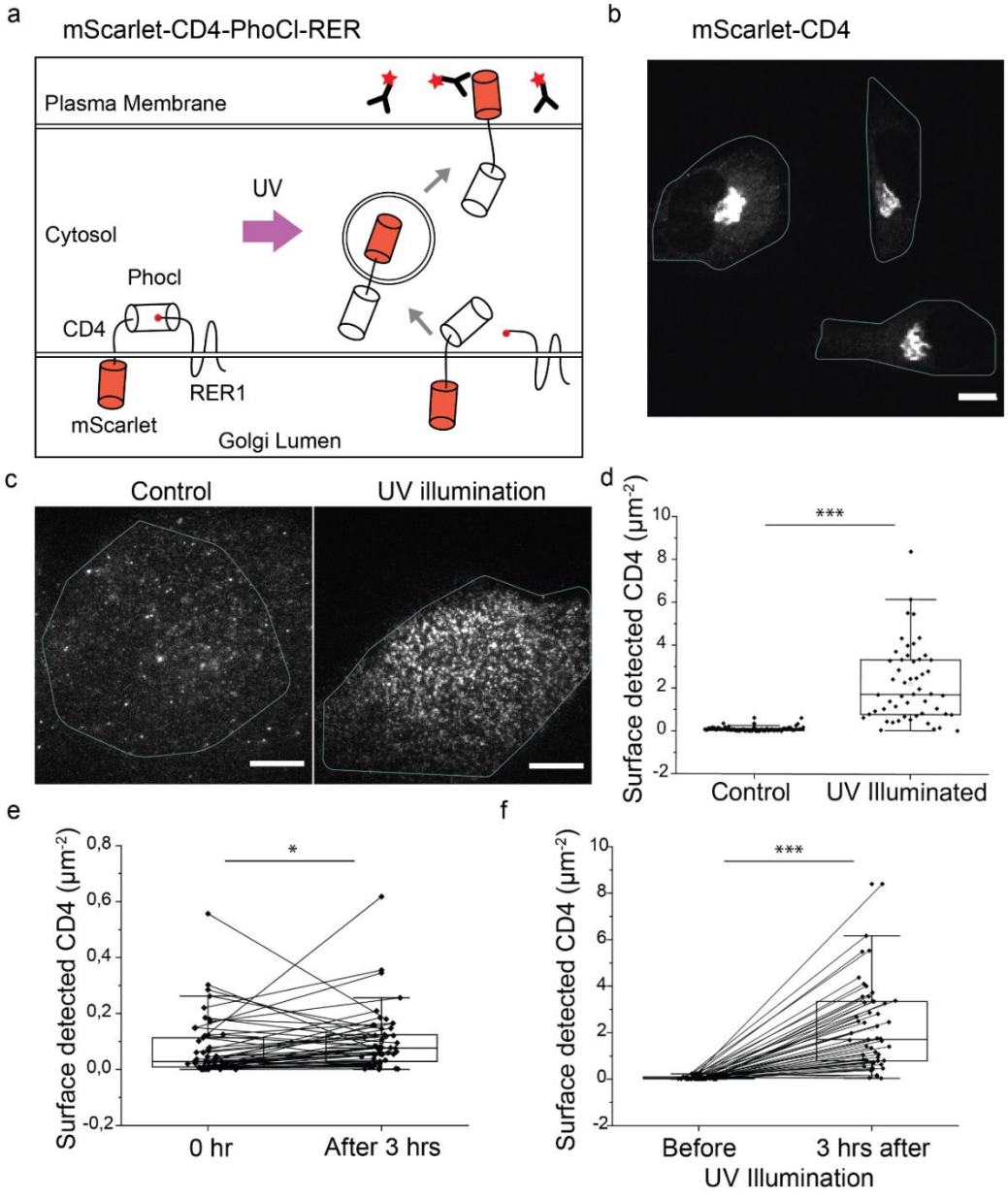

Figure 11: Caging transmembrane protein mScarlet-CD4 using RER. (a) Schematic representation of the fusion protein mScarlet-CD4-PhoCl-RER and its uncaging with UV light. PM localised mScarlet-CD4 is detected using extracellular antibodies against mScarlet. (b) Confocal microscopy of CV1 cells expressing mScarlet-CD4-PhoCl-RER shows its localisation at the Golgi. (c) TIRF microscopy of the same cell with antibodies against mScarlet before and 3 hrs after UV irradiation. (d) Quantification of the number of anti-mScarlet antibodies in the non-illuminated (control) (mean, sd = 0.09 ± 0.1) and UV illuminated cells (mean, sd = 2.2 ± 1.7). Significance tested with unpaired Wilcoxon rank-sum test ($p < 0.001$). (e) Quantification of the number of anti-mScarlet antibodies in control cells at 0 hr (mean, sd = 0.07 ± 0.1) and after 3 hrs (mean, sd = 0.09 ± 0.1). Significance was tested using the paired

Wilcoxon rank-sum test ($p < 0.05$). (f) Quantification of the number of anti-mScarlet antibodies before (mean, sd = 0.06 ± 0.07) and 3 hrs after UV illumination (mean, sd = 2.16 ± 1.7) in the same cells. Significance was tested using the paired Wilcoxon rank-sum test ($p < 0.001$). All scale bars are 10 μm. Plots d,e, and f were made from the same datasets ($N_{replicates}$=11, N_{cells}= ~50 cells for control and activation each). Data was acquired by bachelor student Fenja Blank as part of her bachelor thesis.

Next, I tested whether larger and more complex membrane proteins, such as ion channels, could be caged using the PhoCl-based caging system. Ion channels are large multi-pass transmembrane proteins that span the membrane multiple times. The sequence and length of membrane proteins' transmembrane domains (TMD) play crucial roles in determining their localization. PM-localized membrane proteins tend to have longer TMDs suitable for thicker lipid bilayer of the PM. Therefore, caging a multi-pass membrane protein with multiple TMDs in the Golgi Apparatus via PhoCl might be challenging. Furthermore, most ion channels are oligomeric proteins. It must be verified whether oligomeric and large proteins such as ion channels can be folded and assembled properly under caged conditions. Uncaging of homomers might be specifically challenging since each subunit of the homomer needs to be released for the successful trafficking of the complete functional complex. Finally, ion channels can be tested for functional integrity using electrophysiology methods. Such a test would confirm that fusion with PhoCl and Golgi-resident proteins does not hamper the biological function of the caged POI. Therefore, I tested my PhoCl-based caging tool on the retention of an ion channel next.

I used Big potassium (BK), a calcium-sensitive potassium channel. BK forms a homomer of four identical subunits. Like previous constructs, I designed a fusion protein with BK, PhoCl and TMEM115, the Golgi hook (Figure 12a). Only after all the four PhoCl connected to the four BK channel subunits are cleaved can the ion channel be successfully trafficked to the PM. After UV Illumination, I detected PM localised BK ion channels in TIRF microscopy (Figure 12b-d). PM localised BK ion channels were detected seven hours after UV illumination. We collaborated with Dr. Sara Bertelli and Dr. Andrew Plested from Humboldt University, Berlin, for electrophysiology measurement. Electrophysiology measurements show a drastic

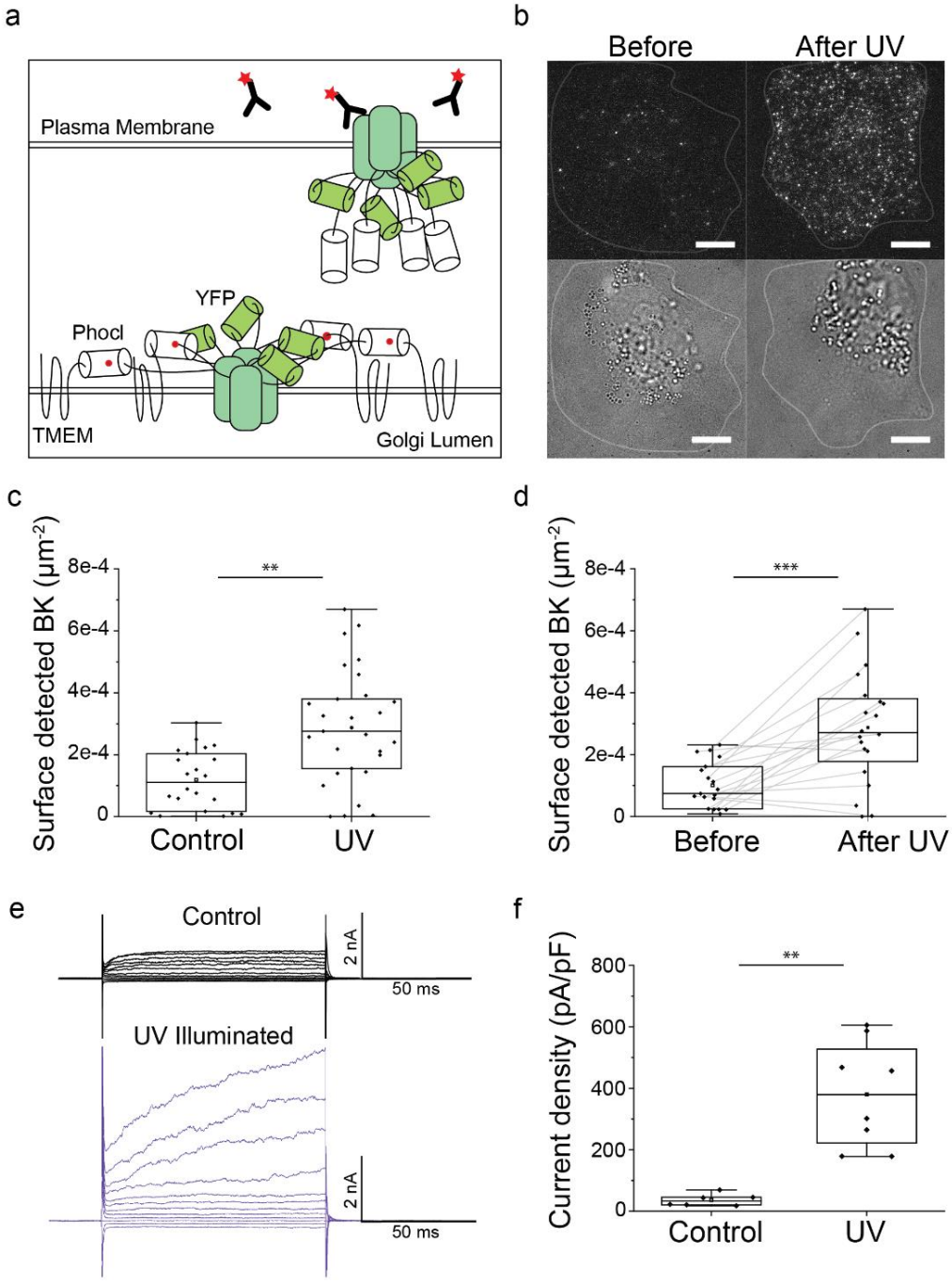

Figure 12: Optogenetic release of BK ion channel. (a) Schematic of FLAG-BK-YFP-PhoCl-TMEM construct. Uncaged and secreted BK is detected using antibodies in the media. (b) TIRF and brightfield images of a cell with antibodies against FLAG before and after UV illumination. (c) Quantification of the number of anti-FLAG antibodies bound to the control (mean, sd = 1.1e-4 ± 9e-5) and UV irradiated cells (mean, sd = 2.8e-4 ± 1e-4). Significance tested with unpaired Wilcoxon rank-sum test ($p < 0.01$).

($N_{replicates}$= 5, N_{cells}= 22 (control), 29 (activated)) (d) Quantification of the number of anti-FLAG antibodies bound to the same cells before (mean, sd = 1e-4 ± 7e-5) and 7 hrs after uncaging (mean, sd = 2.8e-4 ± 1e-4). Significance was tested using the paired Wilcoxon rank-sum test ($p < 0.001$). ($N_{replicates}$= 5, N_{cells}= 20) (e) Representative current traces of BK channel at voltages -20 to 180 mV in control and UV irradiated cells. (f) Quantification of current density at 120 mV in control (mean, sd = 36 ± 20) and UV irradiated cell (mean, sd = 380 ± 172). Significance was tested using the unpaired Wilcoxon rank-sum test ($P <0.01$). ($N_{replicates}$= 3, N_{cells}= 6 (control), 8 (activated)). The scale bar is 10 μm. Electrophysiology data (e and f) was generated in collaboration with Dr. Sara Bertelli and Prof. Andrew Plested.

increase in the characteristic BK currents in the uncaged cells compared to the control cells (Figure 12e,f). Initial experiments with the 3 hr timepoint after uncaging did not show many PMs localised BK channel, and therefore, the 7 hrs timepoint after uncaging was chosen for the experiments.

3.3 DISCUSSION

I here developed a caging system that was compatible with single-molecule microscopy experiments. It is a tool used to control protein levels on a short timescale. Owing to the covalent nature of the caging process, the PhoCl-based caging system provides tight control over the POI, with negligible leakage in the caged state. One can also cage cytosolic POI using this method, which has been impossible until now. I successfully caged the transmembrane protein CD4 at the Golgi and detected them after uncaging with UV light. I also used PhoCl to control the secretion of multi-subunit and larger-sized ion channels and showed that the ion channel's functionality remains intact despite its fusion with PhoCl and a Golgi protein.

3.3.1 Why is PhoCl a better system?

PhoCl, as a caging tool, has a significant advantage over other caging methods. The PhoCl-based caging tool is designed similarly to the popular RUSH system. A POI is tethered to a Golgi resident protein via a linker in both systems. In the RUSH system, the non-covalent streptavidin-biotin interaction between the Golgi resident protein and the POI results in the latter's caging. In such a system, the POI and the Golgi protein hook are synthesized separately, and the POI can be tethered only on encountering the Golgi protein hook. Separate synthesis leads to leakage of untethered POI, and leakage of the POI does not allow for quantitative single-molecule experiments. By contrast, in the PhoCl-based caging system, the linker, i.e., PhoCl, is genetically fused to the POI and the Golgi resident protein, which means the POI is tethered as soon as it is synthesized, eliminating leakage due to untethered protein. Therefore, PhoCl based caging tool provides greater control in the delivery of the POI in the low quantity regime required for single molecule experiments.

My PhoCl-based caging tool also helps control cytosolic proteins of interest. Due to the non-covalent nature of available caging tools, it's so far been nearly impossible to cage cytosolic proteins. Due to the limited dimensions and space of the ER/Golgi membrane and lumen, tethering of transmembrane or secretory proteins is possible through the available caging tools. Cytosolic proteins, on the other hand, cannot be caged via chance interaction with a Golgi hook. Expressing the cytosolic protein as a fusion protein with PhoCl and a Golgi protein allows tethering and control of cytosolic proteins.

3.3.2 Retention via Golgi proteins

There are two aspects of successful caging using PhoCl: good retention and good PhoCl breakage when induced at 405 nm. I tested multiple Golgi resident proteins that serve as anchors, such as ST, TMEM115 and RER-1. TMEM115 and RER1 had better retention capacities, possibly because of a more efficient retention signal. Compared to the single-pass membrane protein ST, TMEM115 has four transmembrane domains (TMD), and RER1 has three TMDs. The TMD of Golgi proteins plays a vital role in

their retention [46]. Lipid composition of the membrane changes across the secretory pathway[47]. The lipid composition determines the membrane's thickness. Proteins with a suitable TMD length and amino acid composition partition into the right organelle due to the membrane characteristics of the organelle[48–50]. Retention of Golgi proteins are highly regulated by their TMDs. Golgi-resident proteins tend to have short TMD to match the Golgi membrane [51,52]. In addition, many Golgi proteins are known to oligomerize through their TMD and form larger protein aggregates that are difficult to transport out of the Golgi[53–58]. If the TMD plays such a vital role in protein localisation, it is expected that in a fusion construct comprising a Golgi protein and a PM protein, there will be a driving force for localisation towards both organelles. Therefore, when CD4, a single-pass PM protein, was fused to single pass Golgi protein like ST, retention at Golgi would likely be difficult (Figure 10), and this could explain why fusion with the multi-pass Golgi protein RER significantly improved retention (Figure 11).

Retention via RER or TMEM, however, is not perfect either. Quantification of secreted CD4 at the PM at 0- and 3-hr time points in non-illuminated samples revealed a slight increase in the secreted of mScarlet-CD4 (Figure 11e). Electrophysiology, a method more sensitive than microscopy, also detected minimal BK currents in control cells without UV illumination (Figure 12e). Golgi retention of proteins involves a variety of mechanisms for retention, which include TMD matching to the membrane, oligomerisation, and sorting by adaptor proteins in a signal-mediated manner[59]. Overexpression of the PhoCl-caged POI might overwhelm the retention mechanisms leading to some leakage. This hypothesis needs to be investigated, and the PhoCl-based caging tool could be further improved using either low-expression vectors or a different Golgi resident protein for a hook in the future for an absolute zero leakage in the caged state. Nonetheless, the leaked amount of molecules is very low and does not hamper the tool's application for quantitative SPT.

This study characterises two Golgi resident proteins, RER and TMEM115, as candidate anchors, providing flexibility for designing the caged constructs. TMEM115 has both termini in the cytosol, while RER1 has a cytosolic N-terminus and a luminal C-terminus. Thus, proteins can be caged at the cytosol and the Golgi lumen depending

on the requirement of the POI. Some POIs may only allow fusion with one terminus to preserve function. POI can be caged through either terminus in the cytosol via TMEM and RER. However, proteins with their termini in the lumen can only be caged at their N-terminus using RER. If the POI is only accessible through its C-terminus and the C-terminus lies in the lumen, we do not have a viable Golgi anchor. Therefore, we should search for candidate Golgi anchors with N-terminus in the lumen in the future.

3.3.3 Uncaging with UV light

The second part of successful caging is the efficient breaking of PhoCl under 405 nm illumination. For the first few experiments with the caged FGF2-GFP, the original PhoCl[45] was used as the caging tool. As FGF2 is a cytosolic protein, the release of FGF2 into the cytosol after uncaging is straightforward. For the experiments with FGF2, the released quantities were sufficient. However, when I tried to use PhoCl to cage the transmembrane protein CD4, I could not detect much CD4 in the PM after uncaging. This might be due to PhoCl's low rate of cleavage and dissociation. PhoCl was shown to have a dissociation percentage of ~70% *in vitro*[60]. This rate must be drastically reduced in cells. I then used the modified PhoCl 2c with better cleavage efficiency (~92%) to cage CD4 and BK to successfully detect the uncaged transmembrane proteins. In the future, efforts to increase the PhoCl cleavage rate in mammalian cells must be made to control a more extensive range of POI concentrations through uncaging.

3.3.4 Applications

The aim of the PhoCl-based caging system is to enable the short-term control of the number of proteins present at its site of action. PhoCl is useful for multiple applications such as quantitative SPT, as a caging tool to observe the effects of a

molecule on a phenomenon and as a tool to estimate the number of proteins required to perform a function.

3.3.4.1 Quantitative SPT

The PhoCl-based caging system can facilitate single-molecule studies of oligomeric proteins. Proteins that function as an oligomeric complex are difficult to observe in their complete state in living cells using SPT due to the conditions required for single molecule observation. Usually, SPT is performed through partial labelling of the POI, which occludes information. Control of the number of proteins via PhoCl would help to achieve single molecule resolution where all the POI at the site of action is labelled. We believe combining PhoCl-based caging with SPT can open new opportunities to understand biological processes that involve oligomers. One can follow a protein's interaction with self or other proteins over the course of time or as a response to stimuli. One can then understand how these actions turn into functions, e.g., cell signalling at the molecular level.

3.3.4.2 Stoichiometry determination

Another exciting application of PhoCl is the study of the stoichiometry of ion channels and their resulting function. Many ion channels are homo/hetero-oligomeric complexes. In the case of the heteromeric ion channels, the subunits associate in a combinatorial fashion and regulate the ion channel's conductivity and opening kinetics[36]. With PhoCl-controlled expression, setting up conditions for stoichiometry measurements of ion channels will be easier. Stepwise photobleaching is a method for determining the stoichiometry of a protein complex. However, having a low number of fully labelled protein complexes is a prerequisite for this method. Researchers perform RNA microinjections where they control the amount of RNA to produce a low number of fully labelled ion channels. Transfection of the PhoCl-caged labelled POI is a more straightforward technique to fulfil this requirement of stepwise photobleaching.

Stoichiometry study of oligomers required that each subunit of the oligomer is fluorescent. Keeping the fluorescent tags for each subunit intact might be challenging when using a high-power 405 nm laser to uncage the POI. This limitation can be, however, easily overcome if Halo/Snap tags are used instead of fluorescent proteins to label the POI. Halo/snap tags are enzymes that react with externally added fluorescently labelled substrates yielding covalently bound fluorophores. Labelling the POI via Halo/Snap substrates after the uncaging step would avoid the photobleaching that may occur due to the UV illumination. Alternatively, it might be possible to uncage PhoCl fused POI with a higher wavelength of ~800nm with two-photon microscopy to avoid UV-mediated photobleaching[61].

3.3.4.3 The quantitative study of biological reactions

PhoCl-based caging could also be used to determine the number of proteins required for a specific function. Functional studies of POI are generally performed through transient transfection under strong promoters, such as the Cytomegalovirus (CMV) promoter, which is far from the endogenous levels of protein expression. Using the PhoCl caging tool, one can systematically identify the number of proteins required for a process, e.g., the number of effector proteins or transfection factors required for a successful signal transduction or gene expression, respectively. The system could also be used to understand how the outcome changes with the change in upstream protein concentration. For example, if steps in a biological process behave like a switch or depend linearly on the concentration of the POI. Such information will be crucial in modelling biological processes in cells and understanding the rules governing biological processes.

3.3.4.4 Caging tool

Finally, PhoCl could be used as a caging tool to understand the role of POI. Transfection-based functional studies of proteins are susceptible to huge variabilities. This is because the cells are not transfected with the same number of plasmids. A large

dataset is required to deal with this variability, especially when the effect of the POI is small. PhoCl-based control provides an opportunity in which, in the same cell, the effect of the POI can be verified before and after its uncaging, providing stronger evidence with lesser effort.

Tight control over the availability of POI can open many opportunities to study the mechanism of the protein's functions at the single-molecule level. Some of these possibilities will be showcased in the coming chapters of the thesis, where PhoCl-based caging has been applied to understand the mechanism of FGF2's unconventional secretion

4 CHAPTER 2: INVESTIGATION OF FGF2 SECRETION USING SINGLE MOLECULE LIVE CELL MICROSCOPY

4.1 INTRODUCTION

Fibroblast Growth Factor 2, or FGF2, is a crucial protein in multiple cell fate decisions. It binds to its receptor and initiates signalling cascades [62] like RAS MAP kinase pathways, PI3K AKT, PLC-y and STAT[63], ultimately resulting in cell growth, cell division, differentiation, and cell migration. The diversity of FGF2's functions stems from its interaction with multiple FGF receptors, their splice variants[64,65] and other regulatory mechanisms[66]. FGF2 is pivotal in development, wound healing, and cancer progression [67–69]. Its role in angiogenesis, a process that involves the breakdown of the ECM, cell migration and formation of new blood vessels from pre-existing ones [68,70–74], makes it crucial for wound healing. Cancerous cells also induce angiogenesis to survive the suffocating tumorous environment for metastasis[75]. Hence, FGF2 has been a critical oncogene to study for targeting cancer[76,77].

FGF2's unique route of secretion adds to its complexity. Unlike most extracellular proteins, FGF2 skips the conventional secretory pathway. It is one of the first proteins known to lack a signal peptide (SP) in its sequence, a compulsory component of most secretory proteins[78].

4.1.1 Conventional secretory pathway

The SP is a sequence stretch at the N-terminus of a protein that is destined for secretion, the PM, or other organelles. Interaction of the signal peptide with the Signal Recognition Particle (SRP) and, finally, the SRP receptor on the ER directs the synthesizing ribosome toward the ER (Figure 13a). After the ribosome is docked at the ER, the nascent polypeptide chain moves into the ER lumen with the help of Sec61 translocon. A secretory protein is entirely imported into the ER lumen, while transmembrane proteins remain within the ER membrane by their hydrophobic stretches. After multiple checkpoints of proper folding at the ER and modifications at the Golgi, these proteins are packaged into vesicles and carried to the PM (Figure 13b). When vesicles reach the PM, they fuse and release their contents into the extracellular space. Transmembrane proteins are also delivered to the PM with this process.

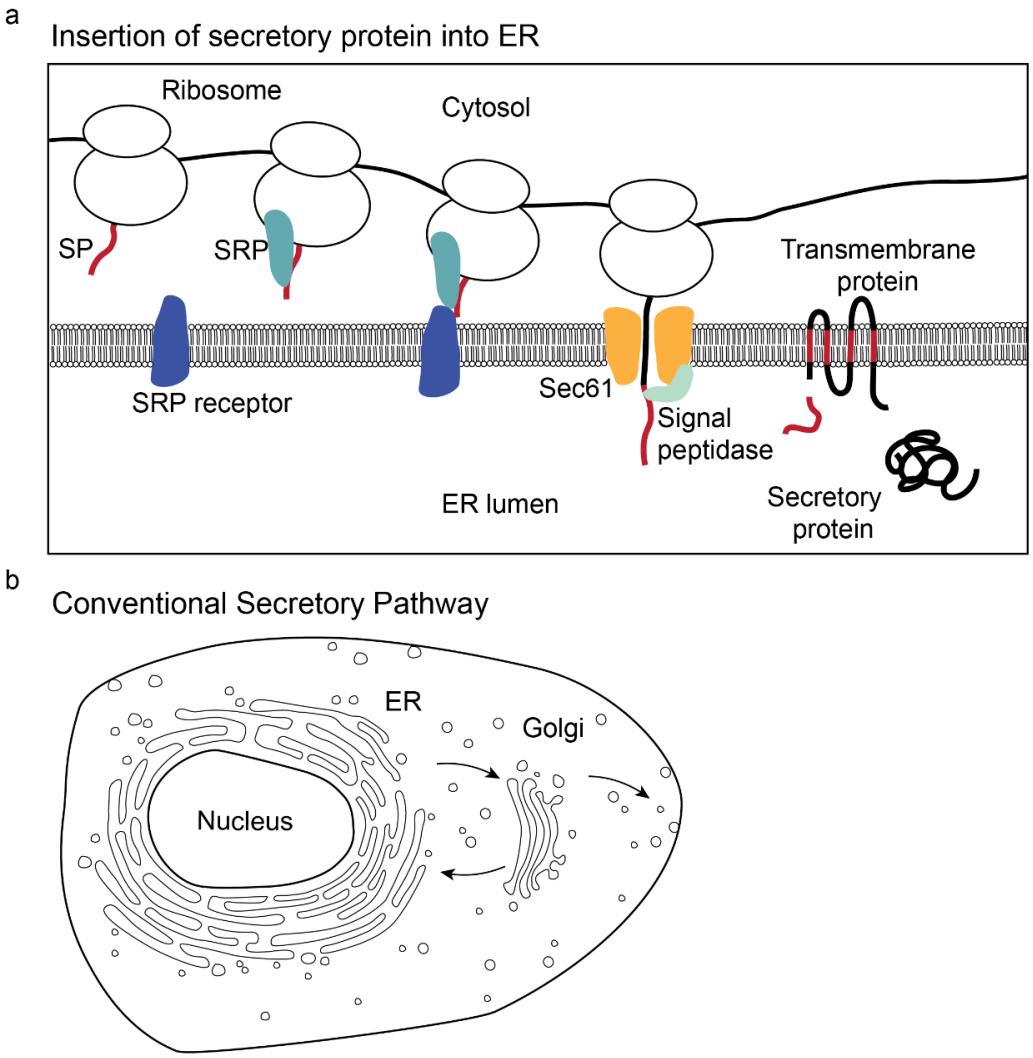

Figure 13: The conventional secretion pathway. (a) Insertion of actively translating peptide into the ER lumen with the help of SP, SRP, SRP receptor, and Sec61 translocation. After insertion, the signal peptide was cleaved by a signal peptidase. The presence of additional hydrophobic stretches (shown in red) in the peptide anchors transmembrane proteins in the membrane. (b) Proteins are transported to the Golgi apparatus. Vesicles carrying secretory proteins fuse to the PM and release secretory proteins from the cell.

This method of protein secretion through the ER and Golgi is predominant and the most well-known. Possession of the SP seems like a prerequisite to undergoing secretion. However, some extracellularly located proteins lack the SP and are secreted via alternative routes. Examples include FGF2, β-galactoside-specific lectins 1 and 3[79–

[81], interleukin1β[82], acyl-coenzyme A-binding protein (AcbA)[83], HMGB1[84–86], thioredoxin [87,88] and engrailed homeoprotein[89–92]. The unconventionally secreted proteins are classified into four groups[93]. Type I, direct protein translocation through lipid pore; Type II, secretion of lipidated protein via specific ABC transporters; Type III, autophagy-based secretion and Type IV, membrane proteins that bypass the Golgi and are directly trafficked from the ER to the PM. FGF2 belongs to the Type I class of unconventionally secreted proteins.

It is hypothesized that the multifunctionality of a protein might be a reason behind the adoption of the unconventional secretion pathway. Proteins that undergo conventional secretion must be unfolded to pass through the ER membrane and enter the ER lumen. If a secretory protein has an additional function as a cytosolic or nuclear protein, it must be folded in the cytosol and the nucleus. Folded state of the protein required in the cytosol makes it difficult for them to enter the conventional secretory pathway. Many unconventionally secreted proteins are known to have dual functionality. These examples include FGF2, Thioredoxin and High mobility group box-1 (HMGB-1). In addition to the primary function of FGF2 in receptor-mediated cell signaling[94], FGF2 can also regulate transcription in a receptor-independent manner[95]. Thioredoxin is a cytosolic protein involved in redox balance[96]. Oxidative stress induces its secretion[97], where it acts as cytokine[98–104]. And HMGB-1 is a nuclear protein involved in nuclear organization and gene expression [105,106]. Inflammatory response to bacterial LPS triggers its secretion to the extracellular space[107], where it acts as a cytokine[108–112].

4.1.2 FGF2's unconventional secretion

FGF2 is one of the earliest known examples of unconventionally secreted proteins. Decades of research on the secretion pathway of FGF2 have brought a model of its secretion to life (Figure 14). FGF2 interacts with the PM by binding to phosphatidylinositol 4,5 bisphosphate ($PI_{(4,5)}P_2$), the α1 subunit of the membrane

protein Na, K-ATPase and the membrane-bound Tec kinase. After binding to the PM, FGF2 oligomerizes and inserts into the PM (Figure 14). Heparan sulphate proteoglycans bind FGF2 from the membrane's extracellular face and potentially pull it out of the membrane.

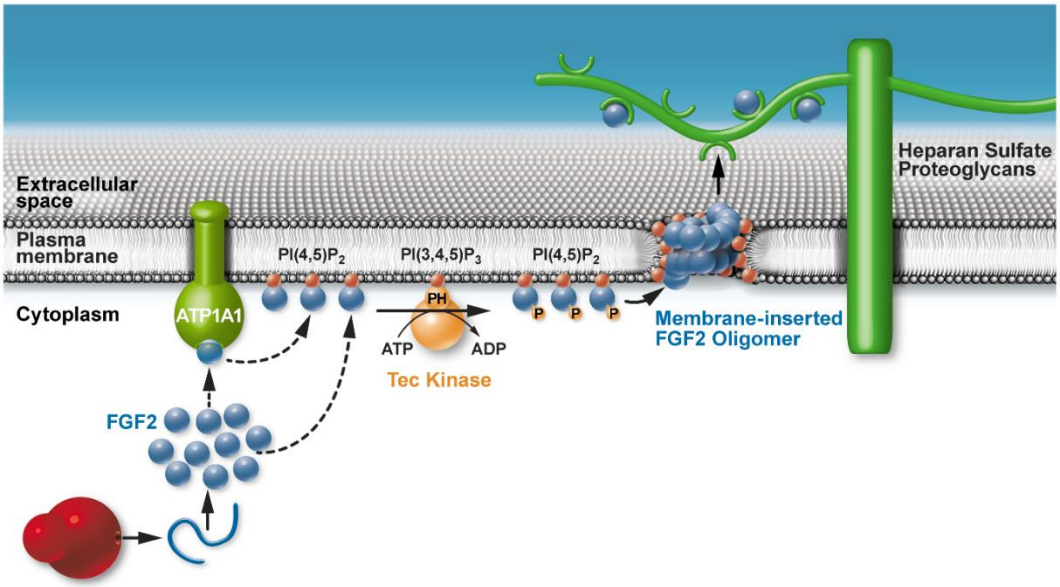

Figure 14: Model of the unconventional secretion pathway of FGF2.[113] From Brough et al. 2017 with permission.

Several facts establish that FGF2 skips the conventional route of ER-Golgi-mediated secretion. It lacks a signal peptide[114,115] and is absent from the ER and Golgi [114–119]. Microscopy images of cells expressing FGF2-GFP show its presence primarily in the cytosol and the nucleus[119]. FGF2 does not show post-translational modifications like glycosylation, typical of proteins passing through the Golgi[114,115]. In fact, FGF2 is rendered non-functional when it is forced through the ER-Golgi pathway by adding SP to its sequence [120]. FGF2 is also not affected by the classical secretion inhibitor Brefeldin A[114,115]. Alternative routes to secretion include channels or vesicle-mediated transportation[93,121] or release due to cell death[122]. The secretion of FGF2 is independent of either of these methods[114,115,123–126]. Finally, it was also possible to reconstitute the secretion process of FGF2 on Giant Unilamellar Vesicles (GUVs) with the help of only two components, $PI_{(4,5)}P_2$ and long-chained heparin[127,128]

FGF2 binds to $PI_{(4,5)}P_2$ via its positively charged C-terminus[129]. Its binding efficiency increases in cholesterol or sphingomyelin lipid environment[129,130]. A detailed investigation was recently conducted on the effects of cholesterol on the $PI_{(4,5)}P_2$-containing membrane and FGF2-$PI_{(4,5)}P_2$ interaction[130]. Via molecular dynamics simulations, it was suggested that cholesterol promotes clustering of $PI_{(4,5)}P_2$, creating dense negative-charged areas at the membrane. This increases and stabilizes the FGF2-$PI_{(4,5)}P_2$ interaction. FGF2 binding to $PI_{(4,5)}P_2$ is essential for its secretion[129,131] as disruption of FGF2-$PI_{(4,5)}P_2$ interaction through drugs impaired membrane recruitment.[132]

Heparan sulfate proteoglycans (HSPGs) are the second essential component of FGF2 secretion[127,131,133]. HSPGs are known to play many vital roles in FGF2 function. After secretion, FGF2 remains bound to cell surface HSPGs. HSPG protects secreted FGF2 from degradation [134–136] and stores them [137,138]. Heparan degrading enzymes release and mobilize FGF2 to distant targets when required[139,140]. HSPGs also form a ternary complex with FGF2 and FGF-receptor on the extracellular side of the membrane to induce signaling[141–143]. Cells that do not synthesize HSPGs do not secrete FGF2[133]. Recently, it was shown that Glypican-1 (GPC1), a GPI-anchored HSPG, is the predominant HSPG involved in FGF2 secretion[144]. Loss of GPC1 greatly impairs secretion, which can be rescued only by overexpression of GPC1 family HSPGs.

A key step in FGF2 secretion is its oligomerization [131,145,146]. Based on the intensity of labelled FGF2 spots in *in vitro* systems and FCS measurements in live cells, they were shown to encompass a range of oligomeric states from dimers to dodecamers[127,131]. High oligomer states of 10-12 were primarily seen in *in vitro* GUV systems[127], whereas oligomer states in cells were limited to less than tetramers[131]. FGF2 oligomerizes through the formation of intermolecular disulphide bridges. Two cysteine residues (C95 and C77) found exclusively in the unconventionally secreted member of the FGF family are essential for its oligomerisation[145]. $PI_{(4,5)}P_2$ and Tyrosine phosphorylation of the FGF2 (Y81p) are also essential for FGF2 oligomerization. FGF2 bound artificially to the membrane via Nickel Nitrilotriacetic acid (NiNTA) instead of $PI_{(4,5)}P_2$ cannot oligomerize. $PI_{(4,5)}P_2$ binding orients FGF2 for a strong dimerization bond via C95-

C95[127], and higher-order oligomers might form via binding to the dimers with the other cysteine (C77). Tyrosine phosphorylation of the FGF2 (Y81p) is postulated to stabilize the higher-order FGF2 oligomers[147].

Oligomers of FGF2 form pores in the PM. In reconstitution experiments, GUVs with high-order FGF2 oligomers on their membrane could translocate small-sized (1kD) dyes [147]. $PI_{(4,5)}P_2$ and tyrosine phosphorylation of FGF2 (Y81p) through their role in high-order FGF2 oligomer assembly are crucial for pore formation [127,147]. $PI_{(4,5)}P_2$ is also a suitable lipid to form toroidal-like pores due to its cone shape. A toroidal-like pore is created when the lipids of the top and the bottom membrane leaflets interact (Figure 10). The addition of Diacylglycerol (DAG), a lipid with an inverted cone shape, results in the loss of the pores. Furthermore, trans-bilayer diffusion of lipids could also be detected in GUVs with FGF2-Y81p-$PI_{(4,5)}P_2$-induced pores. Based on these observations, it is postulated that $PI_{(4,5)}P_2$-bound FGF2 creates toroidal-like pores[148–150].

The toroidal-like pore structure exposes $PI_{(4,5)}P_2$-bound FGF2 to the extracellular surface where the HSPGs reside. The binding of FGF2 to $PI_{(4,5)}P_2$ and HSPGs is mutually exclusive[127]where FGF2's binding affinity to HSPG is a hundred-fold higher than to $PI_{(4,5)}P_2$. Therefore, it is hypothesized that FGF2 is secreted via an assembly-disassembly model wherein FGF2 disassociates from $PI_{(4,5)}P_2$ and binds to extracellular HSPGs[151–153]. The FGF2 oligomers that form the toroidal-like pore structure are named translocon for the purpose of this thesis.

In live cells, two more components, Tec Kinase and the α1 subunit of the Na, K-ATPase, complete the machinery[154,155]. Tec kinase phosphorylates the FGF2 at Tyrosine (Tyr)[154,156]. Phosphorylated Tyr FGF2 is essential for $PI_{(4,5)}P_2$-mediated oligomerization and downstream pore formation[147,149]. All *in vitro* research into FGF2 secretion employ the Tyr phosphorylated version of the FGF2 protein. In contrast, the α1 subunit of the Na, K-ATPase is dispensable for the *in vitro* reconstitution experiments. Na, K-ATPase is an ion channel required to maintain the electrochemical potential of PM[157]. Functional $Na^{\pm}$ K^{+} ATPase or ATP is not a part of the FGF2

secretion process[155]. However, the α1 subunit of this ion channel is required for recruiting FGF2 to the PM in live cells[158].

An enormous amount of information has been produced in the last two decades about the FGF2 secretion pathways. Using *in vitro* and bulk biochemistry experiments, Nickel et al. identified the key players essential for FGF2 secretion and hypothesized a model for its secretion process. However, very few experiments have been conducted using live cells. Visualizing FGF2 action according to the model in live cells will be the ultimate proof. Recently, Dimou et al.[131] demonstrated the recruitment of a single molecule, FGF2, to the PM in live cells. They also showed translocation events in which FGF2 from the PM pore was recognized using extracellular nanobodies against FGF2-GFP. Such single-molecule experiments in live cells support the findings of *in vitro* and bulk biochemistry experiments. Live cell experiments also provide information on the time dynamics and steady-state reality of the process. In addition, live cell experiments with single-particle tracking can shed light on the sequence of events in FGF2 secretion.

This chapter aims to examine the FGF2 secretion process in live cells using TIRF and SPT and unravel the sequence of events involved. FGF2 secretion is a slow and inefficient process. Compared to the number of FGF2 that bind to the inner leaflet of the PM, very few FGF2 molecules form the translocons, the last pore-forming stage of FGF2 secretion (unpublished). Synchronization of the FGF2 secretion process could make the process easy to follow and increase the possibility of visualizing more translocons. In Part 1 of this chapter, I synchronized the FGF2 secretion process using the PhoCl caging system. Uncaging FGF2 creates a zero timepoint of the availability of cytosolic FGF2. This can help decipher the membrane recruitment process and partners important for membrane recruitment.

In Parts 2 and 3 of this chapter, I follow FGF2 molecules on the PM using SPT and analyze the FGF2 molecule's diffusion pattern and its oligomeric state. A molecule's diffusion pattern characterizes its binding partner or the maturity of the molecule in the process. Because oligomerization is a crucial step for FGF2 secretion, the

oligomeric state of the molecule also indicates its maturity. I followed FGF2 molecules from membrane recruitment to secretion using SPT and followed the changes in its diffusion pattern and oligomer state. I can gain information on the sequence of FGF2 secretion by examining how these observables change under mutant conditions.

4.2 PART 1: STUDY OF FGF2 RECRUITMENT USING THE PHOCL CAGING SYSTEM

4.2.1 Results

I employed PhoCl to cage FGF2 at the cytosolic face of the Golgi using a Golgi resident protein, TMEM115. TMEM115 is a multiple-membrane-spanning protein with the C-terminus in the cytosol. FGF2-GFP is connected to the C-terminus of TMEM115 with the PhoCl protein in the middle between the two (Figure 15a). UV illumination breaks PhoCl and releases FGF2-GFP into the cytosol. TIRF imaging showed almost instantaneous recruitment of FGF2-GFP at the inner leaflet of the PM (Figure 15b,c). The shortest time possible to observe membrane-bound FGF2 after activation in our setup was ~30 s. By this time, FGF2-GFP had already occupied the PM. PM-bound FGF2-GFP dissociated on Ionomycin treatment, a reagent that depletes $PI_{(4,5)}P_2$ (Figure 15d). This illustrates that the molecules I visualize are FGF2 molecules directly interacting with the inner leaflet of the PM and not ER-Golgi-derived vesicles carrying the FGF2-GFP construct close to the PM. To show that the recruitment of FGF2 to the PM is based on Brownian diffusion of cytosolic FGF2 and independent of microtubule-based trafficking, I also used a microtubule disrupting agent, Nocodazole. Nocodazole did not affect FGF2's instant recruitment to the PM (Figure 15e), confirming that the uncaged FGF2-GFP does not use active transportation modes. The data show that FGF2-GFP caging and uncaging have been successful. FGF2 particles directly bind to the inner leaflet of the PM and reach the PM by Brownian diffusion.

The uncaged FGF2-GFP is slightly different from FGF2-GFP that is not expressed as PhoCl fusion protein because the uncaged version has an additional short peptide of 23 amino acids at its N-terminus. To test if secretion of the uncaged version of FGF2-GFP is possible, I transfected cells with a plasmid expressing the cleaved version of FGF2-GFP and measured the amount of secreted FGF2-GFP using extracellular GFP nanobodies. The secreted FGF2-GFP binds to the cell's extracellular surface via HSPG and hence can be detected using anti-GFP nanobodies in the media (Figure 15a). Cells expressing the cleaved version of FGF2-GFP showed successful secretion, albeit in lower amounts than wild-type FGF2-GFP (Figure 15f).

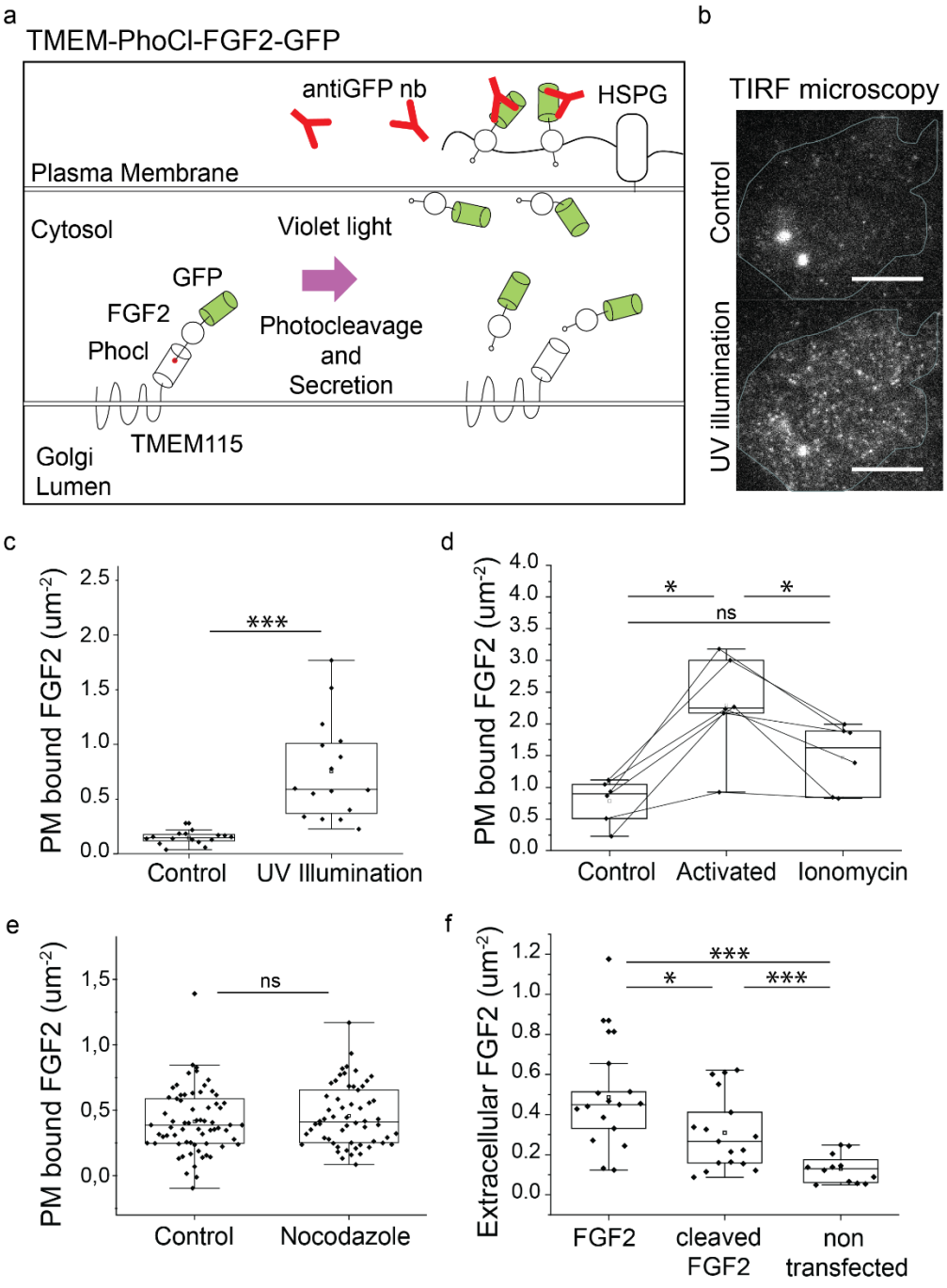

Figure 15: Functionality of the uncaged FGF2. (a) Schematic of the fusion protein TMEM115-PhoCl-FGF2-GFP and its uncaging under UV light. Anti-GFP nanobodies were used to detect secreted extracellular FGF2-GFP. (b) Raw image of TIRF microscopy of a cell expressing the construct before and after activation. After UV illumination, many white spots are observed within the cell boundary (marked in blue). These white spots are the FGF2-GFP molecules that are tracked and quantified. The bright and big spots, especially in the control image, are parts of the Golgi containing the caged FGF2-

GFP close to the PM. Scale bar is 10 μm. (c) Quantification of the PM (PM) bound FGF2-GFP before (mean, sd = 0.14 ± 0.05) and after UV illumination (mean, sd = 0.75 ± 0.4). Statistical significance was tested using the paired Wilcoxon rank-sum test ($p < 0.001$). ($N_{replicate}$= 2, N_{cells}= 16 cells). (d) Quantification of the PM-bound FGF2-GFP before (mean, sd = 0.7 ± 0.3), after UV illumination (mean, sd = 2.29 ± 0.7) and after the addition of Ionomycin (mean, sd = 1.4 ± 0.5). Measurements were done on the same cells across the conditions and are shown by connected lines in the plot. Statistical significance was tested using the paired Wilcoxon rank-sum test ($p < 0.05$). ($N_{replicate/cells}$= 6). (e) Quantification of the PM-bound FGF2 after UV illumination in control (mean, sd = 0.41 ± 0.2) and nocodazole treated cells (mean, sd = 0.45 ± 0.2) ($N_{replicate}$= 3, N_{cells}= 67 (control), 58 (Nocodazole)). (f) Quantification of secreted FGF2 in CV1 cells transfected with plasmids expressing FGF2-GFP (mean, sd = 0.48 ± 0.2), C termini PhoCl-FGF2-GFP (cleaved version of FGF2-GFP) (mean, sd = 0.3 ± 0.1) and in non-transfected CV1 cells (mean, sd = 0.1 ± 0.07). ($N_{replicates}$= 1, N_{cells}= 17 (FGF2), 17 (cleaved FGF2), 12 (control)). Data for plot (c) was acquired by master student Adolf Bierhuizen as part of an internship.

FGF2 interacts with three molecular players, $PI_{(4,5)}P_2$, α1 subunit of $Na^{\pm}$ K^+ ATPase and Tec Kinase at the PM. Caging FGF2-GFP presents a good opportunity to observe FGF2 recruitment at a 0-time point right after the cytosolic FGF2 pool becomes available. Using cells expressing caged mutant FGF2, I tested the molecular component necessary for FGF2's recruitment to the PM (Figure 16). FGF2 mutant defective in binding to both $PI_{(4,5)}P_2$ and α1 subunit, (FGF2 K54/60E/C77/95A/Y81F/K127Q/R128Q/K133Q), also called the full mutant, showed a very low number of FGF2 at the PM. FGF2 defective in binding to $PI_{(4,5)}P_2$ (FGF2 K127Q/R128Q/K133Q), named PIP2 binding mutant, also showed very low recruitment. Meanwhile, FGF2 defective in binding to α1 subunit and defective in dimerizing (K54/60E/C77/95A), named ATP1A1 binding mutant, showed similar number of molecules at the PM as the wild-type FGF2.

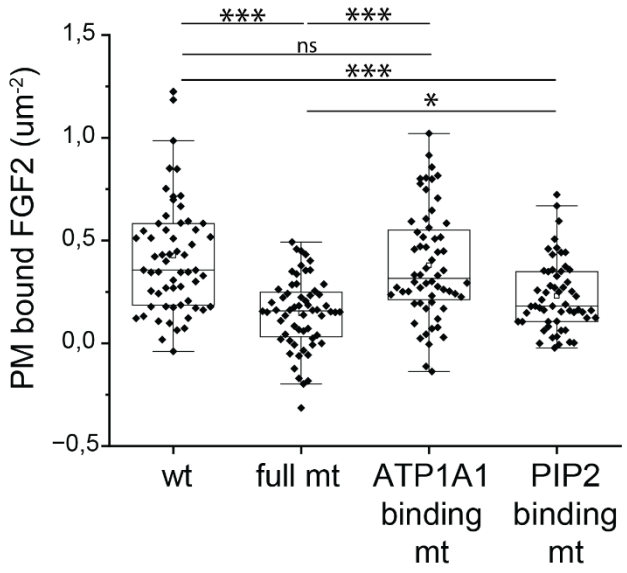

Figure 16: Recruitment of uncaged FGF2 to the PM. Quantification of membrane recruited FGF2-GFP after activation in cells expressing TMEM-PhoCl caged versions of wild-type FGF2-GFP (wt) (mean, sd = 0.42 ± 0.2), FGF2-GFP K127Q/R128Q/K133Q/K5460E/C7795A with a defect in dimerizing and in binding to $PI_{(4,5)}P_2$ and α1 subunit (full mutant) (mean, sd = 0.14 ± 0.1), FGF2-GFP K5460E/C7795A with a defect in dimerization and binding to α1 subunit (ATP1A1 binding mutant) (mean, sd = 0.38 ± 0.2) and FGF2-GFP K127Q/R128Q/K133Q with a defect in binding to $PI_{(4,5)}P_2$ ($PI_{(4,5)}P_2$ binding mutant) (mean,sd = 0.23 ± 0.1). Significance tested with unpaired Wilcoxon rank-sum test ($p < 0.001$ (***), $p < 0.05$ (*)). ($N_{replicates}$= 3, N_{cells}= ~60 for each condition).

4.2.2 Discussion

PhoCl-based caging of FGF2 gives a unique opportunity to study the recruitment of FGF2 to the PM. FGF2 is caged to the Golgi at its cytosolic face. Light-based uncaging breaks FGF2 from PhoCl and the Golgi anchor. On uncaging, almost instantaneous membrane recruitment is observed. The FGF2 molecules detach from the membrane on $PI_{(4,5)}P_2$ depletion, and the recruitment is unaffected by microtubule destabilization, confirming that FGF2 molecules diffuse in the cytosol to bind to the PM and that the FGF2 is not transported to the PM via vesicle trafficking. I also show that the uncaged FGF2 is capable of secretion.

4.2.2.1 Difficult to observe FGF2 translocon and secretion

Synchronization via PhoCl uncaging helped to study FGF2 recruitment to the PM. However, the exciting promise of synchronizing FGF2 was the higher number of secretion events. Unfortunately, the number of observed secretion events remained relatively small even after synchronisation (data not shown). This may be due to the low efficiency of PhoCl cleavage and hence, the insufficient cytosolic FGF2-GFP released after the uncaging. Because FGF2 oligomerization is an essential and rate-limiting step for its secretion, a successful secretion event is probably a concentration-dependent event. The concentration of FGF2 released in the cytosol after uncaging may not be sufficient for successful translocation events. Efforts to increase the PhoCl cleavage rate must be made to control a more extensive range of FGF2 concentrations through uncaging. Recently, a new PhoCl (Phocl 2c) with better cleavage efficiency was designed[159]. I could use PhoCl 2c to cage FGF2 in the future for better uncaging.

Inefficient uncaging of PhoCl and low rate of FGF2 secretion are also why I could not investigate the uncaged FGF2's secretion capacity directly. On uncaging, UV-induced peptide cleavage in PhoCl cuts the protein into a large N-terminus peptide and a short C-terminus peptide. As a result, the uncaged FGF2-GFP harbours the remnant C-

terminus peptide from PhoCl. Testing whether the uncaged FGF2-GFP with this additional peptide can also undergo secretion is crucial.

FGF2-GFP binds to HSPG on the extracellular cell surface after secretion[160]. One can measure secretion efficiency by measuring the extracellular FGF2-GFP on the cell surface with labelled anti-GFP nanobodies in media [131] (Figure 11a). However, when I used the protocol on cells after uncaging, I could not detect the secreted FGF2-GFP (data not shown). Not detecting the secreted FGF2-GFP after uncaging may be due to the additional peptide affecting FGF2's secretion capacity, or it could be due to the experimental setup and the low efficiency of FGF2's secretion.

Although many FGF2 molecules are observed at the inner leaflet at any given time, very few FGF2 molecules successfully undergo secretion (unpublished). Also, once secreted, the FGF2 molecules travel to other cells' surfaces[160]. Therefore, only after many successful secretions the extracellular FGF2-GFP could accumulate enough on the cell surface to be detectable by the GFP-nanobody protocol. High and long duration of FGF2 expression leads to high secretion events and hence, detectability of the extracellular FGF2-GFP. The publication[131] that used this protocol to measure the FGF2 secretion efficiency employed cells that constitutively overexpressed FGF2-GFP. This setup guarantees accumulation and hence, detection of the extracellular FGF2-GFP.

In comparison, in my experiments, the PhoCl-based uncaging system broke only a tiny fraction of the PhoCl, releasing a very low amount of FGF2-GFP in the cytosol. The low number of FGF2-GFP did not produce enough secretion events. Hence, detecting secreted FGF2-GFP was difficult. In addition, due to microscopy setup limitations, I could uncage only one cell at a time leading to the second problem, i.e., even if the secretion were high enough, the secreted FGF2 molecules would travel to neighbouring cell surfaces, and detection would be impossible due to the dilution of the extracellular FGF2 on the cell membrane. Therefore, an indirect experiment was conducted to investigate if the uncaged version of FGF2-GFP with the remnant PhoCl peptide can undergo secretion. Instead of expressing the full construct, TMEM-

PhoCl-FGF2-GFP, and testing secretion efficiency after uncaging, I employed cells overexpressing only the cleaved version of the construct, i.e., FGF2-GFP harbouring the cleaved peptide from PhoCl. Through this setup, I found that the uncaged version of FGF2-GFP is capable of secretion.

4.2.2.2 The curious case of FGF2 membrane recruiter

Using mutant versions of uncaged FGF2-GFP, I found that $PI_{(4,5)}P_2$ plays an essential role in the membrane recruitment of FGF2-GFP. This result is surprising because a previous report stated that the α-subunit is the primary recruiter of FGF2-GFP[158]. Both claims were made using the same experimental method, that is, counting the number of recruited FGF2-GFP molecules using TIRF-SPT in cells. However, there were a few differences between the two studies.

The state of FGF2-GFP differed between the two cases. Our results were derived from newly available FGF2-GFP after uncaging, whereas the results from Legrand et al. were derived from cells constitutively expressing FGF2-GFP. This difference suggests that the new FGF2-GFP might differ from the older FGF2-GFP in the cytosol. As PhoCl-caged FGF2-GFP is already facing the cytosol, it cannot be a modification made in the cytosol. The only difference is that compared to caged FGF2-GFP, FGF2-GFP in a constitutively expressed cell had opportunities to interact with the PM. I hypothesized that FGF2-GFP is recruited multiple times, and the initial recruitment modifies the molecule to have a different binding preference. This hypothesis was further investigated and discussed in the next section of this thesis.

Another difference is that the uncaged FGF2-GFP used in our study had an additional peptide at its N-terminus. Additional peptides may lead to unintentional membrane recruitment. $PI_{(4,5)}P_2$ is a highly negatively charged lipid molecule. The remnant of PhoCl attached to the uncaged FGF2 has six positively charged amino acids: **MHYGNRVFTKYPRGGGGTKLRIQT** (positively charged amino acids are shown in red). This additional peptide may facilitate the electrostatic binding to $PI_{(4,5)}P_2$. However, high binding to $PI_{(4,5)}P_2$ via the additional peptide fragment should be

maintained across all the mutant versions of uncaged FGF2. However, I observed a significant reduction in membrane recruitment in full mutants and FGF2 mutants defective in binding to $PI_{(4,5)}P_2$. Therefore, the additional peptide in the uncaged FGF2-GFP cannot explain the results shown in Figure 16 and the reversal of FGF2 binding preference to its molecular partners at the PM. Nevertheless, the unknown effects of the additional peptide on uncaged FGF2 should be tested in the future. This can be achieved by comparing FGF2-GFP recruitment in cells constitutively expressing the uncaged version of FGF2-GFP with that in cells expressing normal FGF2-GFP.

Yet another difference between our study and Legrand et al.'s study is that I used FGF2-GFP K54/60E/C77/95A instead of FGF2-GFP K54/60E to test the effect of the α-subunit due to cell line unavailability and time constraints. K54/60 are necessary for FGF2 binding to the α-subunit [158]. The additional mutation in this study, C77/95A, inhibits FGF2 dimerization. According to Legrand et al., the inability to bind the α-subunit via the K54/60 affects recruitment. However, I observed PM recruitment of the FGF2-GFP K54/60E/C77/95A mutant at a similar level to the wild-type FGF2-GFP (Figure 12). It is difficult to deduce how the additional non-dimerization mutation would recover FGF2's membrane recruitment that was affected by the K54/60E mutation. Nevertheless, to avoid unknown effects of the additional C77/95A on the recruitment of FGF2, the experiment could be performed without the dimerization mutation in the future.

In conclusion, there were some inconsistencies between the conditions used in this study and those of Legrand et al. These inconsistencies should be addressed in future studies. However, inconsistencies like the additional peptide at the N-terminus of the uncaged FGF2 and the use of a different mutant variant do not explain the results I observe in Figure 16. Therefore, I hypothesise that the time spent by FGF2 in the cytosol gives rise to the observed contrasting results. I hypothesize that FGF2 undergoes multiple recruitments to the PM via different binding partners. The initial recruitment observed in uncaged FGF2-GFP was mediated by $PI_{(4,5)}P_2$. During recruitment, FGF2 undergoes a change in its structure, which modifies its binding affinity and later specifies it to the α subunit. According to this hypothesis, at

equilibrium, the majority of the FGF2 molecules might be modified and recruited to the PM via the α subunit. Legrand et al. observe this matured population of FGF2 molecules in cells expressing FGF2-GFP constitutively.

PhoCl-caged FGF2-GFP is a good tool to see FGF2 movement from the start point of its availability in the cytosol. In this section, using PhoCl uncaged FGF2-GFP, I found some surprising results on its recruitment. I hypothesise that newly uncaged FGF2-GFP is different from FGF2-GFP continuously expressed in constitutively expressing cells. In the next section, I explore this hypothesis further by following FGF2's movement pattern post-recruitment using SPT. I compare the movement of uncaged FGF2 with that of FGF2 under steady-state conditions. By studying the diffusion pattern of FGF2 on the membrane after its recruitment, I also hope to determine the stages of its secretion process.

4.3 PART 2: SINGLE MOLECULE LIVE CELL IMAGING OF FGF2 REVEALS ITS DIFFUSION DYNAMICS

4.3.1 Results

The elements for FGF2's secretion are present in the PM. Therefore, I used SPT to reveal the choreography of FGF2 on the membrane. I measured the diffusion coefficient and alpha for each track obtained from the SPT (see Introduction). I observed that FGF2 moved in multiple ways (Figure 17a). Tracks with alpha < 0.3 represent FGF2 molecules with confined motion and are called immobile. Tracks with a higher alpha are termed mobile. Immobility can stem from interaction with an immobile protein, being trapped in a liquid-ordered high cholesterol domain[161], interaction with cytosketon[162] or a combination of either possible cause. In the case of

FGF2, it is known from *in vitro* studies that higher order FGF2 oligomers (10-12mers) insert themselves into the PM, forming the translocons[128]. These membrane-inserted higher oligomers are expected to be immobile. Analysis of the brightness of the FGF2-GFP spots showed that the mobile and immobile tracks were predominantly dimers (Figure 17b). Therefore, most immobile FGF2 observed were not the membrane inserted higher oligomeric translocons.

Next, I compared the mobility distribution of FGF2-GFP in the caged cell line and the constitutively expressing cell line. I tracked and analyzed the FGF2-GFP molecules seen before and after uncaging in the caged cell line. I observed some FGF2-GFP particles before uncaging. These particles have a broad mobility distribution with a peak at lower alpha values (confined motion). I assumed these particles were ER/Golgi-derived vesicles containing the caged FGF2-GFP. The number of particles on uncaging increases threefold, and these newly released molecules populate the immobile and mobile pool equally (Figure 17c). In contrast, in a constitutively expressing cell line, I observe primarily immobile FGF2-GFP at the PM (Figure 17c). These results suggest that when FGF2 first interacts with the PM, they have a broad mobility distribution. However, the distribution narrows to immobility in equilibrium conditions.

The FGF2-GFP molecules in constitutively expressing cells are in the cytosol for a long time and in a steady state. The newly uncaged FGF2-GFP, on the other hand, had never interacted with the PM before the uncaging step. I, therefore, hypothesized that being in the cytosol for some duration changed FGF2's properties, restricting its binding to a specific 'immobile' substrate. I tested if the mobility distribution of the uncaged FGF2-GFP changes with time. On imaging 3hr after uncaging, I see that the distribution shifts toward immobility, mirroring the population distribution of the FGF2-GFP in constitutively expressing FGF2 cells (Figure 17d). These results support the hypothesis that these immobile molecules are part of the later stage of FGF2 secretion.

To investigate if FGF2's different binding partners are responsible for its various modes of mobility, I employed the caged FGF2-GFP cell line with wild-type and mutant versions of FGF2. As mentioned earlier, in cells expressing the caged FGF2-GFP, I see some fluorescent spots before uncaging that are assumed to be ER/Golgi-derived vesicles containing the caged FGF2-GFP. The mobility distribution is similar for wild-type and mutants before uncaging, bolstering the assumption that these fluorescent spots derive from the same source, i.e., vesicles carrying the caged FGF2-GFP (Figure 17e). Cells expressing caged FGF2 defective in binding to $PI_{(4,5)}P_2$ K127Q/R128Q/K133Q exhibit very low PM recruitment, most of which is immobile (Figures 16 and 17f). Cells expressing caged FGF2 defective in binding to α subunit K54/60E/C77/95A do not show much difference in the mobility distribution and amount of PM recruitment compared to the wild type (Figures 16 and 17f). This data suggests that the newly uncaged FGF2 binds to $PI_{(4,5)}P_2$, and these $PI_{(4,5)}P_2$ bound FGF2 molecules are both mobile and immobile. If FGF2 cannot bind to PI(4,5)P2, they are recruited in low amounts, primarily immobile.

In summary, I find that FGF2 exists in mobile and immobile forms. After uncaging, FGF2 occupy both mobile and immobile states; however, they prefer the immobile state with time. The immobile state is also the dominant state in cells that express FGF2 in a steady state. According to this conclusion, I hypothesised that I should observe molecules changing from mobile to immobile state.

Although the data (Figure 17c,d) indicates that the immobile state forms a later stage of FGF2 secretion, finding mobile tracks that halted towards the end was challenging. Most tracks were either mobile or immobile from start to finish. Very few tracks showed a change in mobility (mean, sd = 21% ± 1%), and the change was not preferred towards a specific state. Only 9% ± 1% of mobile tracks changed into immobility. ($N_{replicates}$= 3, N_{tracks}= ~300 per replicate, N_{cells}= 20 per replicate). Representative mobile tracks with changing mobility are shown in Figure 18a.

The tracks used to generate Figure 17c,d includes all tracks, the molecules already bound to the PM before the start of image acquisition, and the newly recruited

molecules during the acquisition process. I decided to resample the data for tracks that represent newly recruited molecules to observe the mobility just after recruitment and the mobility change with time (Figure 18b,c). The newly recruited molecules were immobile in constitutively expressing cells (Figure 18b). Analysis of newly recruited molecules in cells with uncaged FGF2 showed a mixed mobility population and a slight shift towards the immobile state 3 hrs after activation (Figure 18c). These data suggest that FGF2 molecules do not change their mobility from mobile to immobile while at the PM, but rather the molecules are recruited to mobile or immobile binding partners at the PM. With time and equilibrium, the recruitment of the immobile binding partner is more common. Since FGF2 molecules rarely change their mobility after recruitment, I hypothesise that they undergo multiple recruitment cycles whereby the initial recruitment is to all mobile and immobile binding partners and later recruitments are specified to an immobile binding partner.

According to this hypothesis, I expect fewer recruitment events after the specification because the binding partners are limited, and specialisation reduces the possible number of binding partners. Indeed, I observe fewer recruitment events in constitutively expressing cells, where the FGF2-GFP is in equilibrium than in cells with recently uncaged FGF2-GFP (Figure 18d). The amount of recruited FGF2-GFP should depend on the available reservoir of cytosolic FGF2-GFP and the number of binding partners at the membrane. I observe that the number of PM-bound FGF2-GFP is proportional to the cytosolic pool of FGF2-GFP. At the same amount of cytosolic FGF2-GFP pool, however, there is more recruitment in recently uncaged cells than in constitutively expressing cells.

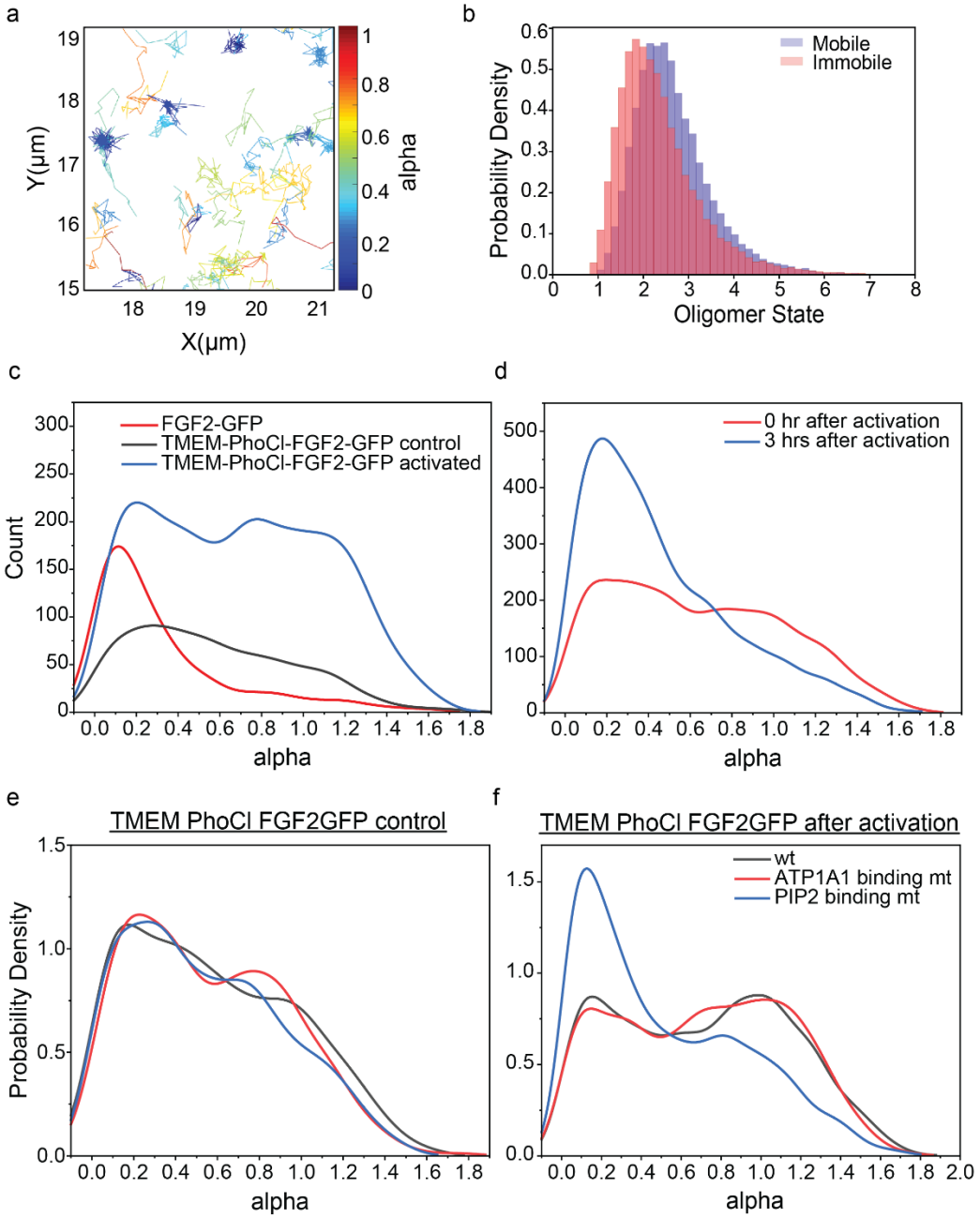

Figure 17: Mobility analysis of FGF2. (a) PM-bound FGF2-GFP tracks colour coded according to the alpha of the track, where low alpha corresponds to confined mobility, and high alpha corresponds to Brownian and directed motion. (b) Oligomer state distribution of mobile and immobile FGF2-GFP tracks. ($N_{replicates}$= 3, N_{cells}= ~60 per condition, N_{tracks}= 27079 (immobile), 25771 (mobile)) (c) Distribution of alpha of FGF2-GFP tracks in cells constitutively expressing FGF2-GFP (FGF2-GFP), in cells expressing a caged version of FGF2-GFP (tmem phocl FGF2-GFP control) and after UV illumination and release of FGF2-GFP into the cytosol (tmem phocl FGF2-GFP activated). ($N_{replicates}$= 3, N_{cells}= ~60 per condition, N_{tracks}= 637 (FGF2-GFP), 812 (caged FGF2-GFP), 2512 (uncaged FGF-

GFP)) (d) Distribution of alpha of FGF2-GFP tracks just after activation in cells expressing caged FGF2-GFP (0hr after activation) and 3 hrs after activation. ($N_{replicates}$= 3, N_{cells}= ~60 per condition, N_{tracks}= 2460 (0 hr), 3169 (3 hrs)). (e-f) Distribution of alpha of the FGF2-GFP tracks in cells expressing wild-type and mutant versions of caged FGF2-GFP before and after activation. ($N_{replicates}$= 4, N_{cells}= ~80 per condition, N_{tracks}= ~450 per condition (control), ~2800 per condition (after activation)). Data were partially acquired by bachelor student Daria Shyshko as part of an internship.

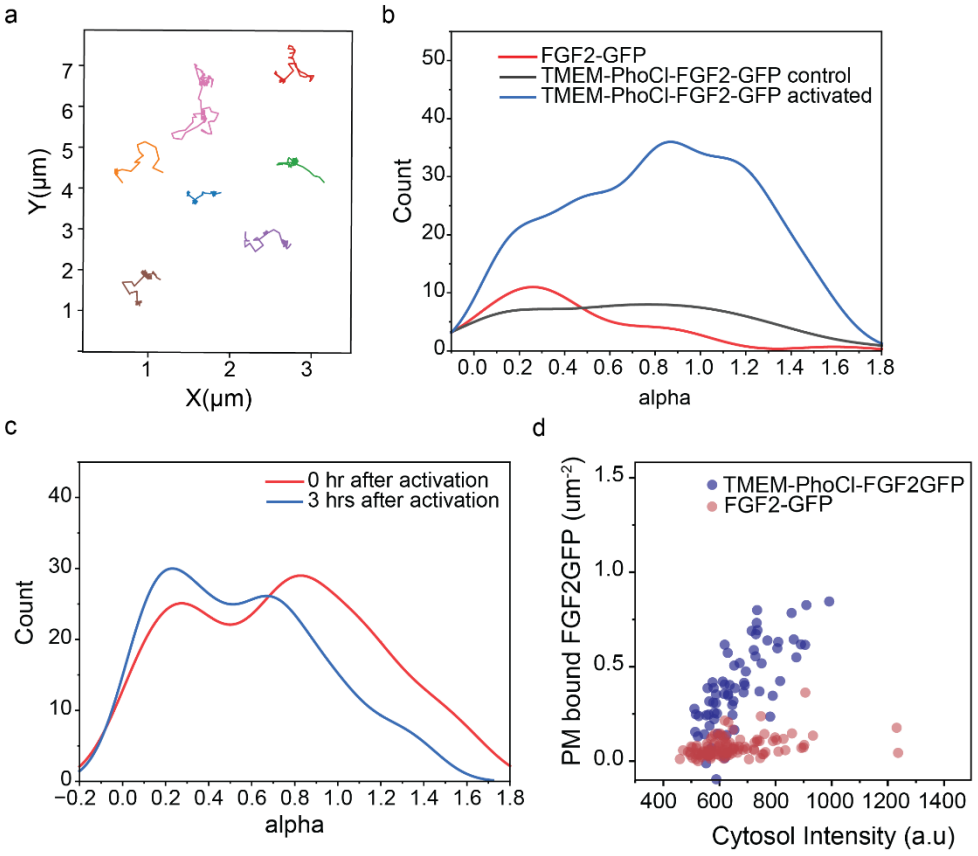

Figure 18: FGF2 is re-recruited to immobile domains. (a) Representative tracks showing mobility type changes. (b) Distribution of alpha of newly recruited FGF2-GFP molecules in cells constitutively expressing FGF2-GFP (FGF2-GFP) and in cells expressing caged FGF2-GFP before (tmem phocl FGF2-GFP control) and after (tmem phocl FGF2-GFP activated) activation. ($N_{replicates}$= 3, N_{cells}= ~60 per condition, N_{tracks}= 28 (FGF2-GFP), 36 (caged FGF2-GFP), 197 (uncaged FGF-GFP)). (c) The distribution of alpha of newly recruited FGF2-GFP molecules in cells expressing caged FGF2-GFP immediately after activation (0 hr after activation) and 3 hrs after activation. ($N_{replicates}$= 3, N_{cells}= ~60 per condition, N_{tracks}= 165 (0 hr), 134 (3 hrs)). (d) Scatter plot of cytosolic intensity and number of PM-bound FGF2-GFP molecules in cells constitutively expressing FGF2-GFP (FGF2-GFP) and after activation in cells expressing caged FGF2-GFP (tmem phocl FGF2-GFP). ($N_{replicates}$= 3, N_{cells}= 111

(FGF2-GFP), 67 (TMEM-PhoCl-FGF2-GFP)). Data were partially acquired by bachelor student Daria Shyshko as part of an internship.

4.3.2 Discussion

I observed two pools of FGF2-GFP, mobile and immobile, where the mobile pool was probably the $PI_{(4,5)}P_2$ bound fraction. I also observed that newly uncaged FGF2-GFP and constitutively expressed FGF2-GFP were fundamentally different in terms of the quantity of recruitment (Figure 18d), binding partner preference (Figure 16, previous section discussion), and mobility (Figure 17c).

4.3.2.1 Reasons behind mobility types

According to the Fluid Mosaic Model[163], the PM is a two-dimensional solution of oriented proteins and lipids, where the constituents have constant mobility. However, protein and lipid mobility in the PM is approximately 20-fold slower than in artificial membranes[164,165]. Clustering of PM proteins and lipids[166–168], physical barriers imposed by the cytoskeletal matrix underlying PM[162], or a specific lipid environment[161] may result in restricted movement and immobility.

$PI_{(4,5)}P_2$, one of the three binding partners of FGF2, is shown to have a diffusion coefficient of 0.5-1 $\mu m^2/s$ at the inner leaflet of the PM[166,169,170]. This value was slower than that observed in blebs or GUVs, as expected for most PM components. $PI_{(4,5)}P_2$ shows a mixed population of free and confined diffusion, where confinement can stem from its interaction with the cytoskeleton, PM proteins, and lipids[166]. Pacheco et al. used SPT-PALM to show that $PI_{(4,5)}P_2$ sensors exhibit mostly free Brownian diffusion, interrupted by transient confined diffusion [170]. Confined diffusion is shown to be a $PI_{(4,5)}P_2$ interaction with membrane-apposed cytoskeletons such as septin and spectrin.

Another molecular binding partner of FGF2, the α-subunit, is also shown to have mobile and immobile characteristics. It exhibited free diffusion in dendrites and restricted movement within the synapses of neurons[171].

Membrane-inserted FGF2 oligomers are another candidate for immobile FGF2 observed in my study. High-order FGF2 oligomers insert into the PM bilayer to form a toroidal pore just before secretion.[145,172,173] Toroidal pores are deformations in a lipid bilayer where the outer and inner leaflets interact, resulting in a tubular structure with a central opening. FGF2 oligomers within these pore structures could be relatively immobile. However, the immobile FGF2 population I observed were not the FGF2 molecules in the pore because they were primarily monomers or dimers (Figure 13b).

Therefore, immobile FGF2 molecules are the FGF2 bound to the $PI_{(4,5)}P_2$ or α subunit, as both can be mobile and immobile. The specific environment in which proteins and lipids are stationed determines their mobility. Our results from Figure 13f with uncaged FGF2 mutants show that both mobile and immobile fractions observed after uncaging are $PI_{(4,5)}P_2$-bound molecules. Since it is known that the α subunit is the principal recruiter of FGF2 in steady state[158], the immobile FGF2 observed in constitutively expressing cells and uncaged cells after 3 hrs is probably FGF2 bound to the α subunit. It has been speculated that FGF2 secretion facilitators, $PI_{(4,5)}P_2$, α subunit and Tec Kinase might be clustered together in raft-like nanodomains mediating quick secretion once recruited to these nanodomains[174]. So, it is also possible that the immobile fraction observed at the later stage is FGF2 bound to either of the molecular partners located at these nanodomains. In the future, an experiment with specific drug inhibitors towards α subunit or $PI_{(4,5)}P_2$ would confirm the identity of the immobile PM-bound FGF2 found in equilibrium and at a later timepoint of uncaged FGF2.

4.3.2.2 Multiple recruitment model

I observed that although there is a shift in mobility distribution over time, at the single molecule level, FGF2 molecules bound to the PM do not seem to change their

mobility. Multiple recruitments of the FGF2 molecules could explain these observations where the initial recruitment to the PM is to a mobile substrate and later recruitments is to immobile substrates. It will be interesting in the future to investigate this hypothesis, and if it's true, the molecular change FGF2 goes through to change its dynamics.

The model of FGF2 multiple recruitments could also explain the difference in binding preference observed between newly uncaged FGF2 and constitutively expressed FGF2. In the previous section, I showed that newly uncaged FGF2 is recruited to the PM via $PI_{(4,5)}P_2$. In contrast, the recruitment of FGF2-GFP at equilibrium is α-subunit dependent[158]. According to the hypothesised multiple recruitment model, FGF2 molecules are recruited to the PM via $PI_{(4,5)}P_2$; the recruited FGF2 undergo modification, e.g., phosphorylation which may reduce its affinity for $PI_{(4,5)}P_2$ resulting in its disassociation. Later, the modified FGF2 is recruited to the speculated immobile nanodomains via the α subunit. Such a speculated nanodomain contains both $PI_{(4,5)}P2$ and α subunit[174]. After recruitment via α subunit, the FGF2 might oligomerise and secrete in $PI_{(4,5)}P_2$ mediated manner as hypothesised in the earlier model[175]. Newly uncaged FGF2-GFP represents the newly available FGF2 molecules, and hence, I observed $PI_{(4,5)}P_2$ as the recruiter. Whereas, according to our model, in constitutively expressing cells, in equilibrium, most cytosolic FGF2 might be modified and hence, observed to be recruited by the α subunit.

In conclusion, from the previous and current sections, I found multiple ways in which newly uncaged FGF2-GFP differs from FGF2-GFP expressed constitutively. I also observed that in terms of mobility, uncaged FGF2-GFP began to resemble constitutively expressed FGF2-GFP over time. To explain these observations, I propose a model of multiple recruitments. The theory can be further tested by checking whether the uncaged FGF2-GFP starts mirroring the constitutively expressed FGF2-GFP in other characteristics with time, such as the binding partner and the number of recruitment events. One can also test if mobility is correlated to the modified, possibly phosphorylated state of FGF2. A single-molecule Fluorescence Resonance Energy Transfer (smFRET) experiment could be set up with FGF2-CFP

and a phosphorylation sensor tagged with YFP[176] to differentiate the phosphorylated FGF2 from the non-phosphorylated FGF2 and observe the mobility of the two populations.

4.3.2.3 Possible reasons for the multiple recruitment model

It has been recently speculated that nanodomains might carry all the essential FGF2 secretion machinery [174]. Having all the machinery, the α-subunit, $PI_{(4,5)}P_2$, Tec kinase, and HSPG close together might enable efficient FGF2 oligomerisation and secretion. Such a domain would also explain the fast kinetics (~200ms) of the translocation step observed earlier in live cells[131]. Multiple recruitments and subsequent FGF2 modifications might have the purpose of redirecting FGF2 towards these nanodomains. FGF2's affinity to the abundantly present $PI_{(4,5)}P_2$ might keep FGF2 away from the proposed nanodomains and interfere with its secretion. Lowering FGF2 binding affinity to $PI_{(4,5)}P_2$ would make them available to be recruited to the 'immobile' raft-like nanodomains by the α subunit. Since the cholesterol-rich environment of these nanodomains increases $PI_{(4,5)}P_2$ visibility and clustering[130], modified FGF2 would still be able to bind to $PI_{(4,5)}P_2$ at these domains, where it will be oligomerized and translocated with the help of $PI_{(4,5)}P_2$.

4.3.2.4 Is the remnant PhoCl responsible for the mobility difference between uncaged FGF2-GFP and FGF2-GFP?

The multiple-recruitment model proposed here is based on observations made using the uncaged version of FGF2-GFP. Uncaged FGF2-GFP and FGF2-GFP are assumed functionally equivalent. However, as described in the previous section, the uncaged FGF2-GFP contains an additional peptide of 23 amino acids at its N-terminus. This additional remnant PhoCl could have resulted in the recruitment and

mobility differences I observed between the uncaged FGF2-GFP and FGF2-GFP in constitutively expressing cells. The remnant PhoCl has a positive charge and could possibly facilitate recruitment to PM, specifically via binding to the negatively charged $PI_{(4,5)}P_2$ leading to more mobile FGF2 due to the mobility of $PI_{(4,5)}P_2$. However, I observed that FGF2 is not recruited to the PM via the extra peptide stretch in the last section (Figure 16) and, therefore, could not be the reason for the mobility differences. However, it is necessary to verify with more experiments if remnant PhoCl influenced the binding and mobility of uncaged FGF2 in an unknown manner in the future. This hypothesis can be tested by using cells that constitutively expressed uncaged-FGF2-GFP and FGF2-GFP and comparing their recruitment and mobility.

In this section, I used mobility analysis to decipher the stages of FGF2 secretion and found out that FGF2 may be re-recruited to the PM where, with time, FGF2's binding preference shifts to the immobile binding partner. Another method for observing the stages of FGF2 secretion is to detect its oligomeric state. FGF2 oligomerization is essential for its secretion. The oligomeric state denotes the maturity of FGF2 during the secretion process. I used SPT and doxycycline-based controlled expression systems to visualize FGF2 oligomers and the oligomerization process in live cells.

4.4 PART3: OLIGOMER STATE OF FGF2

4.4.1 Results

To observe the process of FGF2 oligomerization and to study the sequence of events leading up to its secretion, live-cell SPT using cells expressing FGF2-Halo was performed. First, I looked for evidence of the existence of FGF2-Halo oligomers in cells. Cells expressing FGF2-Halo were sparsely labelled with 10 pM Janelia Fluor (JF) 635 dye. Intensity distribution generated from such a sparsely labelled condition is assumed to represent the intensity of monomeric FGF2-Halo (Figure 19a). Cells labelled with a higher concentration, 1 μM of JF635, showcase a shift in the intensity

distribution, indicating the presence of FGF2-Halo oligomers in the cells (Figure 19a). In a different experimental setup, cells expressing FGF2-Halo (labelled with JF635) and FGF2-GFP were imaged. Colocalization of FGF2-Halo and FGF2-GFP provides further evidence of FGF2 oligomers in live cells (Figure 19b). Randomization of the coordinates of FGF2-GFP molecules significantly reduced the colocalization percentage indicating that the colocalizing spots do not occur through random chance and are indeed FGF2 oligomers.

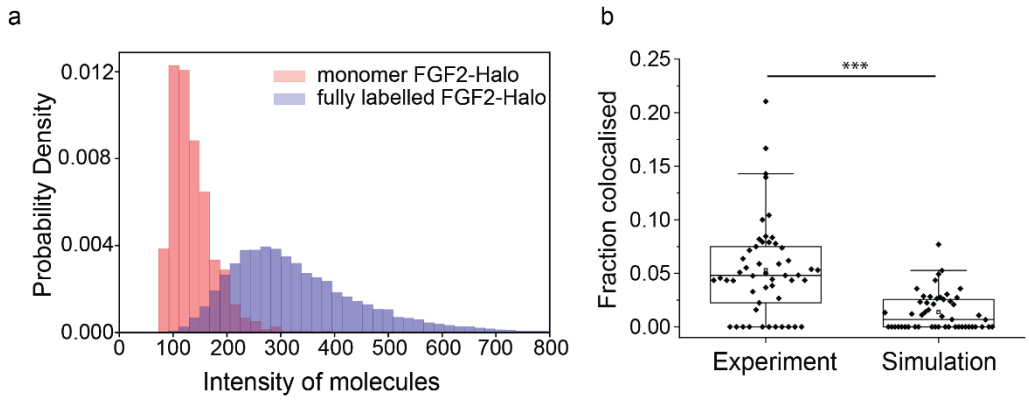

Figure 19: FGF2 oligomerises. (a) The intensity distribution of fully labelled FGF2-Halo (labelled with 1 μM JF635) and partially labelled FGF2-Halo referred to as monomeric FGF2-Halo (labelled with 10 pM JF635). ($N_{replicates}$= 1, N_{cells}= 20, N_{tracks}= 16061 (fully labelled FGF2-Halo), 1028 (monomer FGF2-Halo)) (b) Fraction of FGF2-GFP colocalized with FGF2-Halo in cells expressing both (Experiment) (mean, sd = 0.05 ± 0.04). Positions of tracks were randomized in one of the wavelengths to estimate the percentage of colocalization occurring through chance (Simulation) (mean, sd = 0.01 ± 0.01). ($N_{replicates}$= 1, N_{cells}= 50). Significance tested with unpaired Wilcoxon rank-sum test ($p < 0.001$).

To observe and study oligomerization following membrane recruitment, I traced the intensity of each FGF2 molecule at the PM. The molecules either showed the same intensity level throughout their lifetime on the membrane or had varying intensity levels (Figure 20a,b). The multi-intensity tracks, called multistep molecules, comprise only ~3% ± 2% of the bound FGF2 (Figure 20c). I hypothesize that the multistep molecules represent the actively oligomerizing FGF2 complex where adding a new molecule to a membrane-bound molecule increases the intensity level (up step) and disassembly, secretion, or photobleaching leads to the intensity drop (down step). The multi-intensity tracks are present in a significantly higher fraction in fully labelled

FGF2-Halo cells than in sparsely labelled FGF2-Halo cells (Figure 20c), supporting that these are real events and not artefacts due to intensity fluctuations of the tracked molecules. I observed that 64% (± 5 % sd) of the steps occurring in the multistep tracks are up steps ($N_{replicates}$= 4, N_{tracks}= ~1000 per replicate, N_{cells}= 20 per replicate). This suggests that the multistep tracks comprise both up and down steps, with a slight majority of oligomerizing or up steps.

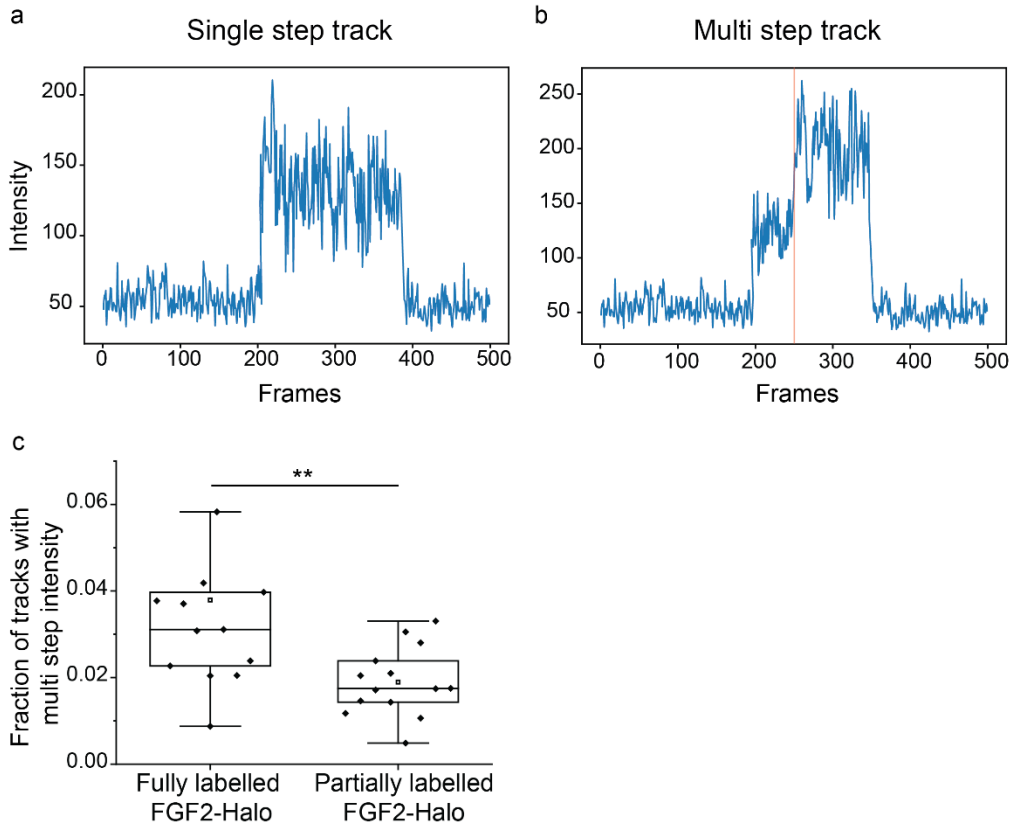

Figure 20: Types of FGF2 tracks. (a) Representative intensity profile of a single-step FGF2 track. The molecule appears at ~200th Frame and disappears at ~400th Frame. Intensity trace before and after the FGF2 sighting represents the background intensity. (b) Representative intensity profile of a multistep track. The molecule appears at ~200th Frame, another molecule joins it at ~250th Frame, and finally, the entire complex disappears at ~350th Frame. The orange line represents the intensity level change detected by the Matlab code (See Appendix) written to recognize such steps in all the FGF2 tracks. (c) Fraction of tracks that show multistep intensity in cells expressing fully labelled FGF2-Halo (mean, sd = 0.037 ± 0.02) and in cells with partially labelled FGF2-Halo (mean, sd = 0.01 ± 0.007) ($N_{replicates}$= 13,

N_{tracks}= ~20,000 per replicate, N_{cells}= 20 per replicate). Significance tested with unpaired Wilcoxon rank-sum test ($p < 0.01$).

SPT allows tracking the intensity of each FGF2-Halo molecule/complex that binds to the PM. The intensity of the FGF2-Halo complex scales linearly with the oligomer state of the complex. Equipped with the knowledge of monomer FGF2-Halo intensity, one can derive the oligomeric state of the tracked molecules. I utilized the sparsely labelled FGF2-Halo molecules to estimate the intensity of monomer FGF2-Halo (Figure 21a-c). The fraction of oligomeric species of the FGF2-Halo complex was derived by fitting the intensity distribution of fully labelled FGF2-Halo molecule/complexes with multiple Gaussians with predicted mean of monomer and higher oligomers (Figure 21d,e).

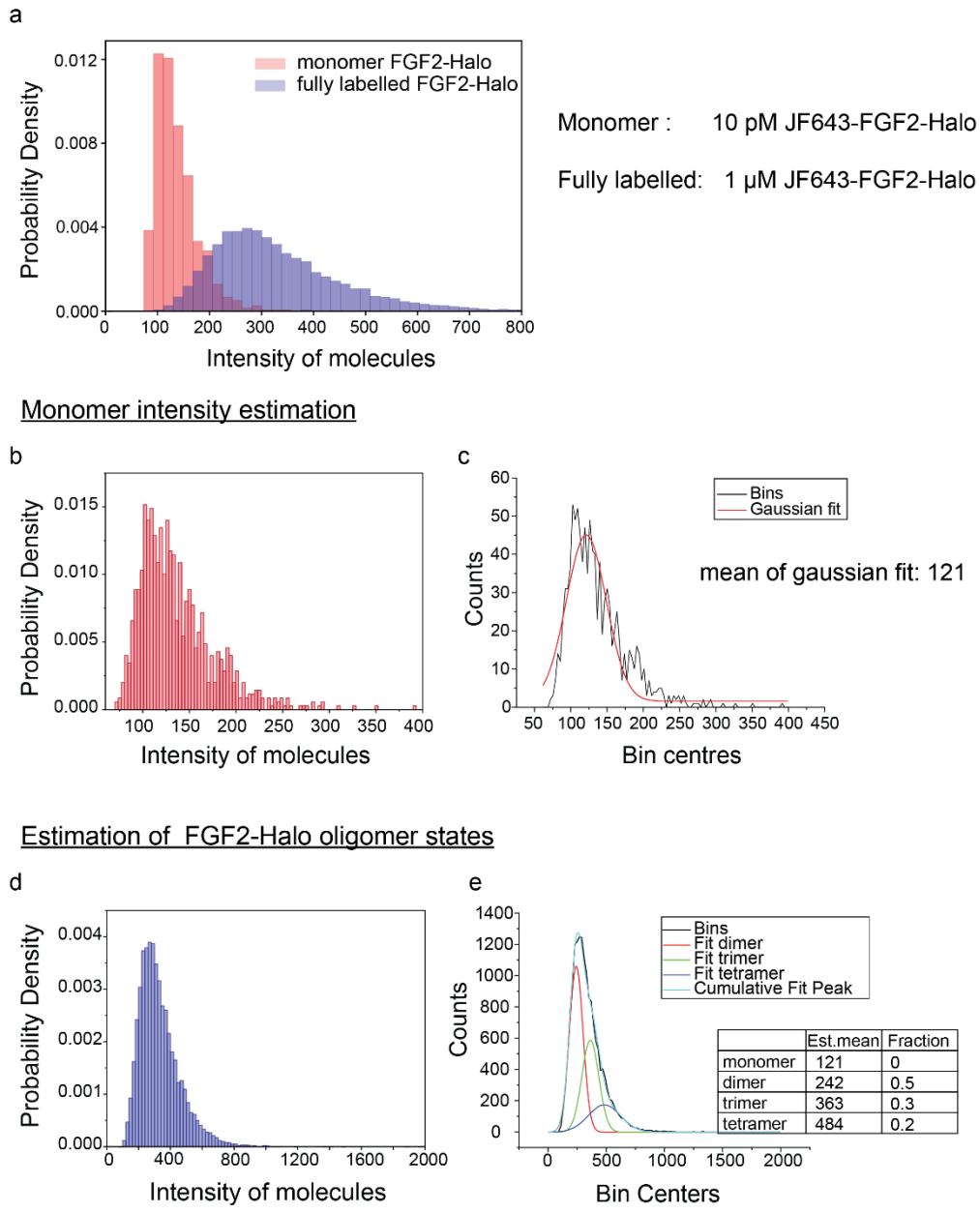

Figure 21: Schematic of FGF2 oligomer analysis. (a) The intensity of each FGF2-Halo molecule on the PM in partially and fully labelled conditions is gathered, and its distribution is plotted. FGF2-Halo molecules detected in cells partially labelled with 10 pM JF635 dye are assumed to represent the monomer Halo-JF635. (b,c) The histogram of monomer intensity distribution is fitted with a single gaussian, and the fit's mean is noted as the monomer intensity. (d,e) The histogram of FGF2-Halo in the fully labelled condition is fitted with the multiples of the estimated monomer intensity to estimate the fraction of each oligomeric species in the cell.

I found that single-step tracks, where FGF2-Halo exhibited only one intensity level, were mostly dimers with a few occurrences of trimers and tetramers (Figure 22a). Since most molecules imaged were already bound to the membrane when first observed, I missed the oligomer state of molecules when they first arrived at the PM. Therefore, I also observed the oligomer distribution of molecules that arrived after the start of image acquisition (Figure 22b). In both cases, dimers overwhelmed the distribution, while a small fraction of higher oligomeric FGF2 also appeared as single-step tracks.

The histogram of the oligomer states exhibited by the multistep molecules shows a strong presence of dimers and trimers (Figure 22c). The molecule or the oligomer that acts as a base for the oligomerization process is likely to be a dimer but could also be a higher-order oligomer (Figure 22d). Moreover, oligomerization proceeds through the stepwise addition of a monomer to a pre-bound FGF2 molecule/oligomer (Figure 22e).

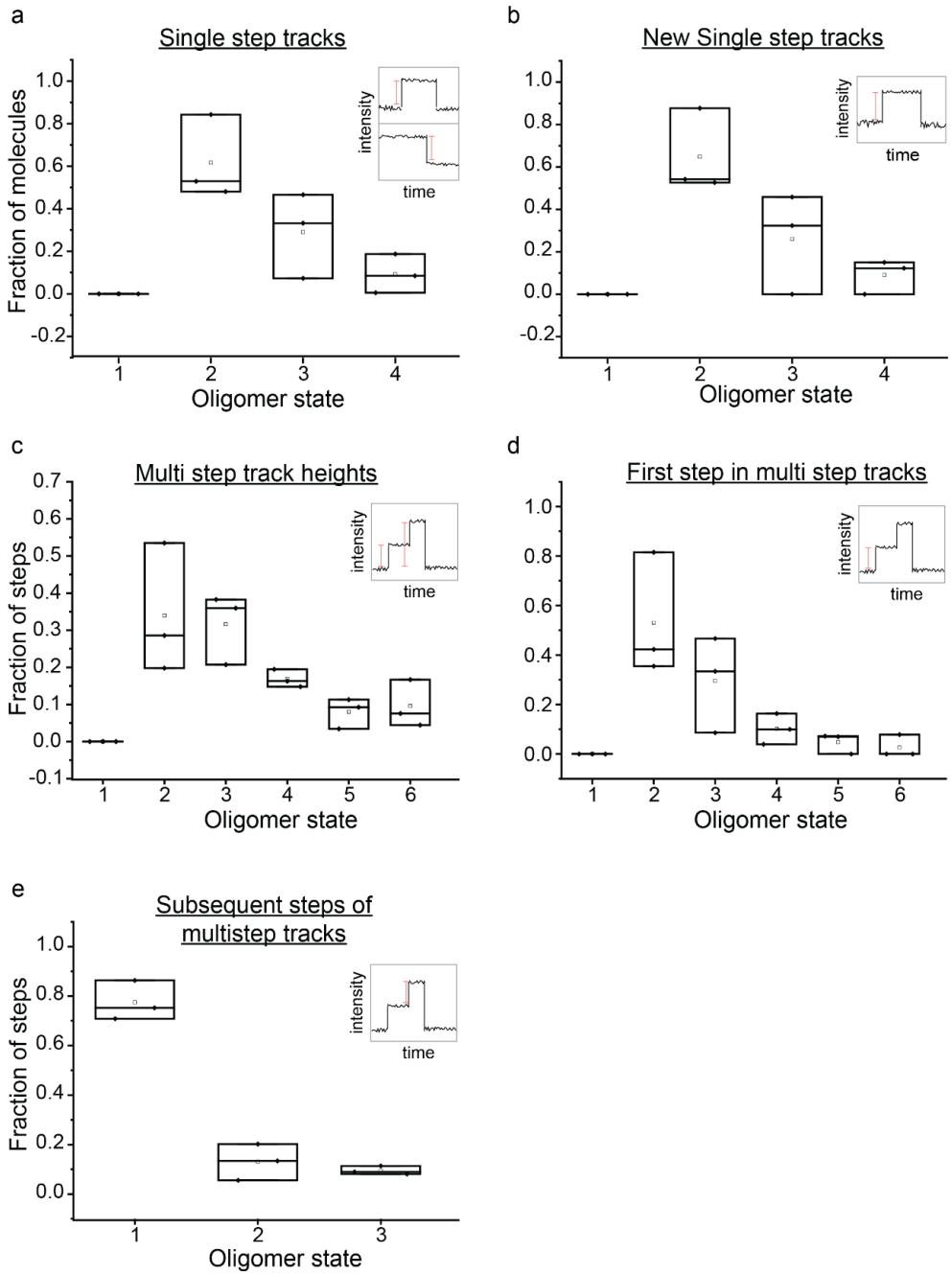

Figure 22: Oligomeric state composition of single and multi step tracks. (a) Oligomeric state distribution of FGF2 molecules in single steps. The inset shows the type of FGF2 track and the specific step used for distribution in all plots. (b) Oligomer-state distribution of newly arriving single-step FGF2 molecules. (c) Oligomeric state distribution of FGF2 molecules showing multistep intensities. (d) Oligomer state of the first step in the multistep tracks. (e) Oligomer state distribution of incoming molecules that assemble on the already bound FGF2 molecules. ($N_{replicates}$= 3, N_{cells}= 20 per replicate,

$N_{steps/tracks\ per\ replicate}$= ~15600 (single step tracks), ~14500 (new single step tracks), ~3500 (multi step tracks), ~1200 (first step of multi step tracks), ~1500 (subsequent steps of multi step tracks))

Most molecules visualized in live cells are dimers, and higher-order oligomers are rare. I observe only 3% of molecules that show multistep intensity. More instances of active oligomerization are required to understand the oligomerization process better. Therefore, conditions that increase oligomerization events must be induced. Recently, it was shown that Glypican1 (GPC1), a type of HSPG, is essential for FGF2 secretion, and overexpression of GPC1 increased FGF2 secretion[144]. Conditions that enhance the secretion rate may also increase the number of high-order FGF2 oligomers. Therefore, I decided to perform the study in GPC1 overexpressing cells. However, the oligomer state distribution of FGF2-Halo in cells overexpressing GPC1 did not show much increase in the high-oligomer FGF2 population compared to the wild-type cells (Figure 23).

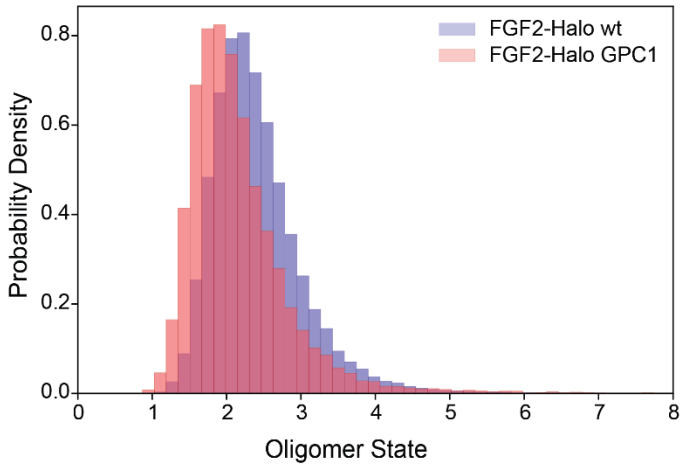

Figure 23: Oligomeric state distribution of FGF2 in GPC1 overexpressing cells. Oligomeric state distribution of FGF2-Halo in wild-type (wt) cells and cells overexpressing GPC1. ($N_{replicates}$= 3, N_{cells}= ~ 60 per condition, N_{tracks}= 63324 (FGF2-Halo wt), 24457 (FGF2-Halo GPC1).

4.4.2 Discussion

FGF2 oligomerization is an essential step in the FGF2 secretion process. According to the model of FGF2 secretion, FGF2 molecules oligomerize with the help of $PI_{(4,5)}P_2$ after its recruitment to the PM. I envisioned that I could visualize and understand this oligomerization process using SPT and live cell imaging. The combination of SPT and a Halo tag enabled detailed visualization of the FGF2 oligomerization process. The results indicate that the FGF2 oligomerization and secretion are inefficient and have low throughput.

4.4.2.1 Oligomerisation is rare and inefficient

I found that ~97% of PM-bound FGF2 exhibited a single-step intensity profile, i.e., they do not change their oligomeric state during their lifetime on the PM. These molecules constitute dimers primarily. Since a higher FGF2 oligomer (10-12 mer) is hypothesized to precede secretion, this indicates that most molecules recruited to the PM dissociate before undergoing oligomerization. Alternatively, the oligomerization process could be slow and missed in the observation window of ~25s or missed due to photobleaching.

Analysis of newly recruited FGF2 molecules shows a similar distribution. The distribution constitutes dimers, trimers and tetramers. This distribution is surprising because it is assumed that FGF2 molecules undergo the entire process of secretion once recruited, and the oligomerisation occurs only on the PM[128]. According to these assumptions, monomer FGF2 would be recruited, and they would remain at the PM, undergo oligomerisation and finally secretion. Observation of recruitment of dimers, trimers, and tetramers, indicates that FGF2 molecules/oligomers dissociate from the PM mid-way before reaching their final oligomer state or secretion.

A small percentage (3%) of PM-bound FGF2 molecules showed a multi-intensity profile. An increase in the intensity level of a PM-bound FGF2 molecule indicates the recruitment of a new molecule to the bound molecule/complex. Reduction of the

intensity level indicates the dissociation of a molecule from a PM-bound FGF2 oligomer or photobleaching of Halo Tag dye. Reduction in the intensity level could also indicate secretion; however, since secretion is an infrequent event and requires a high oligomer FGF2 complex, it has been ruled out as one of the causes. The multi-intensity molecules do not showcase a consistent increase in intensity but rather a mix of increase (also called "up steps") and decrease (also called "down steps") in their intensity profile. The down steps may indicate photobleaching or instability of the oligomers.

In conclusion, oligomerisation is a slow and inefficient process. Very few oligomerisation instances could be detected in the PM-bound FGF2 molecules. In addition, FGF2 molecules/oligomers dissociate from the PM before undergoing the entire secretion process. These observations explain the meagre rate of FGF2 secretion. Such a low oligomerisation rate suggests that there must be specific conditions that need to be met for a successful oligomerisation. These conditions might be the requirement of a specific lipid environment, a collision of two membrane-bound FGF2 molecules, recruitment of an FGF2 molecule to the bound FGF2 molecules or the requirement for the molecules to be in the correct orientation when in proximity.

4.4.2.2 Structure of multi-intensity tracks

Multi-intensity tracks are the molecules that show oligomerisation. I dissected and analysed each step of these multi-intensity tracks. I observed that a broad range of oligomer states could form the base for building the oligomer. Also, oligomerisation resulted from adding monomers to the PM-bound molecule or oligomer.

4.4.2.3 Model

Based on the observations from the SPT study of the FGF2 molecules, I propose the following model of FGF2 dynamics pre-secretion. FGF2 is recruited to the PM.

Seldom, when the right conditions are met, e.g., when two FGF2 molecules collide at the membrane or an FGF2 molecule is recruited close to a prebound molecule, they oligomerise. After some time, the PM-bound FGF2 molecule/oligomers will disassociate from the PM. The FGF2 molecules/oligomers re-bind the PM, maybe oligomerise and dissociate from the PM in multiple such cycles before finally reaching the right oligomer size and undergoing secretion.

4.4.2.4 Limitations

Photobleaching

SPT has been invaluable in our objective to follow FGF2 through its journey towards secretion. However, the method has its limitations. An excellent Signal to Noise ratio (SNR) is required to detect single molecules and confidently decipher a complex's oligomer state. A high SNR can be achieved using bright dyes and high laser powers. The high laser power required to image single molecules comes at the cost of photobleaching. Although a balance between the two was tried, some photobleaching is inevitable, leading to the overrepresentation of lower oligomer states. Photobleaching also leads to incomplete visualisation of a molecule's journey on the PM. I observed most molecules disappearing before undergoing any change in the oligomer state. Also, multi-intensity tracks comprised many down steps, which I assumed were caused by the dissociation of molecules from oligomers. This disappearance of the molecule could also be a result of photobleaching, where I missed out on the progression and oligomerisation of the molecule because it is not fluorescent anymore.

The extent of photobleaching should be measured for a complete interpretation of the data. A PM localised Halo-tagged transmembrane protein of known stoichiometry can be utilised for this purpose. A transmembrane protein would have no possibility of 'dissociation' from the PM, like FGF2. At the same applied laser power, the lifetime of the Halo tag could be used to estimate the degree of photobleaching in the experimental setup.

In the future, photobleaching can also be reduced and the lifetime of the dyes prolonged by using specific media conditions. Lowering the molecular oxygen and using a reducing-plus-oxidizing system (ROXS) in the media has been shown to lengthen the observable track length of single molecules in SPT experiments[177]. Such media modification could be helpful to observe the complete trajectory of the PM-bound FGF2 molecules and see its oligomerisation process.

Limitation of analysis approach and overestimation of dimers

Prediction of the percentage of oligomeric species from intensity values of FGF2-Halo is based on the estimated monomer intensity. Monomer intensity was estimated by fitting a Gaussian to the intensity distribution of a sparsely labelled FGF2-Halo sample. The Gaussian fit is error-prone because the intensity distribution is not a normal distribution. A threshold is set to detect fluorescent molecules over the background for the tracking process, which means that the tracked molecules create an intensity distribution which is cut off at the left tail due to the threshold. Monomer intensity is hence, probably slightly overestimated.

Since FGF2 is a cytosolic protein, they create a significant noise to the membrane-bound FGF2 signal. The sparsely labelled FGF2-Halo sample that is used for monomer intensity prediction has much lower cytosolic fluorescence compared to the fully labelled FGF2-Halo. The high fluorescent background in fully labelled FGF2-Halo samples may add to the signal of the tracked molecule overestimating the oligomeric status of the molecule.

High-expressing cells are inaccessible

Imaging single FGF2 molecules is complicated because cytosolic FGF2 forms a high-intensity background which reduces the SNR. Therefore, cells expressing a low amount of FGF2-Halo were selected for imaging because they had a low background from cytosolic FGF2-Halo, and hence, the best SNR for imaging single FGF2-Halo molecules. Being limited to imaging only low-expressing cells was a major drawback of this study. I assume that high-expressing cells would have a higher secretion rate,

and FGF2 in these cells might be at a more advanced stage of secretion, showing a very different oligomer profile. As I was limited to using low-expressing cells for the SPT experiments, I decided to induce conditions to visualise more oligomerisation events and events at the latter stages of the secretion.

Considering the whole process, i.e., the FGF2 recruitment, oligomerisation and the secretion process as a chemical reaction, increasing the secretion rate might shift the equilibrium to the right towards higher oligomer states. Cells overexpressing GPC1 seemed promising as they are known to improve secretion[144]. Therefore, cells with high GPC1 expression and low FGF2-Halo expression could be used to ensure high SNR and higher secretion rate at the same time. However, my experiments did not show an increase in the higher oligomeric fraction in these low-expressing cells despite the GPC1 overexpression. This indicates that GPC1 overexpression may only influence the last stages of membrane insertion and translocation of the FGF2 secretion process, and the rate-limiting stage of oligomerisation is unaffected by GPC1.

These single-molecule microscopy experiments offered insights into the movements and the oligomerization of FGF2 at the membrane and, ultimately, the sequence of events in the FGF2 secretion process. However, single-molecule microscopy is limited for the time being due to the rarity of successful secretion events and the high cytosolic FGF2 background. Technological advances and new probe development in the single molecule field in the future would likely overcome these limitations. The problems specific to single-molecule imaging of FGF2 secretion could be solved in the future if we could find a method to image PM localised molecules with high SNR despite the presence of cytosolic background. A recently developed technique called Proximity Assisted Photoactivation (PAPA) could be used for this purpose[178]. The method uses two fluorophores, JF549 and JFX650, where JFX650 can be converted to a fluorescent state from a dark state when in proximity to JF549[178]. If we could label the PM with the fluorophore, JF549, we may be able to specifically visualise the fluorescent PM-bound FGF-JFX650 in the non-fluorescent cytosolic FGF2-Halo (JFX650) background. Such a setup would allow observations of PM-bound FGF2 in high-expressing cells.

Transient tracks are overlooked

I used a length cut-off when analyzing the SPT data. I restricted our analysis to FGF2 molecules that remained bound to the PM for longer than 500ms. Considering the recent perspective of the existence of transient nanodomains and the fast kinetics of translocons[174], short-lived FGF2 spots should also be analysed in the future.

4.5 CHAPTER CONCLUSION

In this chapter, the detailed dynamics of FGF2 molecules in live cells were investigated for the first time. The current model of FGF2 secretion has been proposed based on bulk and *in vitro* experiments. *In vitro* experiments have helped identify the key players and steps in the mechanism. However, these measurements are averages, often made in the presence of excess participating molecules, out of equilibrium and may miss out on essential elements required for function in live cells. Observing the same process in live cells at the single molecule level gives one insight into the dynamics of the process under real-time scales and conditions, in equilibrium and with molecular participants in physiological quantities. I used single-molecule microscopy methods to follow FGF2 dynamics in live cells and tested the current model.

I used the oligomer state as an indicator of the FGF2 progression towards secretion and found out that the FGF2 secretion is not as straightforward as the model might imply. The model tells the key steps and the sequence of the process; this might beget a notion that all the steps take place in a unidirectional and single unbreaking continuous sweep. However, tracking FGF2 molecules in live cells revealed an unstable, inefficient, intermittent mechanism. Throughout the investigation, I have implied that FGF2 falls off and is re-recruited multiple times in its progression towards secretion. These were hypothesises made to understand differences observed in the first two parts of the chapter between steady state and out-of-equilibrium data. In the

last part, I saw evidence of such recruitment cycles when I found that higher oligomer FGF2 are recruited to the PM. Such inefficient mode of progression, cycles of binding and unbinding from the PM, explains the meagre rate of secretion partly.

Oligomerisation is also another step that slows the process. I found that most FGF2 molecules do not undergo oligomerisation when they are bound to the PM. This implies that the oligomerisation is a low-probability event. For example, two PM-bound FGF2 colliding in the right orientation might be a low-probability event. The probability is drastically reduced further because oligomerisation must occur a couple of times to obtain a certain oligomeric size that is proposed to be the precursor for successful secretion. This makes oligomerisation a definite bottleneck to the process. This might be faster in case a higher FGF2 pool compensates for the low probability of the oligomerisation event.

Another discovery and contribution to the FGF2 secretion model was made when I utilised the PhoCl caging tool. Using the PhoCl caging system in combination with single-molecule live cell imaging, I revealed the initial phase of FGF2 secretion. Based on the results, I proposed that FGF2 is initially recruited to $PI_{(4,5)}P_2$ at the PM. FGF2 is then modified probably via phosphorylation that reduces its affinity to $PI_{(4,5)}P_2$. The FGF2 falls off the PM and is then re-recruited to the PM via the α1 subunit of the Na, K-ATPase in a steady state. This elaborate phase of PM recruitment might be necessary to prepare FGF2 and redirect them to specific nanodomains. Recruitment and secretion of FGF2 were possible without the necessity of α1 subunit of the Na, K-ATPase in *in vitro* experiments[127]. However, in vivo, the α1 subunit of the Na, K-ATPase was found to be a binding partner and a necessity for FGF2 secretion[155]. Recruitment experiments in steady-state live cells concluded that the α1 subunit of the Na, K-ATPase is the recruiter of FGF2 in live cell conditions[158]. However, during this investigation, it was still assumed that FGF2 undergoes only one recruitment and stays on the PM until secretion. Steady-state conditions also miss out on the initial phase of FGF2 dynamics just after its fresh synthesis in the cytosol. This might have been an insignificant detail. However, caging FGF2 and releasing them simultaneously showcased otherwise and exposed the initial phase of the FGF2 secretion mechanism.

In this chapter, I looked at the FGF2 secretion mechanism through a different perspective of single molecule microscopy and proposed certain modifications to the current model. However, it is still the beginning of understanding the FGF2 dynamics. The theories were made based on exploratory investigation and need to be tested with further controls and experiments.

5 CONCLUSION

Single-molecule live cell microscopy is a powerful tool to investigate biology. The approach can help delineate the kinetics and heterogeneity of a protein population and be used to understand the mechanism and rate of a process. In this thesis, I first established PhoCl as a tool to control the number of proteins. I have shown that PhoCl-based caging and uncaging are suitable for single-molecule microscopy methods, such as SPT. PhoCl-based caging further improves the SPT method, enabling fully labelled SPT, which can be especially useful in studying oligomers. In the second chapter of the thesis, I utilised the fully labelled SPT technique and the established PhoCl-based caging tool to reveal crucial stages of FGF2 secretion. Synchronisation via PhoCl-based caging revealed the initial stages of secretion that were unknown and inaccessible otherwise. In addition, utilising the fully labelled SPT method, I could study the oligomerisation process of FGF2 and, indirectly, the FGF2 molecule's progression towards secretion. The study adds to the understanding of FGF2 dynamics in cells and explains the low rate of FGF2 secretion.

6 MATERIALS AND METHODS

6.1 CLONING

For TMEM-PhoCl-FGF2-GFP cloning, TMEM115 (Human) plasmid was bought from OriGene (cat# RG203956). pcDNA-NLS-PhoCl-mCherry was a gift from Robert Campbell. TMEM115 was cloned into peGFPC1 plasmid using NheI and BsrGI restriction sites. PhoCl, amplified from pcDNA-NLS-PhoCl-mCherry, was cloned into peGFPC1-TMEM115 plasmid using XhoI and HindIII restriction sites. Finally, FGF2-GFP was cloned into the peGFPC1-TMEM115-PhoCl plasmid using EcoRI and SalI restriction sites.

For mScarlet-CD4-PhoCl-RER cloning, a fusion construct comprising of a signal peptide (MWPLVAALLLGSACCGSA), sequences of mScarlet, transmembrane region of CD4 (STPVQPMALIVLGGVAGLLLFIGLGIFFCVRCRHRRR), PhoCl (a gift from R.E Campbell) and RER1 was synthesised by Thermofisher Scientific. The PhoCl was removed using the restriction enzymes HindIII and SacII, and replaced with Phocl 2c by Gibson cloning. The fusion construct was finally cloned into pTREtight2 vector (Addgene) using NheI and XbaI. pTREtight2 was a gift from Markus Ralser (Addgene plasmid # 19407 ; http://n2t.net/addgene:19407 ; RRID:Addgene_19407).

For making the Ca-PhoCl-TMEM and BK-PhoCl-TMEM constructs, Gibson cloning method was used[179]. Gene encoding the voltage gated Calcium channel, CACNA1E with GFP was amplified from pGEMHE-Caa1E-mEGFP plasmid (a gift from Max Ulbrich). Since the CACNA1E GFP sequence is very long(~6000bp), the CACNA1E gene was amplified into four shorter PCR fragments (named ca1, ca2, ca3, ca4-GFP) with overlapping ends of ~20 bp. First, two fragments, ca1 and ca2, with overlapping

ends with each other and with the vector, pTREtight2, were cloned using NEBuilder HiFi DNA Assembly. Next two fragments, ca3 and ca4 GFP, were cloned into the pTREtight2-ca1-ca2 vector. Finally fragments, TMEM115 and PhoCl 2c, were cloned into the pTREtight2-ca1-ca2-ca3-ca4 GFP vector. TMEM-PhoCl-Ca construct was similarly sequentially cloned using the NEBuilder HiFi DNA Assembly kit. BK PhoCl TMEM was constructed from the Ca-PhoCl-TMEM plasmid where the sequence for CACNA1E (Ca) was removed using restriction enzyme AgeI and the BK fragment was inserted using NEBuilder HiFi DNA Assembly. BK fragment was amplified from BK667 YFP plasmid [180], a gift from Teresa Giraldez.

6.2 CELL CULTURE AND TRANSFECTION

Cells were maintained with DMEM (Gibco Life Technologies) supplemented with 10% Fetal Bovine Serum (FBS) and 1% Glutamate (Gibco Life Technologies) at 37°C with 5% CO_2. For live cell experiments, the media was replaced with a live cell imaging media composed of 25mM HEPES in DMEM media supplemented with 10%FBS and 1% Glutamate.

For all experiments unless they were stable cell lines, cells were transfected using the Neon Transfection System (Thermofisher Scientific) or Lipofectamine3000 (Thermofisher Scientific). Fusion constructs with pTRE vectors were cotransfected with rtTA3 plasmids in the presence of 1ug/ul doxycycline.

6.3 OPTICAL SETUPS

6.3.1 Spinning Disk Confocal setup

PhoCl activation and standard fluorescence microscopy were performed on an inverted Olympus IX71 microscope equipped with a Yokogawa CSU-X1 spinning

disk. A 60x/ 1.42 NA oil Olympus objective was used together with 491 nm (100 mW; Cobolt), 561 nm (100 mW; Cobolt) and 645 nm (500 mW; Melles Griot) laser. A quad-edge dichroic beam splitter (446/ 523/ 600/ 677 nm; Semrock) was used to separate fluorescence emission from excitation light, and final images were taken with a sCMOS camera (Hamamatsu). Images were acquired with MetaMorph software.

6.3.2 Custom built TIRF microscope

All TIRF and SPT experiments were performed on a custom-built microscope [181]. Briefly, a 405 nm laser (360mW, Cobalt), 473 nm laser (500 mW; Laserglow Technologies), 561 nm laser (700 mW, Laserglow Technologies) and a 643-nm laser (500 mW; Toptica Photonics) were focused onto the back-focal plane of a TIRF objective (NA, 1.49; 60×; Olympus) for highly inclined plane illumination. A quad-edge dichroic beamsplitter (405/488/561/635 nm; Semrock) separated fluorescence emission from the excitation light. Emission light was filtered by a quad-band bandpass filter (446/523/600/677 nm; Semrock) and focused by a 500-mm tube lens onto the chip of a back-illuminated electron-multiplying charge-coupled device camera (Evolve; Photometrics) that was water-cooled to −85°C. Images were acquired with MicroManager [182].

For dual colour simultaneous microscopy, a long pass dichroic beamsplitter in the emission pathway was used to split the GFP and the far-red emissions and focused onto two halves of the chip of a back-illuminated electron-multiplying charge-coupled device camera.

6.4 LIVE CELL IMAGING

All experiments were performed at room temperature unless stated otherwise.

6.4.1 Uncaging and detecting uncaged proteins

CHO cells stably expressing TMEM-PhoCl-FGF2-GFP were seeded on no.1 18mm glass coverslips. Cells were illuminated with 10 s 405nm laser pulses. Movies were acquired before and after the 405 nm illumination at TIRF in the 491 nm channel for FGF2-GFP.

CV1 cells were co-transfected with rtTA3 and mScarlet-CD4-PhoCl-RER and seeded on grided glass bottom dishes (ibidi) in the presence of doxycycline (Clontech). Cells were incubated with RFP antibodies (Chromotek) labelled with NHS Alexa Fluor 647 for 15 min and imaged at the TIRF setup. The cells were illuminated with 5 s 405 nm laser pulses (12 mW/mm^2) every 15 s for five times. The cells were again incubated with RFP antibodies for 15 mins 3 hrs after the uncaging and subsequently imaged at the TIRF setup.

A similar protocol as that of uncaging of mScarlet-CD4-PhoCl-RER was followed for the uncaging and detecting uncaged BK. HeLa cells expressing BK-PhoCl-TMEM were used for the experiment. Anti-FLAG antibody was used to detect the PM localized BK channel through the extracellular N-terminus containing a FLAG tag. The cells were incubated with the antibodies 7 hrs after uncaging for the detection.

6.4.2 Single particle tracking experiments of FGF2 GFP/Halo

CHO cells stably expressing variant forms of FGF2 were seeded on no.1 18mm coverslips and imaged using the custom-built TIRF microscope setup with 50ms acquisition time.

Drug treatments

For $PI_{(4,5)}P_2$ depletion via ionomycin, cells were treated with 100 μM Ionomycin and 24 μM $CaCl_2$ for 2 mins. For Microtubule destabilization, cells were treated with 2.5 μg/ml Nocadazole for 6 hrs before they were imaged.

Detection of secreted FGF2

CV1 cells were transfected with plasmids encoding the cleaved version of FGF2-GFP or the original version of FGF2-GFP. A day after transfection, cells were incubated with Alexa Fluor 647 tagged anti-GFP nanobodies for 30 mins. Cells were then washed thrice with PBS and replaced with live cell imaging media before imaging.

Sample preparation for FGF2 oligomer study

For the FGF2-Halo experiments, CHO cells expressing FGF2-Halo were incubated with 1 μM JF635 ligand or 50 pM JF635 ligand for one hour. The cells were washed with PBS, and the media was replaced by fresh DMEM media for another hour. Cells were incubated with Heparan Salt for 10 mins and washed with PBS before live cell imaging in live cell imaging media. Cells with lower expression levels indicated by lower cytosolic background were chosen for imaging.

6.5 ELECTROPHYSIOLOGY

The experiments and analysis were performed by Dr. Sara Bertelli from Plested Lab. Whole-cell patch-clamp recordings were performed one day after transfection and doxycycline induction. Transfected HEK293 cells were seeded into gridded glass bottom dishes (Ibidi) and were exposed to UV light. Images of cells pre- and post- UV exposure were captured. Patch clamp experiments were performed in uncaged dishes and control dishes at the 7hrs timepoint after UV exposure.

Currents were acquired using an Axopatch 200B amplifier and the Axograph acquisition program (Axograph Scientific) via an Instrutech ITC-18 D-A interface (HEKA Elektronik). Currents were filtered at 5 kHz and digitized at 20 kHz.

Bath solution was composed as follows (in mM): 145 NaCl, 5 KCl, 1 MgCl2, 10 HEPES, 3 EGTA), pH 7.4. Given the high conductance of BK channels, the following internal (pipette) solution was used to reduce the current and minimize the series

resistance error (in mM): 90 NMDG-Cl, 50 KCl, 4 NaCl, 10 HEPES, 1 Mg-ATP, 10 EGTA, 2 CaCl2 pH 7.3.[183,184]

The series resistance of pipettes, RS, was between 2 and 6 MΩ, and the cell capacitance was between 3 and 25 pF, as measured by the compensating circuit of the amplifier. We accepted a maximal voltage-clamp error (calculated as the product of the maximum current and the uncompensated series resistance) of 10 mV.

The standard IV protocol to elicit BK currents consisted of 100-ms-long voltage steps ranging from -80 mV to +140mV in 20 mV increments, starting from a holding potential of 0 mV. No leak-current subtraction was performed. Figures were prepared using Igor Pro (https://www.wavemetrics.com/products/igorpro).

6.6 DATA ANALYSIS

6.6.1 Quantification of the number of molecules

The TIRF images of PM-bound FGF2, the secreted CD4 and BK molecules on the plasma membrane were analysed using ImageJ. Particles were detected and tracked using Trackmate [185] plugin from ImageJ[186]. Cell-specific Region of Interest (ROI) was manually drawn for every image, and the cell surface area was measured in ImageJ. The number of tracks was normalized to the cell surface area (μm^2) for the final quantification of the number of molecules.

6.6.2 Mobility analysis

TIRF images were tracked with Trackmate Plugin from ImageJ, and the output files, 'Track statistics.csv' and 'Spots in track statistics.csv', were saved for further analysis with Python.

For the classification of tracks as Mobile and Immobile, the maximum distance covered by the FGF2 molecule in x and y was calculated for each track. Tracks with a maximum distance of less than 300nm in x or y were classified as immobile tracks, and the rest as mobile tracks (Appendix 1, function: filter_mob_imm).

For the alpha histogram, the diffusion coefficient and the alpha were measured for each track (Appendix 1). In brief, molecule displacement in lag times of 1 to 5 frames was measured for each particle. The diffusion coefficient and the alpha were obtained from the curve of mean squared displacement and lag times (see Equation 2 from the Introduction). The alpha for all the tracks was pooled from three different days to obtain the final histograms.

6.6.3 Recruitment vs cytosol intensity

TIRF images were acquired and tracked as usual. The number of molecules at the plasma membrane refers to the number of tracks quantified through Trackmate normalised by the cell surface area. The minimum projected image of the movie was produced through ImageJ. This process removes the transient higher-intensity FGF2-GFP molecules at the membrane but retains the low-intensity cytosolic FGF2-GFP background. The cytosol intensity was obtained from the mean intensity of the cell in the projected image.

6.6.4 Dual colour single-molecule imaging

The cells expressing FGF2-GFP and FGF2-Halo were imaged using the dual channel setup at the custom-built TIRF microscope. Tetraspeck beads were diluted to 1:100 and added to plasma-cleaned coverslips, and imaged as references.

The final images were cropped in two, where the left half was the GFP channel, and the right half was the far red channel (Appendix 2). Due to imperfect alignment and chromatic aberration, the two-emission path after splitting does not create perfectly

aligned images on the camera. To correct the alignment, a transformation matrix was created using the cropped tetra speck bead images (Appendix 2). This transformation matrix was then applied to all the right-half images (Appendix 2). Both halves of the images were tracked with Trackmate. The obtained tracks were further analysed using a python code. Each track represents a single molecule. The number of FGF2-GFP molecules within a 100 nm radius of any FGF2-Halo molecule was counted and normalized with the total number of FGF2-GFP molecules on the cell membrane. To find out the number of random colocalisation between FGF2-GFP and FGF2-Halo, the FGF2-GFP tracks were assigned random coordinates within the cell boundary, and the extent of their colocalisation was measured (Appendix 2).

6.6.5 Oligomer state analysis

Generating Oligomer state distribution

CHO-FGF2-Halo cells labelled with 10 pM JF635 were used for monomer calibration. And cells labelled with 1 μM JF635 were assumed as fully labelled FGF2-Halo and were used for the final experiments.

Images were first background subtracted with a rolling ball of a radius of 10 pixels using Image J (Appendix 3). FGF2-Halo molecules were tracked using the Trackmate Plugin in ImageJ (Appendix 3), and the output files, 'Track statistics.csv' and 'Spots in track statistics.csv', were saved for further analysis with Python. Cell-specific ROI was manually drawn for every image, and their coordinates were saved as 'XY_Coordinates.csv'. This ROI is used at the tracking step to track only within the ROI. If it is not used at the tracking step, the XY coordinates of the ROI are used post-tracking (appendix 1c) to filter only tracks found within the cell ROI.

The mean intensity of the cytosol is measured for each cell and saved as 'Plot_Values.csv'. The average mean cytosolic intensity of the monomer samples is subtracted from the spot intensity of all FGF2 tracks (Appendix 3). The mean intensity of each FGF2 track was used to get a distribution for monomer FGF2-Halo as well as

fully labelled FGF2-Halo. The monomer FGF2-Halo intensity distribution was fitted with a single Gaussian in Origin to get the expected mean intensity of an FGF2-Halo monomer molecule.

The fully labelled FGF2-Halo intensities were divided by the expected mean of the monomer FGF2-Halo molecule to visualise the intensities in terms of the oligomer states (Appendix 3).

To estimate the percentage of each oligomeric species, the intensity distribution of fully labelled FGF2-Halo was fitted with multiple Gaussians with means that were multiples of the expected monomer mean using Origin. The area under each gaussian fit was used to find the percentage of each oligomeric state in the sample.

Analysing multi step tracks

The intensity profile (intensity vs time) for each track was run through a Matlab script (Appendix 4) to identify time points where the change in the intensity is bigger than a threshold. This change of intensity represents a recruitment event in case of an increase in intensity and a photobleaching or dissociation event in case of a decrease in intensity. Using this information, I extracted the intensity of different types of tracks (single step and multi-step) and different parts of the multi-step tracks (first step and incoming step) (Appendix 4). The oligomer species in each population (single step track, multi-step track, first step and incoming step) was finally extracted by multi-gaussian fitting with the expected means in Origin.

6.7 MATERIALS

Table 1: Reagents and kits

Reagents	Source
Nebuilder® hifi dna assembly cloning kit	New England Biolabs (NEB)
Gibson assembly® master mix	NEB
QIAquick® Gel extraction kit (250)	Qiagen
QIAGEN® Plasmid Plus Midi Kit	Qiagen
Neon™ Transfection System 10 µL Kit	Invitrogen
Lipofectamine 3000	Thermofisher Scientific
Phusion DNA polymerase	Molox
5X Phusion buffer	NEB
Deoxynucleotide (dNTP) solution mix (10 mM each dNTP)	NEB
ROTIPHORESE®50x Tris-acetate-EDTA (TAE) bufferROTIPHORESE®50x Tris-acetate-EDTA (TAE) buffer	Roth
standard agarose, ROTI®Garose	Roth
GelGreen® Nucleic Acid Gel Stain (10000x in DMSO)	Biotium
Gel Loading Dye, Purple (6X)	NEB
GeneRuler 1kb, DNA Ladder (0.5 µg/µl)	Thermofisher Scientific
AgeI, NheI, HindIII, EcoRI, SalI, BsrGI, XhoI	NEB
CutSmart® Buffer (10x)	NEB
FastAP thermosensitive alkaline phosphatase	Thermofisher Scientific
10X FastAP Buffer	Thermofisher Scientific
T4 DNA Ligase	NEB
10X T4 Ligase DNA Reaction Buffer with 10mM ATP	NEB
Luria Bertani (LB) broth	Roth
Ampicillin (100 mg/ml)	Roth
Kanamycin	Roth
Doxycycline	Clontech
Minimum Essential Medium Eagle. Alpha modification	Sigma-Aldrich
Dulbecco's Modified Eagle Medium (1X)	Gibco Life Technologies
Fetal bovine serum (FBS)	Gibco Life Technologies
GlutaMAX	Gibco Life Technologies
Penicillin-streptomycin	PAN-Biotech
HEPES buffer solution	Gibco Life Technologies
Heparan sodium salt from porcine intestinal mucosa, H3149-25KU	Merck
Ionomycin free acid	Bio-Techne GmbH
Poly-L-Lysine	Gibco Life Technologies

Immersol 518F	Zeiss
Immersion oil Type FF	Cargille

Table 2: Antibodies, ligands and dyes

Antibodies/dyes	Source
Anti-RFP antibody (5F8-α-Red)	Chromotek
Monclonal anti-FLAG antibody-M2 (F1804)	Sigma-Aldrich
GFP-Booster Alexa Fluor® 647	Chromotek
NHS ester Alexa Fluor® 647	ThermoFisher Scientific
Janelia Fluor 635 Halo ligand	Lavis Lab

Table 3: Materials and devices

Materials/Devices	Source	Comment
Glass coverslip 18mm #1	VWR	
µ-Dish 35mm, high Grid-500 glass bottom dish	Ibidi	
Magnetic coverslip holder	Chamlide	
Custom TIRF microscope		60×/NA 1.49 oil objective, EMCCD camera (Photometrics), Toptica Photonics (lasers), Semrock quad-edge dichroic beam splitter (446/ 523/ 600/ 677 nm), Semrock quad-band bandpass filter (446/523/600/677 nm)
Spinning disk confocal microscope	Olympus	Inverted IX71, 60×/NA 1.42 oil objective, CSU-X1 spinning disk (Yokogawa), iLas2 FRAP system (Gataca Systems), ORCA Flash 4.0LT CMOS camera (Hamamatsu)
Zeba Spin Desalting Columns (7 kDa MWCO)	Thermofisher Scientific	
Thermocycler	Eppendorf	
Thermomixer	Eppendorf	
Centrifuge	Eppendorf	Centrifuge 5417R, Centrifuge 5430R
Electrophoresis Power Supply-EPS 301	Amersham Biosciencs	
Neon Transfection System	Invitrogen	
Neubauer cell counting chamber	Assistent	
NanoDrop 1000	ThermoFisher Scientific	

Table 4: Softwares

Software	Use
ImageJ/Fiji	Image Analysis
Metamorph	Imaging software
Micromanager	Imaging software
OriginLab	Analysis
Microsoft Office	Analysis and presentation
Spyder	Integrated Development Environment (IDE) for Python scripting, Data Analysis
Matlab	Matlab scripting, Data Analysis
SnapGene	Cloning design
SerialCloner	Cloning design
Adobe Illustrator	Illustration

Table 5: Plasmids

Construct	Source	Comment
pLenti CMV rtTA3 Hygro (w785-1)	Addgene	pLenti CMV rtTA3 Hygro (w785-1) was a gift from Eric Campeau (Addgene plasmid # 26730 ; http://n2t.net/addgene:26730 ; RRID:Addgene_26730)
pTREtight2	Addgene	pTREtight2 was a gift from Markus Ralser (Addgene plasmid # 19407 ; http://n2t.net/addgene:19407 ; RRID:Addgene_19407)
peGFPC1	Clontech	
peGFPN1	Clontech	
pcDNA-NLS-PhoCl-mCherry	Addgene	pcDNA-NLS-PhoCl-mCherry was a gift from Robert Campbell (Addgene plasmid # 87691 ; http://n2t.net/addgene:87691 ; RRID:Addgene_87691)
TMEM 115 (GFP-tagged) Human transmembrane	OriGene Technologies, Inc.	CAT#: RG203956
PhoCl 2c	ThermoFisher, Genesynth	Sequence information given by Xiaocen Lu, Campbell Lab
pTREtight2-mScarlet-CD4-Phocl 2c-RER	Created within this thesis	
mScarlet-CD4-PhoCl-RER	Thermofisher Scientific, Genesynth	

BK667 plasmid	Gifted by Teresa Giraldez	
peGFPN1-LRRC8A-GFP	Stauber Lab	
pGEMHE-Caa1E-mEGFP	Gifted by Max Ulbrich	
pREV-TRE2-FGF2-GFP	Nickel Lab	
CD4-mRFP	Ewers Lab	

Table 6: Cell lines

Cell lines	Source
CHO-mCAT-TAM/CD2 (CHO-K1)	Received from Nickel Lab
CHO-K1-TMEM-PhoCl-FGF2-GFP	Cell line made by Roberto Salepicco (Nickel Lab)
CHO-K1-TMEM-PhoCl-FGF2-GFP K127Q/R128Q/K133Q	Cloning and Cell line made by Roberto Salepicco (Nickel Lab)
CHO-K1-TMEM-PhoCl-FGF2-GFP K54/60E/C77/95A/Y81F/K127Q/R128Q/K133Q	Cloning and Cell line made by Roberto Salepicco (Nickel Lab)
CHO-K1-TMEM-PhoCl-FGF2-GFP K54/60E/C77/95A	Cloning and Cell line made by Roberto Salepicco (Nickel Lab)
CHO-K1-FGF2-GFP	Received from Nickel Lab
CHO-K1-FGF2-Halo	Received from Nickel Lab
CHO-K1-FGF2-Halo-GPC1	Received from Nickel Lab
CV1	Ewers Lab
HeLA-M1	Ewers Lab
HEK293T	Ewers Lab

7 BIBLIOGRAPHY

1. Taylor, M. J., Husain, K., Gartner, Z. J., Mayor, S. & Vale, R. D. A DNA-Based T Cell Receptor Reveals a Role for Receptor Clustering in Ligand Discrimination. *Cell* **169**, 108-119.e20 (2017).

2. Joo, C., Balci, H., Ishitsuka, Y., Buranachai, C. & Ha, T. Advances in single-molecule fluorescence methods for molecular biology. *Annual Review of Biochemistry* vol. 77 51–76 Preprint at https://doi.org/10.1146/annurev.biochem.77.070606.101543 (2008).

3. Yildiz, A. *et al.* Myosin V walks hand-over-hand: Single fluorophore imaging with 1.5-nm localization. *Science (1979)* **300**, 2061–2065 (2003).

4. Kural, C. *et al.* Cell Biology: Kinesin and dynein move a peroxisome in vivo: A tug-of-war or coordinated movement? *Science (1979)* **308**, 1469–1472 (2005).

5. Jolly, A. L. & Gelfand, V. I. Bidirectional intracellular transport: utility and mechanism. *Biochem Soc Trans* **39**, 1126 (2011).

6. Ali, M. Y. *et al.* Myosin Va and myosin VI coordinate their steps while engaged in an in vitro tug of war during cargo transport. *Proc Natl Acad Sci U S A* **108**, E535 (2011).

7. Noji, H., Yasuda, R., Yoshida, M. & Kinosita, K. Direct observation of the rotation of F1-ATPase. *Nature 1997 386:6622* **386**, 299–302 (1997).

8. Yasuda, R., Noji, H., Yoshida, M., Kinosita, K. & Itoh, H. Resolution of distinct rotational substeps by submillisecond kinetic analysis of F1-ATPase. *Nature* **410**, 898–904 (2001).

9. Cai, L., Friedman, N. & Xie, X. S. Stochastic protein expression in individual cells at the single molecule level. *Nature 2006 440:7082* **440**, 358–362 (2006).

10. Larson, D. R., Singer, R. H. & Zenklusen, D. A Single Molecule View of Gene Expression. *Trends Cell Biol* **19**, 630 (2009).

11. Yu, J., Xiao, J., Ren, X., Lao, K. & Xie, X. S. Probing gene expression in live cells, one protein molecule at a time. *Science (1979)* **311**, 1600–1603 (2006).

12. Golding, I., Paulsson, J., Zawilski, S. M. & Cox, E. C. Real-time kinetics of gene activity in individual bacteria. *Cell* **123**, 1025–1036 (2005).

13. Elf, J., Li, G. W. & Xie, X. S. Probing transcription factor dynamics at the single-molecule level in a living cell. *Science* **316**, 1191–1194 (2007).

14. Li, G. W. & Xie, X. S. Central dogma at the single-molecule level in living cells. *Nature 2011 475:7356* **475**, 308–315 (2011).

15. da Rocha-Azevedo, B. *et al.* Heterogeneity in VEGF Receptor-2 Mobility and Organization on the Endothelial Cell Surface Leads to Diverse Models of Activation by VEGF. *Cell Rep* **32**, 108187 (2020).

16. Wilmes, S. *et al.* Receptor dimerization dynamics as a regulatory valve for plasticity of type I interferon signaling. *J Cell Biol* **209**, 579 (2015).

17. Deliz-Aguirre, R. *et al.* MyD88 oligomer size functions as a physical threshold to trigger IL1R myddosome signaling. *Journal of Cell Biology* **220**, (2021).

18. Sako, Y., Minoghchi, S. & Yanagida, T. Single-molecule imaging of EGFR signalling on the surface of living cells. *Nat Cell Biol* **2**, 168–172 (2000).

19. SHIMOMURA, O., JOHNSON, F. H. & SAIGA, Y. Extraction, Purification and Properties of Aequorin, a Bioluminescent Protein from the Luminous Hydromedusan, Aequorea. *J Cell Comp Physiol* **59**, 223–239 (1962).

20. Abbe, E. Beiträge zur Theorie des Mikroskops und der mikroskopischen Wahrnehmung. *Archiv für Mikroskopische Anatomie 1873 9:1* **9**, 413–468 (1873).

21. Born, M. & Wolf, Emil. Principles of optics : electromagnetic theory of propagation, interference and diffraction of light. (1997).

22. Axelrod, D. Cell-substrate contacts illuminated by total internal reflection fluorescence. *Journal of Cell Biology* **89**, 141–145 (1981).

23. Axelrod, D., Burghardt, T. P. & Thompson, N. L. Total internal reflection fluorescence. *Annu Rev Biophys Bioeng* **13**, 247–268 (1984).

24. Kato-Yamada, Y., Noji, H., Yasuda, R., Kinosita, K. & Yoshida, M. Direct observation of the rotation of epsilon subunit in F1-ATPase. *J Biol Chem* **273**, 19375–19377 (1998).

25. Douglass, A. D. & Vale, R. D. Single-molecule microscopy reveals plasma membrane microdomains created by protein-protein networks that exclude or trap signaling molecules in T cells. *Cell* **121**, 937–950 (2005).

26. Ulbrich, M. H. & Isacoff, E. Y. Subunit counting in membrane-bound proteins. *Nat Methods* **4**, 319–321 (2007).

27. Kohout, S. C., Ulbrich, M. H., Bell, S. C. & Isacoff, E. Y. Subunit organization and functional transitions in Ci-VSP. *Nat Struct Mol Biol* **15**, 106–108 (2008).

28. Tombola, F., Ulbrich, M. H. & Isacoff, E. Y. The voltage-gated proton channel Hv1 has two pores each controlled by one voltage sensor. *Neuron* **58**, 546 (2008).

29. Fujiwara, T., Ritchie, K., Murakoshi, H., Jacobson, K. & Kusumi, A. Phospholipids undergo hop diffusion in compartmentalized cell membrane. *J Cell Biol* **157**, 1071–1081 (2002).

30. V.P.L.S., R. B. F. R. S. Hon. M. R. S. E. & R. I. Acad. XXVII. A brief account of microscopical observations made in the months of June, July and August 1827, on the particles contained in the pollen of plants; and on the general existence of active molecules in organic and inorganic bodies. *https://doi.org/10.1080/14786442808674769* **4**, 161–173 (2009).

31. Nelson, P. biological physics. *Proc Natl Acad Sci U S A* **4**, 1–25 (2013).

32. Einstein, A. Über die von der molekularkinetischen Theorie der Wärme geforderte Bewegung von in ruhenden Flüssigkeiten suspendierten Teilchen. *Ann Phys* **322**, 549–560 (1905).

33. Saffman, P. G. & Delbrueck, M. Brownian motion in biological membranes. *Proceedings of the National Academy of Sciences* **72**, 3111–3113 (1975).

34. Matthews, J. M. & Sunde, M. Dimers, oligomers, everywhere. *Adv Exp Med Biol* **747**, 1–18 (2012).

35. Weiss, A. & Schlessinger, J. Switching signals on or off by receptor dimerization. *Cell* **94**, 277–280 (1998).

36. Voss, F. K. *et al.* Identification of LRRC8 heteromers as an essential component of the volume-regulated anion channel VRAC. *Science (1979)* **344**, 634–638 (2014).

37. Funnell, A. P. W. & Crossley, M. Homo- and heterodimerization in transcriptional regulation. *Adv Exp Med Biol* **747**, 105–121 (2012).

38. Amoutzias, G. D., Robertson, D. L., van de Peer, Y. & Oliver, S. G. Choose your partners: dimerization in eukaryotic transcription factors. *Trends Biochem Sci* **33**, 220–229 (2008).

39. de Oliveira, G. A. P. *et al.* The status of p53 oligomeric and aggregation states in cancer. *Biomolecules* vol. 10 Preprint at https://doi.org/10.3390/biom10040548 (2020).

40. Schmidt, T. Local stoichiometries determined by counting individual molecules. *Anal Chem* **68**, 4397–4401 (1996).

41. Huseyin, M. K. & Klose, R. J. Live-cell single particle tracking of PRC1 reveals a highly dynamic system with low target site occupancy. *Nature Communications 2021 12:1* **12**, 1–20 (2021).

42. Boncompain, G. *et al.* Synchronization of secretory protein traffic in populations of cells. *Nat Methods* **9**, 493–498 (2012).

43. Chen, D., Gibson, E. S. & Kennedy, M. J. A light-triggered protein secretion system. *Journal of Cell Biology* **201**, 631–640 (2013).

44. Bourke, A. M. *et al.* zapERtrap: A light-regulated ER release system reveals unexpected neuronal trafficking pathways. *Journal of Cell Biology* **220**, (2021).

45. Zhang, W. *et al.* Optogenetic control with a photocleavable protein, Phocl. *Nat Methods* **14**, 391–394 (2017).

46. Banfield, D. K. Mechanisms of Protein Retention in the Golgi. *Cold Spring Harb Perspect Biol* **3**, 1–14 (2011).

47. van M Eer, G. *LIPID TRAFFIC IN ANIMAL CELLS*. *Annu. Rev. Cell BioI* vol. 5 www.annualreviews.org (1989).

48. Bretscher, M. S. & Munro, S. Cholesterol and the golgi apparatus. *Science (1979)* **261**, 1280–1281 (1993).

49. Mitra, K., Ubarretxena-Belandia, I., Taguchi, T., Warren, G. & Engelman, D. M. Modulation of the bilayer thickness of exocytic pathway membranes by membrane proteins rather than cholesterol. *Proc Natl Acad Sci U S A* **101**, 4083–4088 (2004).

50. Sharpe, H. J., Stevens, T. J. & Munro, S. A Comprehensive Comparison of Transmembrane Domains Reveals Organelle-Specific Properties. *Cell* **142**, 158–169 (2010).

51. Munro, S. A comparison of the transmembrane domains of Golgi and plasma membrane proteins. *Biochem Soc Trans* **23**, 527–530 (1995).

52. Bretscher, M. S. & Munro, S. Cholesterol and the golgi apparatus. *Science (1979)* **261**, 1280–1281 (1993).

53. Nilsson, T., Slusarewicz, P., Hoe, M. H. & Warren, G. Kin recognition. *FEBS Lett* **330**, 1–4 (1993).

54. Weisz, O. A., Swift, A. M. & Machamer, C. E. Oligomerization of a membrane protein correlates with its retention in the Golgi complex. *Journal of Cell Biology* **122**, 1185–1196 (1993).

55. Nilsson, T., Rabouille, C., Hui, N., Watson, R. & Warren, G. The role of the membrane-spanning domain and stalk region of N-acetylglucosaminyltransferase I in retention, kin recognition and structural maintenance of the Golgi apparatus in HeLa cells. *J Cell Sci* **109**, 1975–1989 (1996).

56. Opat, A. S., Houghton, F. & Gleeson, P. A. Medial Golgi but not late golgi glycosyltransferases exist as high molecular weight complexes. Role of luminal domain in complex formation and localization. *Journal of Biological Chemistry* **275**, 11836–11845 (2000).

57. Qian, R., Chen, C. & Colley, K. J. Location and Mechanism of α2,6-Sialyltransferase Dimer Formation. *Journal of Biological Chemistry* **276**, 28641–28649 (2001).

58. Fenteany, F. H. & Colley, K. J. Multiple signals are required for α2,6-sialyltransferase (ST6Gal I) oligomerization and golgi localization. *Journal of Biological Chemistry* **280**, 5423–5429 (2005).

59. Stalder, D. & Gershlick, D. C. Direct trafficking pathways from the Golgi apparatus to the plasma membrane. *Semin Cell Dev Biol* **107**, 112 (2020).

60. Lu, X. *et al.* Photocleavable proteins that undergo fast and efficient dissociation. *Chem Sci* **12**, 9658–9672 (2021).

61. Adam, V. *et al.* Data storage based on photochromic and photoconvertible fluorescent proteins. *J Biotechnol* **149**, 289–298 (2010).

62. Spivak-Kroizman, T. *et al.* Heparin-induced oligomerization of FGF molecules is responsible for FGF receptor dimerization, activation, and cell proliferation. *Cell* **79**, 1015–1024 (1994).

63. Ornitz, D. M. & Itoh, N. The Fibroblast Growth Factor signaling pathway. *Wiley Interdiscip Rev Dev Biol* **4**, 215–266 (2015).

64. Ornitz, D. M. *et al.* Receptor specificity of the fibroblast growth factor family. *Journal of Biological Chemistry* **271**, 15292–15297 (1996).

65. Zhang, X. *et al.* Receptor specificity of the fibroblast growth factor family: The complete mammalian FGF family. *Journal of Biological Chemistry* **281**, 15694–15700 (2006).

66. Goetz, R. & Mohammadi, M. Exploring mechanisms of FGF signalling through the lens of structural biology. *Nature Reviews Molecular Cell Biology* vol. 14 166–180 Preprint at https://doi.org/10.1038/nrm3528 (2013).

67. Chandler, L. A. *et al.* Prevalent expression of fibroblast growth factor (FGF) receptors and FGF2 in human tumor cell lines. *Int J Cancer* **81**, 451–458 (1999).

68. Ahmad, I., Iwata, T. & Leung, H. Y. Mechanisms of FGFR-mediated carcinogenesis. *Biochim Biophys Acta* **1823**, 850–860 (2012).

69. Bikfalvi, A., Klein, S., Pintucci, G. & Rifkin, D. B. Biological Roles of Fibroblast Growth Factor-2. *Endocr Rev* **18**, 26–45 (1997).

70. Werner, S. & Grose, R. Regulation of wound healing by growth factors and cytokines. *Physiological Reviews* vol. 83 835–870 Preprint at https://doi.org/10.1152/physrev.2003.83.3.835 (2003).

71. Sepp, N. T. *et al.* Bacic fibroblast growth factor increases epression of the αvβ3 integrin complex on human microvascular endothelial cells. *Journal of Investigative Dermatology* **103**, 295–299 (1994).

72. Gualandris, A. & Presta, M. Transcriptional and posttranscriptional regulation of urokinase-type plasminogen activator expression in endothelial cells by basic fibroblast growth factor. *J Cell Physiol* **162**, 400–409 (1995).

73. Presta, M., Besser, D. & Nagamine, Y. *Elucidation of a Signaling Pathway Induced by FGF-2 Leading to uPA Gene Expression in NIH 3T3 Fibroblasts'. Cell Growth & Differentiation* vol. 6 https://www.researchgate.net/publication/14653729 (1995).

74. Powers, C. J., Mcleskey, S. W. & Wellstein, A. *Fibroblast growth factors, their receptors and signaling. Endocrine-Related Cancer* vol. 7 http://www.endocrinology.org (2000).

75. Nishida, N., Yano, H., Nishida, T., Kamura, T. & Kojiro, M. Angiogenesis in Cancer. *Vasc Health Risk Manag* **2**, 213–219 (2006).

76. Akl, M. R. *et al.* Molecular and clinical significance of fibroblast growth factor 2 (FGF2 /bFGF) in malignancies of solid and hematological cancers for personalized therapies. *Oncotarget* **7**, 44735–44762 (2016).

77. Arnedos, M., Andre, F., Soria, J. C. & Dieci, M. V. Fibroblast growth factor receptor inhibitors as a cancer treatment: From a biologic rationale to medical perspectives. *Cancer Discov* **3**, 264–279 (2013).

78. Owji, H., Nezafat, N., Negahdaripour, M., Hajiebrahimi, A. & Ghasemi, Y. A comprehensive review of signal peptides: Structure, roles, and applications. *Eur J Cell Biol* **97**, 422–441 (2018).

79. Cooper, D. N. W. & Barondes, S. H. Evidence for export of a muscle lectin from cytosol to extracellular matrix and for a novel secretory mechanism. *Journal of Cell Biology* **110**, 1681–1691 (1990).

80. Hughes, R. C. Secretion of the galectin family of mammalian carbohydrate-binding proteins. *Biochimica et Biophysica Acta (BBA) - General Subjects* **1473**, 172–185 (1999).

81. Cho, M. & Cummings, R. D. Galectin-1, a β-Galactoside-binding Lectin in Chinese Hamster Ovary Cells: I. PHYSICAL AND CHEMICAL CHARACTERIZATION. *Journal of Biological Chemistry* **270**, 5198–5206 (1995).

82. Rubartelli, A., Cozzolino, F., Talio, M. & Sitia, R. A novel secretory pathway for interleukin-1 beta, a protein lacking a signal sequence. *EMBO J* **9**, 1503–1510 (1990).

83. Kinseth, M. A. *et al.* The Golgi-Associated Protein GRASP Is Required for Unconventional Protein Secretion during Development. *Cell* **130**, 524–534 (2007).

84. Scaffidi, P., Misteli, T. & Bianchi, M. E. Release of chromatin protein HMGB1 by necrotic cells triggers inflammation. *Nature 2002 418:6894* **418**, 191–195 (2002).

85. Gardella, S. *et al.* The nuclear protein HMGB1 is secreted by monocytes via a non-classical, vesicle-mediated secretory pathway. *EMBO Rep* **3**, 995–1001 (2002).

86. Bonaldi, T. *et al.* Monocytic cells hyperacetylate chromatin protein HMGB1 to redirect it towards secretion. *EMBO J* **22**, 5551–5560 (2003).

87. Ericson, M. L., Horling, J., Wendel-Hansen, V., Holmgren, A. & Rosen, A. Secretion of thioredoxin after in vitro activation of human B cells. *Lymphokine Cytokine Res* **11**, 201–207 (1992).

88. Rubartelli, A., Bajetto, A., Allavena, G., Wollman, E. & Sitia, R. Secretion of thioredoxin by normal and neoplastic cells through a leaderless secretory pathway. *Journal of Biological Chemistry* **267**, 24161–24164 (1992).

89. Maizel, A. *et al.* Engrailed homeoprotein secretion is a regulated process. *Development* **129**, 3545–3553 (2002).

90. Maizel, A., Bensaude, O., Prochiantz, A. & Joliot, A. A short region of its homeodomain is necessary for engrailed nuclear export and secretion. *Development* **126**, 3183–3190 (1999).

91. Joliot, A. *et al.* Identification of a signal sequence necessary for the unconventional secretion of Engrailed homeoprotein. *Current Biology* **8**, 856–863 (1998).

92. Dupont, E., Prochiantz, A. & Joliot, A. Identification of a Signal Peptide for Unconventional Secretion *. *Journal of Biological Chemistry* **282**, 8994–9000 (2007).

93. Rabouille, C., Malhotra, V. & Nickel, W. Diversity in unconventional protein secretion. *J Cell Sci* **125**, 5251–5255 (2012).

94. Ornitz, D. M. & Itoh, N. The Fibroblast Growth Factor signaling pathway. *Wiley Interdiscip Rev Dev Biol* **4**, 215 (2015).

95. Nakanishi, Y. *et al.* Direct effect of basic fibroblast growth factor on gene transcription in a cell-free system. *Proc Natl Acad Sci U S A* **89**, 5216–5220 (1992).

96. J Arne Â, E. S. & Holmgren, A. Physiological functions of thioredoxin and thioredoxin reductase.

97. Kondo, N. *et al.* Redox-Sensing Release of Human Thioredoxin from T Lymphocytes with Negative Feedback Loops. *The Journal of Immunology* **172**, 442–448 (2004).

98. Pekkari, K., Gurunath, R., Arner, E. S. J. & Holmgren, A. Truncated Thioredoxin Is a Mitogenic Cytokine for Resting Human Peripheral Blood Mononuclear Cells and Is Present in Human Plasma *. *Journal of Biological Chemistry* **275**, 37474–37480 (2000).

99. Pekkari, K., Goodarzi, M. T., Scheynius, A., Holmgren, A. & Avila-Cariño, J. Truncated thioredoxin (Trx80) induces differentiation of human CD14+ monocytes into a novel cell type (TAMs) via activation of the MAP kinases p38, ERK, and JNK. *Blood* **105**, 1598–1605 (2005).

100. Pekkari, K. *et al.* Truncated thioredoxin (Trx80) exerts unique mitogenic cytokine effects via a mechanism independent of thiol oxido-reductase activity. *FEBS Lett* **539**, 143–148 (2003).

101. Pekkari, K. *et al.* Truncated thioredoxin (Trx80) induces production of interleukin-12 and enhances CD14 expression in human monocytes. *Blood* **97**, 3184–3190 (2001).

102. Angelini, G. *et al.* Antigen-presenting dendritic cells provide the reducing extracellular microenvironment required for T lymphocyte activation. *Proc Natl Acad Sci U S A* **99**, 1491–1496 (2002).

103. Nishinaka, Y., Nakamura, H. & Yodoi, J. Thioredoxin cytokine action. *Methods Enzymol* **347**, 332–338 (2002).

104. Nakamura, H., Masutani, H. & Yodoi, J. Extracellular thioredoxin and thioredoxin-binding protein 2 in control of cancer. *Semin Cancer Biol* **16**, 444–451 (2006).

105. Bianchi, M. E. & Agresti, A. HMG proteins: dynamic players in gene regulation and differentiation. *Curr Opin Genet Dev* **15**, 496–506 (2005).

106. Bianchi, M., Agresti, A., Bianchi, M. E., Tamkun, J. & Stillman, D. HMGB proteins and gene expression HMGB proteins and gene expression This review comes from a themed issue on Chromosomes and expression mechanisms Edited by. *Curr Opin Genet Dev* **13**, 170–178 (2003).

107. Gardella, S. *et al.* The nuclear protein HMGB1 is secreted by monocytes via a non-classical, vesicle-mediated secretory pathway. *EMBO Rep* **3**, 995–1001 (2002).

108. Erlandsson, L., Andersson, K., Sigvardsson, M., Lycke, N. & Leanderson, T. Mice with an inactivated joining chain locus have perturbed IgM secretion. doi:10.1002/(SICI)1521-4141(199808)28:08.

109. Yang, H., Wang, H., Czura, C. J. & Tracey, K. J. The cytokine activity of HMGB1. *J Leukoc Biol* **78**, 1–8 (2005).

110. Wang, H. *et al.* HMG-1 as a late mediator of endotoxin lethality in mice. *Science (1979)* **285**, 248–251 (1999).

111. Wang, H. *et al.* Cholinergic agonists inhibit HMGB1 release and improve survival in experimental sepsis. *Nature Medicine 2004 10:11* **10**, 1216–1221 (2004).

112. Wang, H., Yang, H., Tracey, K. J., Wang, A. H. & North Shore-, T. K. Extracellular role of HMGB1 in inflammation and sepsis. *J Intern Med* **255**, 320–331 (2004).

113. Brough, D., Pelegrin, P. & Nickel, W. An emerging case for membrane pore formation as a common mechanism for the unconventional secretion of FGF2 and IL-1β. *J Cell Sci* **130**, 3197–3202 (2017).

114. Hughes, R. C. Secretion of the galectin family of mammalian carbohydrate-binding proteins. *Biochimica et Biophysica Acta (BBA) - General Subjects* **1473**, 172–185 (1999).

115. Cleves, A. E. Protein transport: The nonclassical ins and outs. *Current Biology* **7**, R318–R320 (1997).

116. Monzat, V. *et al.* Expression of two FGF-2 isoforms in pancreatic acinar cells (AR4-2J). Intracellular localization and role in the regulation of the extracellular matrix biosynthesis. *Eur J Cell Biol* **69**, 316–326 (1996).

117. Bugler, B., Amalric, F. & Prats2, H. Alternative initiation of translation determines cytoplasmic or nuclear localization of basic fibroblast growth factor. *Mol Cell Biol* **11**, 573–577 (1991).

118. Renko, M., Quarto, N., Morimoto, T. & Rifkin, D. B. Nuclear and cytoplasmic localization of different basic fibroblast growth factor species. *J Cell Physiol* **144**, 108–114 (1990).

119. Engling, A. *et al.* Biosynthetic FGF-2 is targeted to non-lipid raft microdomains following translocation to the extracellular surface of CHO cells. *J Cell Sci* **115**, 3619–3631 (2002).

120. Wegehingel, S., Zehe, C. & Nickel, W. Rerouting of fibroblast growth factor 2 to the classical secretory pathway results in post-translational modifications that block binding to heparan sulfate proteoglycans. *FEBS Lett* **582**, 2387–2392 (2008).

121. Nickel, W. & Rabouille, C. Mechanisms of regulated unconventional protein secretion. *Nat Rev Mol Cell Biol* **10**, 148–155 (2009).

122. McNeil, P. L., Muthukrishnan, L., Warder, E. & D'Amore, P. A. Growth factors are released by mechanically wounded endothelial cells. *Journal of Cell Biology* **109**, 811–822 (1989).

123. Nickel, W. The mystery of nonclassical protein secretion: A current view on cargo proteins and potential export routes. *Eur J Biochem* **270**, 2109–2119 (2003).

124. Florkiewicz, R. Z., Majack, R. A., Buechler, R. D. & Florkiewicz, E. Quantitative export of FGF-2 occurs through an alternative, energy-dependent, non-ER/Golgi pathway. *J Cell Physiol* **162**, 388–399 (1995).

125. Trudel, C., Faure-Desire, V., Florkiewicz, R. Z. & Baird, A. Translocation of FGF2 to the Cell Surface Without Release Into Conditioned Media. *J. Cell. Physiol* **185**, 260–268 (2000).

126. Mignatti, P., Morimoto, T. & Rifkin, D. B. Basic fibroblast growth factor, a protein devoid of secretory signal sequence, is released by cells via a pathway independent of the endoplasmic reticulum-Golgi complex. *J Cell Physiol* **151**, 81–93 (1992).

127. Steringer, J. P. *et al.* Key steps in unconventional secretion of fibroblast growth factor 2 reconstituted with purified components. *Elife* **6**, 1–36 (2017).

128. Steringer, J. P. & Nickel, W. The molecular mechanism underlying unconventional secretion of Fibroblast Growth Factor 2 from tumour cells. *Biol Cell* **109**, 375–380 (2017).

129. Temmerman, K. *et al.* A Direct Role for Phosphatidylinositol-4,5-bisphosphate in Unconventional Secretion of Fibroblast Growth Factor 2. *Traffic* **9**, 1204–1217 (2008).

130. Lolicato, F. *et al.* Cholesterol promotes both head group visibility and clustering of PI (4 , 5) P 2 driving unconventional secretion of Fibroblast Growth Factor 2. **2**, 1–30 (2021).

131. Dimou, E. *et al.* Single event visualization of unconventional secretion of FGF2. *Journal of Cell Biology* **218**, (2019).

132. Sparn, C. *et al.* Glypican-1 drives unconventional secretion of Fibroblast Growth Factor 2. doi:10.1101/2021.11.11.468179.

133. Wegehingel, S., Scha, T., Nickel, W. & Zehe, C. Cell-surface heparan sulfate proteoglycans are essential components of the unconventional export machinery of FGF-2. **103**, 15479–15484 (2006).

134. Sommer, A. & Rifkin, D. B. Interaction of heparin with human basic fibroblast growth factor: Protection of the angiogenic protein from proteolytic degradation by a glycosaminoglycan. *J Cell Physiol* **138**, 215–220 (1989).

135. Saksela, O., Moscatelli, D., Sommer, A. & Rifkin, D. B. Endothelial cell-derived heparan sulfate binds basic fibroblast growth factor and protects it from proteolytic degradation. *Journal of Cell Biology* **107**, 743–751 (1988).

136. Gospodarowicz, D. & Cheng, J. Heparin protects basic and acidic FGF from inactivation. *J Cell Physiol* **128**, 475–484 (1986).

137. Ornitz, D. M. & Itoh, N. Protein family review Fibroblast growth factors. *Genome Biol* **2**, reviews3005.1 (2001).

138. Vlodavsky, I., Miao, H. Q., Medalion, B., Danagher, P. & Ron, D. Involvement of heparan sulfate and related molecules in sequestration and growth promoting activity of fibroblast growth factor. *Cancer Metastasis Rev* **15**, 177–186 (1996).

139. Gould, S. E., Upholt, W. B. & Kosher, R. A. Characterization of chicken syndecan-3 as a heparan sulfate proteoglycan and its expression during embryogenesis. *Dev Biol* **168**, 438–451 (1995).

140. Cohn, M. J., Izpisúa-Belmonte, J. C., Abud, H., Heath, J. K. & Tickle, C. Fibroblast growth factors induce additional limb development from the flank of chick embryos. *Cell* **80**, 739–746 (1995).

141. Klagsbrun, M. & Baird, A. A dual receptor system is required for basic fibroblast growth factor activity. *Cell* **67**, 229–231 (1991).

142. BAIRD, A. & KLAGSBRUN, M. The Fibroblast Growth Factor Family An Overview. *Ann N Y Acad Sci* **638**, xi–xii (1991).

143. Pellegrini, L. Role of heparan sulfate in fibroblast growth factor signalling: a structural view. *Curr Opin Struct Biol* **11**, 629–634 (2001).

144. Sparn, C. *et al.* Glypican-1 drives unconventional secretion of Fibroblast Growth Factor 2. *Elife* **11**, (2022).

145. Müller, H. M. *et al.* Formation of Disulfide Bridges Drives Oligomerization, Membrane Pore Formation, and Translocation of Fibroblast Growth Factor 2 to Cell Surfaces. *J Biol Chem* **290**, 8925 (2015).

146. Steringer, J. P. *et al.* Key steps in unconventional secretion of fibroblast growth factor 2 reconstituted with purified components. *Elife* **6**, 1–36 (2017).

147. Steringer, J. P. *et al.* Phosphatidylinositol 4,5-bisphosphate (PI(4,5)P2)-dependent oligomerization of fibroblast growth factor 2 (FGF2) triggers the formation of a lipidic membrane pore implicated in unconventional secretion. *Journal of Biological Chemistry* **287**, 27659–27669 (2012).

148. Nickel, W. & Seedorf, M. Unconventional Mechanisms of Protein Transport to the Cell Surface of Eukaryotic Cells. *http://dx.doi.org/10.1146/annurev.cellbio.24.110707.175320* **24**, 287–308 (2008).

149. Nickel, W. The unconventional secretory machinery of fibroblast growth factor 2. *Traffic* **12**, 799–805 (2011).

150. Qian, S., Wang, C., Yang, L. & Huang, H. W. Structure of transmembrane pore induced by Bax-derived peptide: Evidence for lipidic pores. *Proceedings of the National Academy of Sciences* **105**, 17379–17383 (2008).

151. Steringer, J. P., Müller, H. M. & Nickel, W. Unconventional Secretion of Fibroblast Growth Factor 2—A Novel Type of Protein Translocation across Membranes? *J Mol Biol* **427**, 1202–1210 (2015).

152. la Venuta, G., Zeitler, M., Steringer, J. P., Müller, H. M. & Nickel, W. The startling properties of fibroblast growth factor 2: How to exit mammalian cells without a signal peptide at hand. *Journal of Biological Chemistry* **290**, 27015–27020 (2015).

153. Steringer, J. P. & Nickel, W. The molecular mechanism underlying unconventional secretion of Fibroblast Growth Factor 2 from tumour cells. *Biol Cell* **109**, 375–380 (2017).

154. Ebert, A. D. *et al.* Tec-Kinase-Mediated Phosphorylation of Fibroblast Growth Factor 2 is Essential for Unconventional Secretion. *Traffic* **11**, 813–826 (2010).

155. Zacherl, S. *et al.* A Direct Role for ATP1A1 in Unconventional Secretion of Fibroblast Growth Factor 2 *. *Journal of Biological Chemistry* **290**, 3654–3665 (2015).

156. Nickel, W. Pathways of unconventional protein secretion. *Curr Opin Biotechnol* **21**, 621–626 (2010).

157. Kaplan, J. H. Biochemistry of Na,K-ATPase. *Annu Rev Biochem* **71**, 511–535 (2002).

158. Legrand, C. *et al.* The Na,K-ATPase acts upstream of phosphoinositide PI(4,5)P2 facilitating unconventional secretion of Fibroblast Growth Factor 2. *Commun Biol* **3**, 1–16 (2020).

159. Lu, X. *et al.* Improved Photocleavable Proteins with Faster and More Efficient Dissociation. *bioRxiv* 2020.12.10.419556 (2020) doi:10.1101/2020.12.10.419556.

160. Zehe, C., Engling, A., Wegehingel, S., Schäfer, T. & Nickel, W. Cell-surface heparan sulfate proteoglycans are essential components of the unconventional export machinery of FGF-2. *Proc Natl Acad Sci U S A* **103**, 15479 (2006).

161. Levental, I., Levental, K. R. & Heberle, F. A. Lipid Rafts: Controversies Resolved, Mysteries Remain. *Trends Cell Biol* **30**, 341–353 (2020).

162. Fujiwara, T., Ritchie, K., Murakoshi, H., Jacobson, K. & Kusumi, A. Phospholipids undergo hop diffusion in compartmentalized cell membrane. *Journal of Cell Biology* **157**, 1071–1081 (2002).

163. Singer, S. J. & Nicolson, G. L. The Fluid Mosaic Model of the Structure of Cell Membranes. *Science (1979)* **175**, 720–731 (1972).

164. Kusumi, A. *et al.* Dynamic Organizing Principles of the Plasma Membrane that Regulate Signal Transduction: Commemorating the Fortieth Anniversary of Singer and Nicolson's Fluid-Mosaic Model. *https://doi.org/10.1146/annurev-cellbio-100809-151736* **28**, 215–250 (2012).

165. Trimble, W. S. & Grinstein, S. Barriers to the free diffusion of proteins and lipids in the plasma membrane. *J Cell Biol* **208**, 259 (2015).

166. Golebiewska, U., Nyako, M., Woturski, W., Zaitseva, I. & Mclaughlin, S. Diffusion Coefficient of Fluorescent Phosphatidylinositol 4,5-bisphosphate in the Plasma Membrane of Cells. *Mol Biol Cell* **19**, 1663–1669 (2008).

167. McLaughlin, S. & Murray, D. Plasma membrane phosphoinositide organization by protein electrostatics. *Nature 2005 438:7068* **438**, 605–611 (2005).

168. van den Bogaart, G. *et al.* Membrane protein sequestering by ionic protein–lipid interactions. *Nature 2011 479:7374* **479**, 552–555 (2011).

169. Hammond, G. R. V., Sim, Y., Lagnado, L. & Irvine, R. F. Reversible binding and rapid diffusion of proteins in complex with inositol lipids serves to coordinate free movement with spatial information. *Journal of Cell Biology* **184**, 297–308 (2009).

170. Pacheco, J., Cassidy, A. C., Zewe, J. P., Wills, R. C. & Hammond, G. R. v. Free diffusion of PI(4,5)P2 in the plasma membrane in the presence of high density effector protein complexes. doi:10.1101/2022.01.07.475414.

171. Liebmann, T. *et al.* Regulation of Neuronal Na,K-ATPase by Extracellular Scaffolding Proteins. *International Journal of Molecular Sciences 2018, Vol. 19, Page 2214* **19**, 2214 (2018).

172. Steringer, J. P. *et al.* Phosphatidylinositol 4,5-Bisphosphate (PI(4,5)P2)-dependent Oligomerization of Fibroblast Growth Factor 2 (FGF2) Triggers the Formation of a Lipidic Membrane Pore Implicated in Unconventional Secretion. *Journal of Biological Chemistry* **287**, 27659–27669 (2012).

173. Steringer, J. P. & Nickel, W. A direct gateway into the extracellular space: Unconventional secretion of FGF2 through self-sustained plasma membrane pores. *Semin Cell Dev Biol* **83**, 3–7 (2018).

174. Lolicato, F. & Nickel, W. A Role for Liquid-Ordered Plasma Membrane Nanodomains Coordinating the Unconventional Secretory Pathway of Fibroblast Growth Factor 2? *Front Cell Dev Biol* **10**, (2022).

175. Sparn, C., Meyer, A., Saleppico, R. & Nickel, W. Unconventional secretion mediated by direct protein self-translocation across the plasma membranes of mammalian cells. *Trends Biochem Sci* **47**, 699–709 (2022).

176. Sato, M., Ozawa, T., Inukai, K., Asano, T. & Umezawa, Y. Fluorescent indicators for imaging protein phosphorylation in single living cells. *Nature Biotechnology 2002 20:3* **20**, 287–294 (2002).

177. Tsunoyama, T. A. *et al.* Super-long single-molecule tracking reveals dynamic-anchorage-induced integrin function. *Nature Chemical Biology 2018 14:5* **14**, 497–506 (2018).

178. Graham, T. G. W., Ferrie, J. J., Dailey, G. M., Tjian, R. & Darzacq, X. Detecting molecular interactions in live-cell single-molecule imaging with proximity-assisted photoactivation (PAPA). *Elife* **11**, 1–46 (2022).

179. DG, G. *et al.* Enzymatic assembly of DNA molecules up to several hundred kilobases. *Nat Methods* **6**, 343–345 (2009).

180. Miranda, P. *et al.* State-dependent FRET reports calcium- and voltagedependent gating-ring motions in BK channels. *Proc Natl Acad Sci U S A* **110**, 5217–5222 (2013).

181. E, P., CM, W. & H, E. A simple method for GFP- and RFP-based dual color single-molecule localization microscopy. *ACS Chem Biol* **10**, 1411–1416 (2015).

182. Edelstein, A., Amodaj, N., Hoover, K., Vale, R. & Stuurman, N. Computer Control of Microscopes Using μManager. *Curr Protoc Mol Biol* **92**, 14.20.1-14.20.17 (2010).

183. Lippiat, J. D., Standen, N. B. & Davies, N. W. Block of cloned BK(Ca) channels (rSlo) expressed in HEK 293 cells by N-methyl D-glucamine. *Pflugers Arch* **436**, 810–812 (1998).

184. Wang, Z., Wong, N. C., Cheng, Y., Kehl, S. J. & Fedida, D. Control of voltage-gated K+ channel permeability to NMDG+ by a residue at the outer pore. *Journal of General Physiology* **133**, 361–374 (2009).

185. Tinevez, J. Y. *et al.* TrackMate: An open and extensible platform for single-particle tracking. *Methods* **115**, 80–90 (2017).

186. Schindelin, J. *et al.* Fiji: an open-source platform for biological-image analysis. *Nature Methods 2012 9:7* **9**, 676–682 (2012).

187. Pavon Arocas, O. (2021). A Thesis Template in Word (Version 1.0.0). https://doi.org/10.5281/zenodo.6418337

8 APPENDIX

Python, ImageJ and Matlab scripts are used for data processing and analysis. Important factors and functions of the code are marked in green.

8.1 MEASUREMENT OF ALPHA AND DIFFUSION COEFFICIENT

```
import os, pandas as pd, numpy as np
# selecting files-----------------------------------------------
-------directoryPath = input('Directory for csv files: ')
f = os.listdir(directoryPath)
ff = [os.path.join(directoryPath, x) for x in f]
paths = list(filter(os.path.isdir, ff))
paths = [x for x in paths if 'track.csv' in
os.listdir(x+"\\Pos0")]
paths = [x + "\\Pos0" for x in paths]
#functions-----------------------------------------------------------
-------
#assignment of mobility to each track
def filter_mob_imm(spot, track):
    mobility = []
    for j in track["TRACK_ID"]:
        current = spot.loc[spot["TRACK_ID"] == j]
        xspread = max(current["POSITION_X"]) -
min(current["POSITION_X"])
        yspread = max(current["POSITION_Y"]) -
min(current["POSITION_Y"])
        if (xspread and yspread) < 0.3:
            mobility.append('Immobile')
        else:
            mobility.append('Mobile')
```

```
    track['Mobility'] = mobility
#calculation of mean square displacement for each track
def compute_msd_1_5_np(xy, dt): # modify if there is gap.
    #shifts = np.floor(t / t_step).astype(int)
    shifts = np.arange(1,6)
    t = shifts*dt
    msds = np.zeros(shifts.size)
    msds_std = np.zeros(shifts.size)

    for i, shift in enumerate(shifts):
        delx = xy[:-shift if shift else None]
        dely = xy[shift:]
        #find the rows with nan and remove the rows from both
array
        a = np.isnan(delx)
        b = np.isnan(dely)
        c = np.logical_or(a, b)
        delx = delx[~c[:,0]]
        dely = dely[~c[:,0]]
        diffs = delx-dely
        sqdist = np.square(diffs).sum(axis=1)
        msds[i] = sqdist.mean()
        msds_std[i] = sqdist.std(ddof=1)
    msds = pd.DataFrame({'msds': msds, 'tau': t, 'msds_std':
msds_std})
    return msds

def correct_missing_frames(xy):
    full_ind = pd.Series(np.arange(min(xy.index),max(xy.index)+1))
    ins = full_ind.index.difference(xy.index)
    a = np.full([len(ins), 2], np.nan).tolist()
    df = pd.DataFrame(a, index=pd.Index(ins),
columns=pd.Index(['POSITION_X','POSITION_Y']))
    xy.append(df)
    xy = xy.sort_index()
    return xy
#main code----------------------------------------------------------
-------
filetype1 = '\\spot.csv'
filetype2 = '\\track.csv'
t = 10
dt = 0.05 #50ms in s
for filename in paths:
    alpha_all = []
    D_all = []
    if os.path.exists(filename + filetype1):
        print(filename)
        spots = pd.DataFrame(pd.read_csv(filename + filetype1))
        tracks = pd.DataFrame(pd.read_csv(filename + filetype2))
```

```
        filter_mob_imm(spots, tracks)
        tracks.to_csv(filename + '\\Tracks statistics roi
filtered.csv')
        long_tracks = tracks[tracks['NUMBER_SPOTS'] > t] #filter
out short tracks
        long_tracks = long_tracks.reset_index(drop=True)
        for j in long_tracks["TRACK_ID"]: #loop through each track
            current = spots.loc[spots["TRACK_ID"] == j]
            current = current.set_index("FRAME")
            xy =
current.loc[:,['POSITION_X','POSITION_Y']]#collect xy coordinates
            xy = correct_missing_frames(xy)
            xy = xy.to_numpy()
            msd = compute_msd_1_5_np(xy, dt)
            reg =
stats.linregress(np.log(msd['tau']),np.log(msd['msds']))
            #measurement of alpha and Diffusion Coefficient
            alpha = reg.slope
            D = np.exp(reg.intercept)/4
            alpha_all.append(alpha)
            D_all.append(D)
        long_tracks['Diffusion_Coefficient'] = D_all
        long_tracks['alpha'] = alpha_all
        #save all alpha and diffusion coefficient and plot...
```

8.2 PIPELINE FOR COLOCALISATION ANALYSIS

Pipeline outline:

a) Creating a transformation matrix. Matlab code

b) Cropping and aligning left and right images. Matlab code

c) Tracking. (not shown)

d) Measuring colocalization and Simulation. Python code

a) Creating a transformation matrix. (Matlab code)

```
%Manually crop tetraspeck bead image into two halves using
rectangular ROI of 256 x 512 pixels. Save the left images as
'left.png' and right image as 'right.png' before running the
following code.%
```

```
red= imread('right.png');
green = imread('left.png');
cpselect(red,green)

%An interactive window with the left and right image will appear.
Select the beads that appear in both the images and make sure they
are labelled with the same number. Save the selected points before
running the next lines.%

tform = fitgeotrans(movingPoints,fixedPoints,'affine');
Roriginal = imref2d(size(green));
recoveredred= imwarp (red,tform,'OutputView',Roriginal);
imwrite(recoveredred,'transformed_red.tif');

%The tform matrix is the transformation matrix we need to apply on
all the images. It can be saved for later use.%
```

b) Cropping and Aligning left and right images. (Matlab code)

```
%Load the 'tform.mat' file obtained from the last step before
running the following lines.%
% Finds and crops TIF images in that folder
% code to select folder is omitted here%

% Process all image files in those folders.
for k = 1 : numberOfFolders
    % Get this folder and print it out.
    thisFolder = listOfFolderNames{k};
    fprintf('Processing folder %s\n', thisFolder);
    filePattern = sprintf('%s/*.tif', thisFolder);
    baseFileNames = dir(filePattern);
    numberOfImageFiles = length(baseFileNames);
    % Now we have a list of all files in this folder.
    if numberOfImageFiles >= 1
        % Go through all those image files.
        mkdir(fullfile(thisFolder,'leftImages'));
        mkdir(fullfile(thisFolder,'rightImages'));
        for f = 1 : numberOfImageFiles
            fullFileName = fullfile(thisFolder,
baseFileNames(f).name);
            I = imread(fullFileName);
           %crop image
            rect = [0,0,256,512];
            left = imcrop(I, rect);
            rect2 = [257,0,256,512];
            right = imcrop(I, rect2);
            Roriginal = imref2d(size(left));
           %apply transformation matrix
```

```
            recoveredred =
imwarp(right,tform,'OutputView',Roriginal);

imwrite(left,strcat(thisFolder,'\leftImages\',baseFileNames(f).nam
e));
imwrite(recoveredred,strcat(thisFolder,'\rightImages\',baseFileNam
es(f).name));
        end
```

c) Tracking

d) Measuring colocalisation. (Python code)

```
#only showing the core parts of the code.# file selection section
is shortened. Some lines for variable saving is also omitted.
import os, pandas as pd, matplotlib.pyplot as plt, pickle, numpy
as np
from scipy.spatial import ConvexHull, convex_hull_plot_2d
from scipy.spatial import Delaunay
import random

#functions-----------------------------------------------------------
#function to find colocalisation
def coloc(green, red):
    d = 0.1
    neighbours = []
    neighboursred = []
    for i in range(len(green)):
        x = green.iloc[i,13]
        y = green.iloc[i,14]
        match = []
        matchred = []
        for j in range(len(red)):
            if ((abs(red.iloc[j,13]-x)<d) and (abs(red.iloc[j,14]-
y)<d)):
                match.append(green.iloc[i,1])
                matchred.append(red.iloc[j,1])
                break
        if len(match)>0:
            neighbours.append(match)
            neighboursred.append(matchred)
    return neighbours,neighboursred

#functions required for the randomisation process
#triangle coordinates
def tri_points(tri,points):
    triangle = []
    for i in range(len(tri.vertices)):
        m = []
```

```
        for j in range(3):
            coor = tri.vertices[i][j]
            m.append([points.iloc[coor][0], points.iloc[coor][1]])
        triangle.append(m)
    return triangle

def tri_area(tri,points):
    area = []
    n = len(tri.vertices) #number of triangles
    for i in range(n):
        cur = tri.vertices[i]
        #Area =1/2[x1(y2 - y3) + x2(y3 - y1) + x3(y1 - y2)]

area.append(1/2*abs(points.iloc[cur[0],0]*(points.iloc[cur[1],1] -
points.iloc[cur[2],1]) +
points.iloc[cur[1],0]*(points.iloc[cur[2],1] -
points.iloc[cur[0],1]) +
points.iloc[cur[2],0]*(points.iloc[cur[0],1] -
points.iloc[cur[1],1])))
    return area


#given triangle coordinates: generates a point within the triangle
def point_on_triangle(pt):
    pt1 = pt[0]
    pt2 = pt[1]
    pt3 = pt[2]
    s, t = sorted([random.random(), random.random()])
    return (s * pt1[0] + (t-s)*pt2[0] + (1-t)*pt3[0],
            s * pt1[1] + (t-s)*pt2[1] + (1-t)*pt3[1])

#variable definition, file selection-----------------------------
-------
paths = []
filename = []
m = []  #fraction of green spots that colocalise
r = [] # fraction of randomised green spot colocalising
# file selection
directoryPath= input('Directory for csv files: ')
for x in os.walk(directoryPath):
    if any(s.startswith('All') for s in x[2]):
        paths.append(x[0])
for i in paths:
    if 'left' in i:
        filename.append(i.split('left')[0])

#main code-------------------------------------------------------
-------
for f in filename:
```

```
    g = 0
    counts = 0
    spots = []
    spotsred = []
    green = pd.DataFrame(pd.read_csv(f + 'leftImages\\' + 'Track
statistics.csv'))
    red = pd.DataFrame(pd.read_csv(f + 'rightImages\\' + 'Track
statistics.csv'))
    #only select immobile green and red particles
    red = red.loc[red["TRACK_DISPLACEMENT"]<0.25]
    green = green.loc[green["TRACK_DISPLACEMENT"]<0.25]
    g = g + len(green)
    [b,c] = coloc(green, red)#run colocalisation function
    counts = counts + len(b)
    m.append(counts/g) #collecting fraction of FGF2-GFP that
colocalise
    proxy = f.split('\\')

#simulation-----------------------------------------------------
-------

#generate randomised coodinates for green spots within cell
boundary
# red channel is very dense and all spots are used to map the cell
border. N random spots are generated within the cell boundary
where N is the number of FGF2-GFP molecules(green spots) observed
in the experiment. The random spots are tested for colocolisation
with the red spots from the experiment.

points = red[["TRACK_X_LOCATION", "TRACK_Y_LOCATION"]].to_numpy()
hull = ConvexHull(points) #generate polygon for the boundary of
the cell
boundary = pd.DataFrame(zip(points[hull.vertices,0],
points[hull.vertices,1])) # xy coordinates of cell boundary
polygon
tri = Delaunay(boundary) # generate triangles within the polygon
total = len(green) # number of points to randomly place within the
shape
area = []
n = len(tri.vertices) #number of triangles
area = tri_area(tri,boundary) #get vector with areas of triangles
p = area/sum(area) #get probab vector based on the area of each
triangle
particles = np.random.multinomial(total, p, size=1) # generate
number of #spots to add in each triangle based on area of the
triangle
triangle = tri_points(tri,boundary)
rndm = [] #list of generated coordinates
for i in range(len(tri.vertices)):
        for j in range(particles[0,i]):
```

```
            rndm.append(point_on_triangle(triangle[i]))

coord = pd.DataFrame(rndm, columns =['X', 'Y']) # tuple to
dataframe
green_rd = green.copy()
green_rd[["TRACK_X_LOCATION", "TRACK_Y_LOCATION"]] = coord
#replace x,y coordinates to new random x,y coordinates
[b,c] = coloc(green_rd, red)
 r.append(len(b)/g) #fraction of randomised FGF2-GFP that
colocalise

# saving list of fraction of FGF2-GFP molecules that colocalise to
FGF2-Halo molecules.
with open(directoryPath + '\\fraction_colocalise.txt', "wb") as
fp:
   pickle.dump(m, fp)
with open(directoryPath + '\\randomised_fraction_colocalise.txt',
"wb") as fp:
   pickle.dump(r, fp)
```

8.3 PIPELINE FOR OLIGOMER STATE ANALYSIS

Pipeline outline:

a) Background subtraction. Image J Macro (not shown)

b) Tracking. Python code run in Image J

c) Collecting intensity values of the tracks. Python code

d) Converting intensity values to oligomer state and extracting percentage of oligomer species. Origin (not shown)

a) Background subtraction

b) Tracking

```
###
Modified script from a posted script on image.sc forum by Jean-
Yves Tinevez, the creator of trackmate plugin.###
# trackmate core script
```

```
import sys
from ij import IJ
from ij import WindowManager
from fiji.plugin.trackmate import Model
from fiji.plugin.trackmate import Settings
from fiji.plugin.trackmate import TrackMate
from fiji.plugin.trackmate import SelectionModel
from fiji.plugin.trackmate import Logger
from fiji.plugin.trackmate.detection import LogDetectorFactory
from fiji.plugin.trackmate.tracking import LAPUtils
from fiji.plugin.trackmate.action import ExportStatsToIJAction
from fiji.plugin.trackmate.tracking.sparselap import
SparseLAPTrackerFactory
from fiji.plugin.trackmate.providers import SpotAnalyzerProvider
from fiji.plugin.trackmate.providers import EdgeAnalyzerProvider
from fiji.plugin.trackmate.providers import TrackAnalyzerProvider
import
fiji.plugin.trackmate.visualization.hyperstack.HyperStackDisplayer
as HyperStackDisplayer
import fiji.plugin.trackmate.features.FeatureFilter as
FeatureFilter
from java.io import File
from fiji.plugin.trackmate.io import TmXmlWriter
from ij.plugin import FolderOpener

def trackmate(stack):
      imp = WindowManager.getCurrentImage()
      dims = imp.getDimensions();
      imp.setDimensions( dims[ 2 ], dims[ 4 ], dims[ 3 ] );

      #----------------------------
      # Create the model object now
      #----------------------------
      model = Model()
      model.setLogger(Logger.IJ_LOGGER)

      #------------------------
      # Prepare settings object
      #------------------------
      settings = Settings()
      settings.setFrom(imp)

      # spot detection variables
      # Configure detector - We use the Strings for the keys
      settings.detectorFactory = LogDetectorFactory()
      settings.detectorSettings = {
          'DO_SUBPIXEL_LOCALIZATION' : True,
          'RADIUS' : .3,
          'TARGET_CHANNEL' : 1,
```

```
        'THRESHOLD' : 50., #changes based on experiment or cell
        'DO_MEDIAN_FILTERING' : False,
    }

    #tracking variables
    settings.trackerFactory = SparseLAPTrackerFactory()
    settings.trackerSettings = {
    'MAX_FRAME_GAP' : 2,
    'ALTERNATIVE_LINKING_COST_FACTOR' : 1.05,
    'LINKING_FEATURE_PENALTIES' : {},
    'LINKING_MAX_DISTANCE' : 0.4,
    'GAP_CLOSING_MAX_DISTANCE' : 0.4,
    'MERGING_FEATURE_PENALTIES' : {},
    'SPLITTING_MAX_DISTANCE' : 1.50,
    'BLOCKING_VALUE' : float("inf"),
    'ALLOW_GAP_CLOSING' : True,
    'ALLOW_TRACK_SPLITTING' : False,
    'ALLOW_TRACK_MERGING' : False,
    'MERGING_MAX_DISTANCE' : 1.50,
    'SPLITTING_FEATURE_PENALTIES' : {},
    'CUTOFF_PERCENTILE' : 0.9,
    'GAP_CLOSING_FEATURE_PENALTIES' : {}}

    spotAnalyzerProvider = SpotAnalyzerProvider()
    for key in spotAnalyzerProvider.getKeys():
        print( key )
        settings.addSpotAnalyzerFactory(
spotAnalyzerProvider.getFactory( key ) )

    edgeAnalyzerProvider = EdgeAnalyzerProvider()
    for  key in edgeAnalyzerProvider.getKeys():
        print( key )
        settings.addEdgeAnalyzer(
edgeAnalyzerProvider.getFactory( key ) )

    trackAnalyzerProvider = TrackAnalyzerProvider()
    for key in trackAnalyzerProvider.getKeys():
        print( key )
        settings.addTrackAnalyzer(
trackAnalyzerProvider.getFactory( key ) )

    #-------------------
    # Instantiate plugin
    #-------------------

    trackmate = TrackMate(model, settings)

    #--------
```

```
# Process
#--------

ok = trackmate.checkInput()
if not ok:
    sys.exit(str(trackmate.getErrorMessage()))

ok = trackmate.process()
if not ok:
    sys.exit(str(trackmate.getErrorMessage()))


#----------------
# Display results
#----------------

selectionModel = SelectionModel(model)
displayer =  HyperStackDisplayer(model, selectionModel, imp)
displayer.render()
displayer.refresh()

# Echo results with the logger we set at start:
model.getLogger().log(str(model))

# export needed files for further analysis
outfile = TmXmlWriter(File(stack + 'model.xml'))
outfile.appendModel(model)
outfile.writeToFile()

#to get tracksta,link,spots file
esta = ExportStatsToIJAction(selectionModel)
esta.execute(trackmate)

# saving the output files
from ij import IJ, ImagePlus, ImageStack
dir = stack
IJ.selectWindow("Track statistics");
IJ.saveAs("text", dir + "track40" + ".csv");
IJ.run("Close");
IJ.selectWindow("Links in tracks statistics");
IJ.saveAs("text", dir + "link40" + ".csv");
IJ.run("Close");
IJ.selectWindow("Spots in tracks statistics");
IJ.saveAs("text", dir + "spot40" + ".csv");
IJ.run("Close");
imp.changes = False
imp.close();
```

```
from ij import IJ
from ij.plugin import FolderOpener
import os

#select the folder that needs batch analysis
path =
"E:\\gpc1mcherry_fgf2halo\\220503\\gpc1hafgf2halowt\\50pM_bgsubs";
#listing only top level folders in the path
f = os.listdir(path)
ff = [os.path.join(path, x) for x in f]
folders= list(filter(os.path.isdir, ff))
print(folders)
for i in folders:
      if not os.path.exists(i + '\\track40.csv'):
            if not len(os.listdir(i))<10:
                  print(i);
                  stack = i + '\\'
                  imp = FolderOpener.open(i, "")
                  imp.show()
                  imp.setRoi(125, 99, 180, 221); # roi for
cropping image depends on the illumination on the given day to
have a uniform illumination
                  imp2 = imp.crop("stack");
                  imp.close();
                  imp2.show();
                  #setting scale
                  IJ.run(imp2, "Set Scale...", "distance=1
                  known=0.1 unit=µm");

                  #open roi manager
                  from ij.plugin.frame import RoiManager
                  rm = RoiManager.getInstance()
                  if not rm:
                    rm = RoiManager()
                  rm.reset()

                  #find name of roi file
                  l = os.listdir(i);
                  for fname in l:
                      if fname.endswith('.roi'):
                              f = fname

                  #opening cell specific roi file
                  rm.runCommand("open", stack + f);
                  #imp2.close();
                  rm.select(0)

                  #running trackmate on stack
                  trackmate(stack)
```

```
#closing roi manager
roiManager = rm.getRoiManager();
roiManager.close();
```

c) Collecting intensity values of the tracks

```
###Uses tracking output files to gather all intensity values of
the tracked FGF2 molecules. Each track represents a single FGF2
molecule tracked over some time. Filters out tracks that are
outside the cell region. Defines tracks as mobile or immobile
based on the track displacements. Saves all FGF2 intensities,
mobile and immobile FGF2 intensities and modified track statistics
file with only tracks of duration higher than 10 frames.

import matplotlib.pyplot as plt
import os
import pandas as pd
import pickle
from numpy import histogram
from scipy import stats
from shapely.geometry import Point
from shapely.geometry.polygon import Polygon
import numpy as np

#fileselection ----------------------------------------------------
-----
directoryPath = input('Directory for csv files: ')
f = os.listdir(directoryPath)
ff = [os.path.join(directoryPath, x) for x in f]
paths = list(filter(os.path.isdir, ff))

#functions---------------------------------------------------------
-------
#defines tracks as mobile or immobile based on net track
displacement
def filter_mob_imm(spot, track):
    mobility = []
    for j in track["TRACK_ID"]:
        current = spot.loc[spot["TRACK_ID"] == j]
        xspread = max(current["POSITION_X"]) -
min(current["POSITION_X"])
        yspread = max(current["POSITION_Y"]) -
min(current["POSITION_Y"])
        if (xspread and yspread) < 0.3: #threshold of 300nm for
immobile spots
            mobility.append('Immobile')
        else:
```

```
            mobility.append('Mobile')
    track['Mobility'] = mobility

#filters out tracks outside of cell specific roi. If not used in
tracking step
def remove_tracks_outside_roi(track, coor):  # coor is x,y
coordinate of roi
    lons_lats_vect = coor.to_numpy()  # needs it to be in numpy
array
    polygon = Polygon(lons_lats_vect)
    track_xy = track[["TRACK_X_LOCATION",
"TRACK_Y_LOCATION"]].to_numpy()
    track_xy = track_xy * 10  # roi coordinates always in pixels.
need to *10 if track coor in um
    boolean = []
    for i in range(len(track_xy)):
        point = Point(track_xy[i])
        boolean.append(polygon.contains(point))
    new_tracks = track[boolean]
    return new_tracks

#main code-----------------------------------------------------------
-------
#get mean background intensity from monomer data for the day.
monopath = path + "\\10pM_bgsubs\\no_od_stepanalyser_input"
mf = os.listdir(monopath)
mff = [os.path.join(monopath, x) for x in mf]
mpaths = list(filter(os.path.isdir, mff))
filetype4 = "\\Plot Values.csv"
all_bg = []
all_s_height = []# multi step intensities: level
all_ups = 0 # to check the direction of step data
all_downs = 0 # same
all_start_height = [] #first steps in multistep cases
all_build_height = [] # intensity of incoming particles on
multistep spots
all_drop_height = []
for i in mpaths:
    bg = pd.DataFrame(pd.read_csv(i + filetype4))
    #clean bg and get bg value
    z_scores = stats. zscore(bg["Mean"]) #calculate z-scores of
`df`
    abs_z_scores = np. abs(z_scores)
    filtered_entries = (abs_z_scores < 3)
    bg = bg[filtered_entries]
    bg_mean= bg['Mean'].mean()
    all_bg.append(bg_mean)

#names of output files from tracking
```

```
filetype1 = '\\spot40.csv'
filetype2 = '\\track40.csv'
filetype3 = '\\XY_Coordinates.csv'
filetype4 = "\\Plot Values.csv"  # Mean intensity of the cytosolic
background
t = 10
allheightimmobile = []
allheightmob = []
for filename in paths:
    if os.path.exists(filename + filetype1):
        print(filename)
        height = []
        height_mob = []
        height_imm = []
        spots = pd.DataFrame(pd.read_csv(filename + filetype1))
        tracks = pd.DataFrame(pd.read_csv(filename + filetype2))
        bg_mean = np.mean(all_bg)
        #modify all intensity values by subtracting it with bg
means (cytosolic background)
        spots['MEAN_INTENSITY'] =  spots['MEAN_INTENSITY']-bg_mean
        coor_path = filename + filetype3
        if os.path.exists(coor_path):  # if file exists:
            coor = pd.DataFrame(pd.read_csv(filename + filetype3))
               new_tracks = remove_tracks_outside_roi(tracks,
coor)
               tracks = new_tracks
               tracks = tracks.reset_index(drop=True)
        filter_mob_imm(spots, tracks)
        tracks = tracks[tracks['NUMBER_SPOTS'] > 10] #filter out
too short tracks
        tracks = tracks[tracks['TRACK_DURATION']<450] #filter out
too long tracks
        tracks = tracks.reset_index(drop=True)
        for j in tracks["TRACK_ID"]:
               current = spots.loc[spots["TRACK_ID"] == j]
               spotaverage = current['MEAN_INTENSITY'].mean()
               height.append(spotaverage)

        # segregate mobile and immobile heights into seperate
lists
        height = pd.Series(height)
        im_entries = tracks['Mobility'] == 'Immobile'
        mob_entries = tracks['Mobility'] == 'Mobile'
        height_mob = height[mob_entries]
        height_imm = height[im_entries]
        allheightimmobile.extend(height_imm)
        allheightmob.extend(height_mob)

# saving all intensity variables
```

```
#save allheightimmobile and allheightmob and plot
```

8.4 PIPELINE FOR MULTI STEP TRACK ANALYSIS

Pipeline outline:

a) Selecting long tracks (>10 frames) for the analysis

b) Identifying time points of changes in mean intensity levels. Matlab code. Written by Dr. Amin Zehtabian.

c) Gathering intensity levels of specific categories. Python code

d) Conversion of Intensity to oligomer state and plotting. Python code (not shown)

a) Selecting tracks for the analysis

b) Identifying timepoints of changes in mean intensity levels

```
%%Takes in filtered track statistics and spots in track statistics
output files from trackmate analysis. Finds timepoints in each
track where a change in mean intensity level is detected. Saves
the track-id and the frames with the change in a file called
allstep.csv.

fileinfo = dir ("steppy/no_od_stepanalyser_input/");
fnames = {fileinfo.name};
filetype1 = "/spot40.csv";
filetype2 = "/Tracks statistics roi filtered_minlength10.csv";
for i = 1: length(fnames)
if (length(fnames{i}) > 10)
track =
readtable(strcat("steppy/no_od_stepanalyser_input/",fnames{i},file
type2));
spot =
readtable(strcat("steppy/no_od_stepanalyser_input/",fnames{i},file
type1));
allstepmatrix = [];
for j = 1: height(track)
Track_id = track{j,'TRACK_ID'}; % ID of the desired track
rows = spot.TRACK_ID == Track_id;
mean_series = spot(rows,"MEAN_INTENSITY");
```

```
mean_series = table2array(mean_series);
Error1 = 27; % biggervalue less noisy
x =
findchangepts(mean_series,'Statistic','std','MinThreshold',Error1)
;
A = [] ;
n = size(x,1);
A(1:n,1) = Track_id;
stepmat = [A,x];
allstepmatrix = [allstepmatrix;stepmat];
end
writematrix(allstepmatrix,
strcat("steppy/no_od_stepanalyser_input/",fnames{i},'/allstep.csv'
));
end
end
```

c) Gathering intensity levels of specific categories

```
###Opens the output files from trackmate and the 'allstep.csv'
file from 2b script. Finds out the mean intensity of each step of
a multi-step track. Collects mean intensities of a single-step
track, mean intensities of all levels of a multi-step track, mean
intensities of the first step of a multi-step track and mean
intensities of molecules that bind to existing spots.
import os, pandas as pd, matplotlib.pyplot as plt, pickle, numpy
as np
from numpy import histogram
from scipy import stats
#file selection----------------------------------------------------
-------
#%%
path = r"D:\purba\211018" #name of the folder to analyse
directoryPath = path + \\1uM_bgsubs\\no_od_stepanalyser_input
#address for fully labelled data

#main code---------------------------------------------------------
-------
##get mean bg from 10pM data.
monopath = path + "\\10pM_bgsubs\\no_od_stepanalyser_input"
mf = os.listdir(monopath)
mff = [os.path.join(monopath, x) for x in mf]
mpaths = list(filter(os.path.isdir, mff))
filetype4 = "\\Plot Values.csv"
all_bg = []
all_s_height = []# multi step intensities: level
all_ups = 0 # to check the direction of step data
all_downs = 0 # same
all_start_height = [] #first steps in multistep cases
all_build_height = [] # intensity of incoming particles on
multistep spots
```

```
all_drop_height = []
for i in mpaths:
    bg = pd.DataFrame(pd.read_csv(i + filetype4))
    #clean bg and get bg value
    z_scores = stats. zscore(bg["Mean"]) #calculate z-scores of
`df`
    abs_z_scores = np. abs(z_scores)
    filtered_entries = (abs_z_scores < 3)
    bg = bg[filtered_entries]
    bg_mean= bg['Mean'].mean()
    all_bg.append(bg_mean)

f = os.listdir(directoryPath)
ff = [os.path.join(directoryPath, x) for x in f]
paths = list(filter(os.path.isdir, ff))

filetype1 = "\\allstep.csv"
filetype2 = "\\spot40.csv"
filetype3 = "\\Tracks statistics roi filtered_minlength10.csv"
#only tracks with min length of 10 frames

all_steppy_fraction = []#% of total immobile spots that show
multiple steps
all_ns_height = []# only single step intensities
all_s_height = []# multi step intensities: level
all_ups = 0 # to check the direction of step data
all_downs = 0 # same
all_start_height = [] #first steps in multistep cases
all_build_height = [] # intensity of incoming particles on
multistep spots

for i in paths:
    print(i)
    tracks = pd.DataFrame(pd.read_csv(i + filetype3))
    tracks = tracks[tracks['TRACK_DURATION']<450]
    spots = pd.DataFrame(pd.read_csv(i + filetype2))
    step = pd.DataFrame(pd.read_csv(i + filetype1, header=None))
    step.columns =['TRACK_ID', 'FRAME']
    bg_mean = np.mean(all_bg)

    #modify all intensity values by subtracting it with bg means
(cytosolic background)
    spots['MEAN_INTENSITY'] =  spots['MEAN_INTENSITY']-bg_mean

    #% of tracks that show multiple steps
    Number_of_steppy_data = len(step['TRACK_ID'].unique())
    Total_immobile = len(tracks)
    steppy_fraction = Number_of_steppy_data/Total_immobile
    all_steppy_fraction.append(steppy_fraction)
```

```
    steppy_track_id = step['TRACK_ID'].unique()
    s_track = tracks[tracks['TRACK_ID'].isin(steppy_track_id)]
    ns_track = tracks[~tracks['TRACK_ID'].isin(steppy_track_id)]

    # collecting intensity of single step tracks
    ns_height = []
    for j in ns_track["TRACK_ID"]:
        current = spots.loc[spots["TRACK_ID"] == j]
        spotaverage = current['MEAN_INTENSITY'].mean()
        ns_height.append(spotaverage)
    all_ns_height.extend(ns_height)

    # processing intensity of multi-step tracks
    s_height = []
    for j in s_track["TRACK_ID"]:
        track_step = step[step["TRACK_ID"] == j]
        n = len(track_step)
        current = spots.loc[spots["TRACK_ID"] == j]
        current = current.reset_index(drop=True)
        start = 0
        for k in range(n):
            end = track_step.iloc[k,1]
            spotaverage = current.iloc[start:end-1,12].mean()
            s_height.append(spotaverage)
            start = end
        spotaverage = current.iloc[start::,12].mean()
        s_height.append(spotaverage)

    # make another dataframe that includes the mean intensity of
each step of a track.
    mod_step = pd.DataFrame()
    for j in s_track["TRACK_ID"]:
        track_step = step[step["TRACK_ID"] == j]
        #stop = tracks[tracks["TRACK_ID"] == j].TRACK_STOP.iloc[0]
        stop = len(spots.loc[spots["TRACK_ID"] == j])
        new_row = {"TRACK_ID":j, 'FRAME':stop +1}
        track_step = track_step.append(new_row, ignore_index=True)
        mod_step = mod_step.append(track_step)
    mod_step = mod_step.reset_index()
    mod_step['Height'] = s_height
    mod_step['build'] = mod_step['Height'].diff()
    mod_step.loc[mod_step['index'] == 0, 'build'] = np.nan

    #filtering multistep data
    #1.REMOVE STEPS WITH TOO SHORT DURATION
```

```
    starts = pd.DataFrame({"TRACK_ID": s_track["TRACK_ID"],
"FRAME":0})
    mod_step = pd.concat([starts,mod_step])
    mod_step =
mod_step.sort_values(['TRACK_ID','FRAME']).reset_index(drop=True)

    spot_frame = []
    for j in range(len(mod_step)): #the position of index row
keeps changing
        track_id = mod_step.loc[j,'TRACK_ID']
        ind = mod_step.loc[j,'FRAME']
        current = spots.loc[spots["TRACK_ID"] ==
track_id].reset_index(drop=True)
        spot_frame.append(current.iloc[ind,8])
    mod_step['spot_FRAME'] = spot_frame
    mod_step['duration'] = mod_step['spot_FRAME'].diff()
    mod_step.loc[mod_step['index'].isna(), 'duration'] = np.nan

    #duration threshold for a step is set at 7 frames
    mod_step = mod_step[~mod_step['duration'].between(0,7)]


    #3.REMOVE PHOTOBLEACHING TRACKS
    upward_tracks = []
    for j in s_track["TRACK_ID"]:
        track_step = mod_step[mod_step["TRACK_ID"] == j]
        if (track_step['build'] > 0).any() == True:
            upward_tracks.append(j)
    mod_step = mod_step[mod_step['TRACK_ID'].isin(upward_tracks)]

    #3. REMOVE SINGLE STEP TRACKS AFTER all filtering
    singles = []
    for j in mod_step['TRACK_ID'].unique():
        mod_curr = mod_step[mod_step['TRACK_ID'] == j]
        if len(mod_curr)<3:
            singles.append(j)
    mod_step = mod_step[~mod_step['TRACK_ID'].isin(singles)]

    #UPDATE THE TRACK FILE
    s_track =
tracks[tracks['TRACK_ID'].isin(mod_step['TRACK_ID'])]

    #DATA GATHERING FOR PLOTS:
    mod_step['Height_oli'] = mod_step['Height']/np.mean(mono)
    #for oligomer state distribution plot of multistep tracks
    all_s_height.extend(mod_step['Height_oli'])
    #for oligomer state distribution plot of first step in
multistep tracks
    start_height = mod_step[mod_step['index'] == 0].Height_oli
```

```
    all_start_height.extend(start_height)
    #for oligomer state distribution plot of subsequent step in
multistep track

all_build_height.extend(mod_step[mod_step['build_oli']>0].build_ol
i)
    #number of steps with increasing intensity
    up = len(mod_step[mod_step['build'] > 0])
    #number of steps with dropping intensity
    down = len(mod_step[mod_step['build'] < 0])
    all_ups = all_ups + up
    all_downs = all_downs + down

#save all variables..
```